

Aus dem Walther-Straub-Institut für Pharmakologie und Toxikologie  
der Ludwig-Maximilians-Universität München

Vorstand: Prof. Dr. med. Thomas Gudermann



# Analysis of P2X7 protein complexes in a P2X7-EGFP BAC transgenic mouse model

Dissertation

zum Erwerb des Doktorgrades der Naturwissenschaften an der Medizinischen  
Fakultät der Ludwig-Maximilians-Universität zu München

vorgelegt von

**Robin Edwin Kopp (geb. Stocklauser)**

aus

Lindenberg i. Allgäu

München,

2019

Mit Genehmigung der Medizinischen Fakultät  
der Universität München

Betreuerin: Prof. Dr. phil. nat. Annette Nicke

Zweitgutachter: PD Dr. Sven Lammich

Dekan: Prof. Dr. med. dent. Reinhard Hickel

Tag der mündlichen Prüfung: 08.04.2020

## Summary

P2X receptors are trimeric non-selective cation channels, gated by extracellular ATP. The P2X7 subtype differs from the other six P2X receptor family members (P2X1 - P2X6) among other things, by its low sensitivity to ATP and its extended cytoplasmic C-terminal domain. The receptor is expressed in a variety of cell types, with high expression in immune cells. Activation of P2X7 leads to the assembly of the NLRP3 inflammasome, resulting in caspase-1 activation and subsequent release of the mature proinflammatory cytokines IL-1 $\beta$  and IL-18. Accordingly, P2X7 signaling has been associated with a variety of inflammatory diseases, like pulmonary diseases, rheumatoid arthritis, inflammatory bowel disease, and neurodegenerative diseases. Thus, the receptor has gained attention as a promising drug target.

However, its cell type-specific localization, as well as the proteins involved in its trafficking, signaling, and functional modulation are still ambiguous. In addition, a heteromeric assembly with the P2X4 subtype is still a matter of debate. These uncertainties stand in sharp contrast to its role as a drug target.

Herein, a novel P2X7-EGFP BAC transgenic mouse model was used to determine P2X7 localization and its interaction with novel proteins, as well as the P2X4 subtype.

In this study, the mouse model was characterized in detail. To exclude an aberrant expression of the transgenic protein, membrane localization and distribution in different brain regions was biochemically investigated. By using conditional *P2rx7<sup>-/-</sup>* mice, a previously observed dominant expression in microglia and oligodendrocytes was validated. This was further confirmed by immunofluorescence labeling and confocal microscopy.

Additionally, the postulated interaction with the P2X4 subunit was investigated to examine the distribution, mutual interrelation, and the physical interaction of both subunits *in vivo*. In contrast to previous reports, no significant interaction was observed in native mouse tissue.

As the major part of this study, the BAC transgenic mouse line was used to

identify novel interaction partners of the P2X7 receptor. Therefore, a protocol for quantitative *in situ* cross-linking of P2X7 complexes in native lung tissue was established and used to co-purify interacting proteins cross-linked to P2X7. Subsequent analysis by mass spectrometry identified 41 significantly enriched proteins, of which several are involved in leukocyte migration. This allows us to link a previously described P2X7-mediated infiltration of leukocytes to a direct physical interaction of P2X7 with distinct cell adhesion molecules, like Integrin  $\beta$ -2, ICAM-1, PECAM-1 and MCAM.

Overall, this study addressed long discussed questions in P2X7 research and can help to understand signaling effects of P2X7 activation. This could lead to new treatment strategies of disease, in which P2X7 plays a major role.

## Zusammenfassung

P2X Rezeptoren sind trimere, nicht-selektive Kationenkanäle, die durch extrazelluläres ATP aktiviert werden. Der P2X7 Subtyp unterscheidet sich von den anderen sechs Mitgliedern der P2X Rezeptorfamilie (P2X1 - P2X6) unter anderem durch seine geringe Sensitivität gegenüber ATP und seiner langen zytoplasmatischen, C-terminalen Domäne. Der Rezeptor wird in verschiedenen Zelltypen exprimiert, mit einer hohen Expressionsrate in Immunzellen. P2X7 Aktivierung führt zur Assemblierung des NLRP3 Inflammasoms, was zur anschließenden Freisetzung der reifen proinflammatorischen Zytokine IL-1 $\beta$  und IL-18 führt. Entsprechend wurde der Rezeptor mit einer Vielzahl von inflammatorischen Krankheiten, wie beispielsweise Lungenerkrankungen, rheumatoider Arthritis, chronisch-entzündlichen Darmerkrankungen und neurodegenerativen Erkrankungen in Verbindung gebracht und als vielversprechendes Zielprotein für Arzneimittel in Betracht gezogen.

Trotzdem sind die zelltyp-spezifische Lokalisation des Rezeptors sowie die Proteine, die an dessen Transport, Signalwegen und funktioneller Modulation beteiligt sind, nach wie vor weitestgehend unbekannt. Darüber hinaus ist auch die heteromere Assemblierung mit dem P2X4 Subtyp immer noch umstritten. Diese Ungewissheiten stehen in einem starken Kontrast zu seiner Rolle als Zielprotein für die Arzneimittelherstellung.

In der vorliegenden Arbeit wurde ein neues P2X7-EGFP BAC transgenes Mausmodell verwendet, um die Lokalisation von P2X7 und dessen Interaktion mit neuen Proteinen sowie mit dem P2X4 Subtyp aufzuklären.

Im ersten Teil der Arbeit wurde das Mausmodell im Detail charakterisiert. Um eine abweichende Expression des transgenen Proteins auszuschließen, wurde die Membranlokalisierung und dessen Präsenz in verschiedenen Gehirnregionen biochemisch untersucht. Mit Hilfe von konditionellen *P2rx7*<sup>-/-</sup> Mäusen wurde eine zuvor beobachtete dominante Expression in Mikroglia und Oligodendrozyten bestätigt. Dies wurde desweiteren mit Hilfe von Immunfluoreszenzfärbung und Konfokalmikroskopie validiert.

Im zweiten Teil wurde die postulierte Interaktion mit dem P2X4 Rezeptor untersucht, um die Verteilung der beiden Subtypen, deren gegenseitige Beeinflussung, sowie deren physikalische Interaktion *in vivo* zu analysieren. Im Gegensatz zu bisherigen Studien, wurde in nativem Mausgewebe keine signifikante Interaktion beobachtet.

Als Hauptteil dieser Arbeit wurde die BAC transgene Mauslinie verwendet, um neue Interaktionspartner des P2X7 Rezeptors zu identifizieren. Hierfür wurde ein Protokoll etabliert, welches quantitatives *in situ* Quervernetzen von P2X7 Proteinkomplexen in nativem Mausgewebe ermöglicht, um interagierende, an P2X7 kovalent gebundene Proteine mit aufzureinigen. Durch die anschließende massenspektrometrische Analyse wurden 41 signifikant angereicherte Proteine identifiziert, von denen einige in die Migration von Leukozyten involviert sind. Dies ermöglicht es, eine zuvor beschriebene P2X7-vermittelte Einwanderung von Leukozyten mit der direkten, physikalischen Interaktion von P2X7 mit Zelladhäsionsmolekülen, wie Integrin  $\beta$ -2, ICAM-1, PECAM-1 und MCAM in Verbindung zu bringen.

Zusammenfassend behandelte diese Arbeit langjährig diskutierte Fragestellungen im Forschungsfeld des P2X7 Rezeptors und kann dabei helfen, die Effekte der P2X7 Aktivierung auf verschiedene Signalwege zu verstehen. Dies könnte dazu beitragen, neue Behandlungsstrategien für Krankheiten zu eröffnen, bei denen P2X7 eine entscheidende Rolle spielt.

# Contents

<b>Summary</b>	<b>3</b>
<b>Zusammenfassung</b>	<b>5</b>
<b>List of Abbreviations</b>	<b>5</b>
<b>1. Introduction</b>	<b>10</b>
1.1. Purinergic signaling . . . . .	10
1.2. P2X receptors . . . . .	11
1.3. The P2X7 receptor . . . . .	14
1.3.1. Properties . . . . .	14
1.3.2. Protein localization . . . . .	14
1.3.3. Signaling . . . . .	15
1.3.4. Interaction partners . . . . .	18
1.3.4.1. Heat shock protein HSP 90 . . . . .	20
1.3.4.2. Pannexin-1 . . . . .	21
1.3.4.3. Calmodulin . . . . .	21
1.3.4.4. Caveolins . . . . .	22
1.3.4.5. Myosin-9 . . . . .	22
1.3.4.6. Proteins involved in P2X7 receptor internalization	23
1.3.4.7. Proteins involved in P2X7-mediated interleukin	
secretion . . . . .	23
1.3.4.8. Anoctamin channels . . . . .	24
1.3.4.9. P2X4 receptor . . . . .	25
1.4. Preliminary work and aim of the study . . . . .	28
<b>2. Materials and Methods</b>	<b>31</b>
2.1. Materials . . . . .	31
2.1.1. Mouse lines . . . . .	31
2.1.2. Chemicals and materials . . . . .	32
2.1.3. Commercial kits and solutions . . . . .	33

---

2.1.4.	Buffers and media . . . . .	33
2.1.4.1.	Buffers and media for molecular biology . . . . .	33
2.1.4.2.	Buffers for <i>X. laevis</i> oocytes . . . . .	34
2.1.4.3.	Buffers for biochemical applications . . . . .	34
2.1.4.4.	Buffers and media for immunohistochemistry . . . . .	35
2.1.4.5.	Buffers and media for FACS analysis and cell culture . . . . .	35
2.1.5.	Antibodies . . . . .	36
2.1.6.	Enzymes . . . . .	37
2.1.7.	Oligonucleotides . . . . .	38
2.1.8.	Special equipment . . . . .	39
2.2.	Methods . . . . .	39
2.2.1.	Animal breeding and experiments . . . . .	39
2.2.2.	Molecular biology . . . . .	40
2.2.2.1.	Gibson assembly . . . . .	40
2.2.2.2.	Heat shock transformation . . . . .	40
2.2.2.3.	Polymerase chain reaction . . . . .	41
2.2.2.4.	Plasmid DNA preparation . . . . .	42
2.2.2.5.	Agarose gel electrophoresis . . . . .	42
2.2.2.6.	Quantification of nucleic acid samples . . . . .	43
2.2.2.7.	<i>In-vitro</i> cRNA synthesis . . . . .	43
2.2.2.8.	Southern blot analysis . . . . .	43
2.2.3.	Protein biochemical methods . . . . .	44
2.2.3.1.	<i>X. laevis</i> oocytes as expression system . . . . .	44
2.2.3.2.	Protein extraction from <i>X. laevis</i> oocytes . . . . .	44
2.2.3.3.	Protein extraction from mouse tissue . . . . .	44
2.2.3.4.	Glycosylation analysis . . . . .	45
2.2.3.5.	Purification of affinity-tagged proteins . . . . .	45
2.2.3.6.	Fluorescent labeling of proteins . . . . .	46
2.2.3.7.	Protein cross-linking . . . . .	46
2.2.3.8.	Sample preparation for LC-MS/MS analysis . . . . .	47
2.2.3.9.	SDS-PAGE . . . . .	47
2.2.3.10.	Western blot analysis . . . . .	48
2.2.3.11.	LC-MS/MS analysis . . . . .	48
2.2.4.	Flow cytometry . . . . .	50
2.2.5.	Immunohistochemistry . . . . .	51
2.2.5.1.	Immunostaining of lung and DRG cryosections . . . . .	51

---

2.2.5.2.	Free floating immunostaining of brain slices . . . . .	52
2.2.5.3.	Immunostaining of adherent cells . . . . .	53
2.2.6.	Isolation and cultivation of primary cells . . . . .	53
2.2.6.1.	Cells in the bronchoalveolar lavage fluid . . . . .	53
2.2.6.2.	Isolation of peritoneal macrophages . . . . .	54
2.2.6.3.	Primary microglia culture . . . . .	54
<b>3.</b>	<b>Results</b>	<b>55</b>
3.1.	Characterization of the P2X7-EGFP BAC transgenic mouse model	55
3.1.1.	Protein expression levels and stability of expression . . . . .	55
3.1.2.	Influence on endogenous P2X7 expression . . . . .	57
3.1.3.	Protein expression pattern . . . . .	58
3.1.4.	Plasma membrane targeting . . . . .	59
3.1.5.	Receptor assembly . . . . .	61
3.1.6.	Receptor function . . . . .	63
3.2.	Localisation of P2X7 protein in the nervous system . . . . .	64
3.2.1.	Central nervous system . . . . .	64
3.2.2.	Peripheral nervous system . . . . .	69
3.3.	Interaction and interrelation of P2X4 and P2X7 subunits . . . . .	71
3.3.1.	Localization of P2X4 and P2X7 subunits . . . . .	71
3.3.2.	Mutual interrelation . . . . .	75
3.3.3.	Physical interaction . . . . .	77
3.4.	Identification of novel interaction partners of P2X7 . . . . .	78
3.4.1.	Co-immunoprecipitation experiments . . . . .	78
3.4.2.	Protein cross-linking of membrane extracts . . . . .	79
3.4.3.	Optimization of the cross-linking protocol to allow <i>in-situ</i> cross-linking of lung tissue . . . . .	80
3.4.4.	Optimization of the purification protocol . . . . .	83
3.4.5.	Identification of novel interaction partners of P2X7 by <i>in-</i> <i>situ</i> cross-linking mass spectrometry . . . . .	86
3.4.6.	Validation of identified interaction partners . . . . .	91
3.4.7.	Identification of modified peptides and mapping of cross- linking sites . . . . .	94
<b>4.</b>	<b>Discussion</b>	<b>97</b>
4.1.	P2X7 mouse models . . . . .	97
4.2.	Validation of the P2X7-EGFP BAC transgenic mouse model . . . . .	99



## List of Abbreviations

- AA** amino acid  
**ACN** acetonitrile  
**ADAM17** disintegrin and metalloproteinase domain-containing protein 17  
**ADP** adenosine 5'-diphosphate  
**ALI** acute lung injury  
**AMP** adenosine 5'-monophosphate  
**ambic** ammonium bicarbonate  
**AQP5** aquaporin-5  
**ASC** apoptosis-associated speck-like protein containing a CARD  
**AT** alveolar type  
**ATP** adenosine 5'-triphosphate
- BAC** bacterial artificial chromosome  
**BALF** bronchoalveolar lavage fluid  
**BSA** bovine serum albumin  
**bp** base pairs  
**BzATP** 3'-O-(4-Benzoyl)benzoyl-adenosine 5'-triphosphate
- cAMP** cyclic adenosine monophosphate  
**CARD** caspase activation and recruitment domain  
**CASK** calcium/calmodulin-dependent serine protein kinase  
**CCR2** C-C chemokine receptor type 2  
**CD** cluster of differentiation  
**cDNA** complementary DNA  
**CNS** central nervous system  
**COPD** chronic obstructive pulmonary disease  
**CRH** corticotropin-releasing hormone  
**cRNA** complementary RNA

<b>DAMP</b>	danger/damage associated molecular pattern
<b>DAPI</b>	4',6-diamidino-2-phenylindole
<b>DMEM</b>	Dulbecco's modified Eagle's medium
<b>DMSO</b>	dimethyl sulfoxide
<b>DNA</b>	deoxyribonucleic acid
<b>DRG</b>	dorsal root ganglion
<b>DSS</b>	disuccinimidyl suberate
<b>DTT</b>	dithiothreitol
<b>E-cadherin</b>	epithelial cadherin
<b>EDTA</b>	ethylenediaminetetraacetic acid
<b>EE</b>	early endosome
<b>EGFP</b>	enhanced green fluorescent protein
<b>Endo H</b>	endoglycosidase H
<b>ER</b>	endoplasmic reticulum
<b>FA</b>	formic acid
<b>FACE</b>	fusion-activated Ca <sup>2+</sup> entry
<b>FACS</b>	fluorescence-activated cell sorting
<b>FBS</b>	fetal bovine serum
<b>FDR</b>	false discovery rate
<b>FISH</b>	fluorescence <i>in situ</i> hybridization
<b>FRET</b>	Förster resonance energy transfer
<b>GFAP</b>	glial fibrillary acidic protein
<b>GFP</b>	green fluorescent protein
<b>GRK</b>	G-protein-coupled receptor kinase
<b>GS</b>	glutamine synthetase
<b>GTP</b>	guanosine 5'-triphosphate
<b>HBSS</b>	Hanks' balanced salt solution
<b>HCD</b>	higher-energy collision-induced dissociation
<b>HEK</b>	human embryonic kidney
<b>HPLC</b>	high performance liquid chromatography
<b>hrs</b>	hours
<b>HSP</b>	heat shock protein

- Iba1** ionized calcium-binding adapter molecule 1  
**ICAM-1** intercellular adhesion molecule 1  
**IL** interleukin
- JAM** junctional adhesion molecule
- kb** kilobases  
**kDa** kilodalton
- LAMP-1** lysosome-associated membrane glycoprotein 1  
**LB** lysogeny broth  
**LC-MS/MS** liquid chromatography tandem mass spectrometry  
**LPS** lipopolysaccharide
- MCAM** cell surface glycoprotein MUC18  
**min** minutes  
**MHC** major histocompatibility complex  
**MPZ** myelin protein zero  
**mRNA** messenger RNA  
**MS** mass spectrometry  
**MyD88** myeloid differentiation primary response 88
- NAC** N-acetylcysteine  
**NEK** NIMA-related kinase  
**NF-kappaB** nuclear factor 'kappa-light-chain-enhancer' of activated B-cells  
**NHS** N-hydroxysuccinimide  
**Ni-NTA** nickel nitrilotriacetic acid  
**NIMA** never in mitosis gene a  
**NLR** NOD-like receptor  
**NLRP** NOD-like receptor pyrin domain-containing  
**NMDG** N-methyl-D-glucamine  
**NMR** nuclear magnetic resonance  
**NOD** nucleotide-binding oligomerization domain  
**nPAGE** native polyacrylamide gel electrophoresis  
**NRK** normal rat kidney

- p120** p120 catenin  
**PAGE** polyacrylamide gel electrophoresis  
**PAMP** pathogen-associated molecular pattern  
**PB** sodium phosphate buffer  
**PBS** phosphate-buffered saline  
**PCR** polymerase chain reaction  
**PFA** paraformaldehyde  
**PECAM-1** platelet endothelial cell adhesion molecule 1  
**PLA** proximity ligation assay  
**PLVAP** plasmalemma vesicle-associated protein  
**PMP** peripheral myelin protein  
**PPIA** peptidylprolyl isomerase A  
**ppm** parts per million  
**PS** phosphatidylserine  
**PVDF** polyvinylidene difluoride
- qRT-PCR** real-time quantitative reverse transcription PCR
- ROS** reactive oxygen species  
**RNA** ribonucleic acid  
**RPLP0** ribosomal protein lateral stalk subunit P0  
**rpm** revolutions per minute  
**RT** room temperature
- SD** standard deviation  
**SDS-PAGE** sodium dodecylsulfate polyacrylamide gel electrophoresis  
**sec** seconds  
**SEM** standard error of the mean  
**shRNA** short hairpin RNA  
**SOC** super optimal broth with catabolite repression  
**SNAP** synaptosomal-associated protein  
**SNARE** soluble N-ethylmaleimide-sensitive-factor attachment receptor  
**SNP** single nucleotide polymorphism

- TAE** tris-acetate-EDTA  
**TMEM** transmembrane protein  
**TFA** trifluoroacetic acid  
**tg** transgenic  
**TH** tyrosine hydroxylase  
**TLR** toll-like receptor  
**TBS** tris-buffered saline
- UDP** uridine 5'-diphosphate  
**UTP** uridine 5'-triphosphate
- VAMP** vesicle associated membrane protein  
**VE-cadherin** vascular endothelial-cadherin  
**VCAM-1** vascular cell adhesion protein 1
- wt** wild type
- XL-MS** cross-linking mass spectrometry

# 1. Introduction

## 1.1. Purinergic signaling

Adenosine 5'-triphosphate (ATP) is commonly known as the universal currency of energy of living cells. The resulting free energy of the exergonic cleavage of ATP can be used in metabolic processes. Cell movement and muscle contraction carried out by the molecular motor proteins actin and myosin are the best-known mechanisms for the consumption of ATP. ATP serves also as a precursor for DNA and RNA synthesis. Since its discovery in 1929, ATP attracted the attention of researchers due to its role as a signaling molecule. ATP serves as a substrate for kinases to phosphorylate proteins, which subsequently leads to the activation of signaling cascades. In addition, ATP is the precursor of the well-known second messenger molecule cyclic adenosine monophosphate (cAMP). Furthermore, extracellular ATP, for example released following cell injury or as a neurotransmitter, can get metabolized by ectoATPases to generate adenosine 5'-diphosphate (ADP), adenosine 5'-monophosphate (AMP), and finally adenosine. ATP itself and all breakdown products can directly act on cells as agonists of purinergic receptors, which were proposed by Geoffrey Burnstock in 1972 [Burnstock, 1972]. Purinergic receptors, also known as purinoceptors, are ligand-gated transmembrane proteins and are widely expressed in all tissues. They comprise two families of receptors, which were introduced by Burnstock in 1978 (Figure 1) [Burnstock, 2012]. The P2 subgroup are nucleotide-sensitive receptors, whereas P1 receptors are gated by the breakdown product adenosine. The P2 receptors are subdivided into P2Y and P2X receptors based on differences in their structure and the cellular response upon their activation. Activation of the G protein-coupled metabotropic P2Y receptors sets off an intracellular signaling cascade that can regulate many different cellular processes. In contrast, the ionotropic P2X receptors open a channel which allows cations to enter the cell. This in turn leads to membrane depolarization and the activation of further signaling events, which can alter gene activation or influence the release of transmitters. Although the P2 receptors are commonly

referred to as ATP receptors, they have a mixed selectivity for nucleotides. In addition to ATP, the native nucleotides ADP, uridine 5'-triphosphate (UTP), uridine 5'-diphosphate (UDP) and UDP-glucose can also act on the P2Y receptors. P2Y11 is the only subunit where ATP serves exclusively as an endogenous agonist. On P2X receptors, in contrast, other native nucleotides, except ATP, are inactive [Jacobson and Müller, 2016].

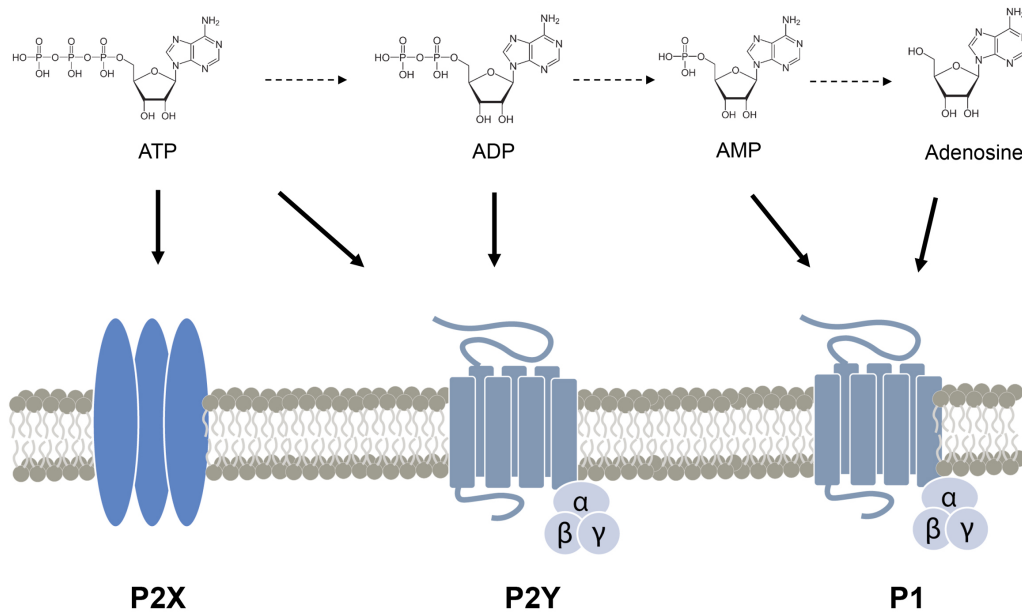


Figure 1 – **Different classes of purinergic receptors:** P2X receptors are ionotropic non-selective cation channels, whereas P2Y and P1 receptors are metabotropic G protein-coupled receptors. ATP can act on P2X as well as P2Y receptors. A second activator of P2Y receptors is the breakdown product ADP. P1 receptors are activated by AMP or adenosine, but not by ATP and ADP.

## 1.2. P2X receptors

P2X receptors are trimeric ligand-gated, non-selective cation channels with a high permeability for  $\text{Ca}^{2+}$ . The first P2X receptor genes were identified in 1994 and so far seven mammalian P2X subtypes are known and have been cloned [Brake et al., 1994], [North, 2002], [Valera et al., 1994]. The P2X6 receptor represents the smallest member of the P2X receptor family comprising 379 amino acids (AAs), whereas P2X7 is the largest subtype consisting of 595 AAs. All

subtypes share a common conserved structure with a relatively short intracellular N-terminus, two  $\alpha$ -helical hydrophobic transmembrane domains, a large ectodomain, and an intracellular C-terminus that varies in length among the subtypes (Figure 2 A). The ectodomain comprises the ATP binding site, glycosylation sites, and ten conserved cysteine residues that form disulfide bonds [North, 2002]. Twenty-two residues in the ectodomain are highly conserved in organisms which are distantly related through phylogeny and form most likely the ATP binding sites [Browne et al., 2010]. The C-terminus is the most diverse part of the P2X family and varies greatly in length between the subtypes from 28 (P2X6) to 240 (P2X7) AAs. It is therefore thought to be related to subtype specific properties. The first crystal structure of a P2X receptor was obtained from a truncated zebrafish P2X4 in its closed state and revealed the folding of each subunit [Kawate et al., 2009]. The overall structure of the P2X monomer is often described as a dolphin-like shape (Figure 2 B). The  $\beta$ -sheets formed by the highly conserved residues of the extracellular domain represent the body of the dolphin. The more flexible parts of the extracellular domain constitute the head, fin and flippers, while the  $\alpha$ -helical transmembrane domains make up the tail of the dolphin. The crystal structure also resolved the global architecture, since it confirmed the trimeric structure which was first proposed by Nicke et al. [Nicke et al., 1998]. Three P2X subunits are necessary to form the functional trimeric ion channel, either in form of a homomer or a heteromer with other subunits (Figure 2 C). All P2X subtypes but P2X6 can assemble as a homomer and form a functional channel on their own [Torres et al., 1999]. In an initial interaction study, a possible heteromerization of each P2X subunit was shown, but the co-assembly of P2X7 with one of the other subtypes was excluded [Torres et al., 1999]. A variety of possible P2X heteromers are characterized, but the precise stoichiometry of the subunit assembly is only known for a few of them and the appearance of most heteromers in native tissue is poorly described [Saul et al., 2013]. In total three ATP molecules can bind to the P2X receptor at the interface of the subunits and at least two ATP molecules are necessary for its activation and the opening of the ion channel (Figure 3 C, right side) [Stelmashenko et al., 2012], [Wilkinson et al., 2006].

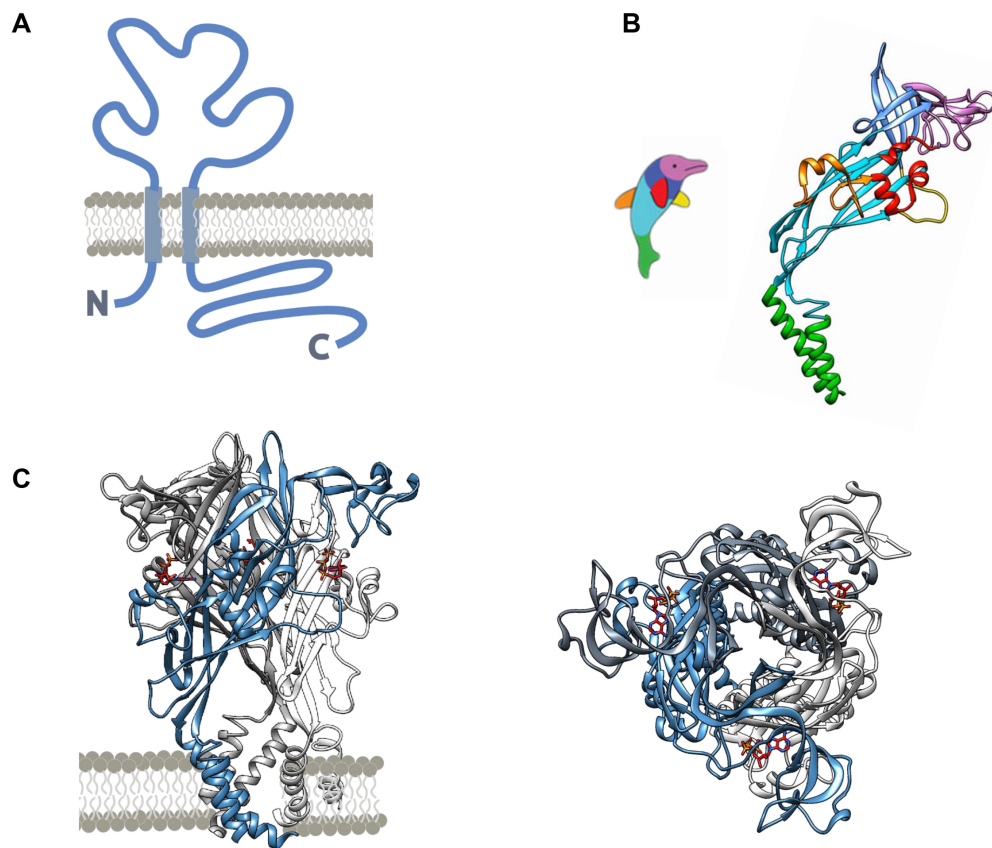


Figure 2 – **Structure of P2X receptors:** (A) Schematic illustration of one P2X subunit consisting of a short intracellular N-terminus, two transmembrane domains, a large ectodomain and a cytoplasmic C-terminal tail, which varies in length between subtypes. (B) The structure of the P2X monomer is commonly described as a dolphine-like shape. The transmembrane domains form the tail of the dolphine. The highly conserved beta sheets in the ectodomain form the body and the more flexible parts represent the flippers, fin and head of the dolphine. (C) P2X receptors assemble as homo- or heterotrimers to form a functional channel. Binding of ATP opens the non-selective cation channel. Crystal structure of truncated P2X4 in ATP-bound, open state (PDB ID: 4dw1) was visualized using UCSF Chimera v1.13.1. ATP is shown in red. Dolphine illustration was taken from [Jiang et al., 2013].

## 1.3. The P2X7 receptor

### 1.3.1. Properties

The P2X7 protein is encoded by the *P2rx7* gene, located on the human chromosome 12q24.31. The encoded receptor differs from all other P2X subunits due to several unique properties: P2X7 is the largest member of the P2X family with an intracellular C-terminal domain consisting of 240 AAs that is significantly longer than any other P2X subunit. In addition, P2X7 seems to be the only subunit that assembles exclusively in form of homotrimers and shows no heterotrimeric assembly [Antonio et al., 2011], [Nicke, 2008], [Torres et al., 1999]. A functional interaction with the P2X4 subtype is still a controversial issue and discussed in more detail in section 1.3.4.9. The affinity for ATP is up to 100-fold lower compared to the other subtypes and it is preferentially activated by 3'-O-(4-Benzoyl)benzoyl adenosine 5'-triphosphate (BzATP). It is speculated that the missing residue, corresponding to Leu217 of P2X4, is responsible for this unique pharmacological property [Jiang et al., 2013]. The binding of the agonist opens the channel within milliseconds, which leads to a cationic inward current. In contrast to the other family members, the P2X7 subtype is able to open a large non-selective pore, which allows permeation of molecules up to 900 Da. This pore formation can be analyzed by uptake of N-methyl-D-glucamine (NMDG)<sup>+</sup>, Yo-Pro-1, or ethidium bromide. It was discussed that recruitment of an accessory protein is necessary to allow the formation of the pore and Pannexin-1 was identified as candidate to fulfill this effect [Pelegriin and Surprenant, 2006]. However, recent studies showed that the uptake of large dyes is an intrinsic property of P2X7 and does not require accessory proteins [Karasawa et al., 2017], [Pippel et al., 2017]. For a more detailed view regarding the potential interaction with Pannexin-1 and the pore-formation refer to section 1.3.4.2 and the recent review by Di Virgilio et al. [Di Virgilio et al., 2018].

### 1.3.2. Protein localization

The P2X7 subtype is expressed in a variety of cell types. The most prominent expression is found in immune cells. However, P2X7 is also found in

other cells, like smooth muscle cells, ventricle myocytes, keratinocytes, microvascular endothelial cells, fibroblasts, epithelial cells, glial cells, and erythrocytes among others [Barth and Kasper, 2009],[Burnstock and Knight, 2004], [Burnstock, 2014]. In the brain, it was originally thought that the expression of P2X7 is limited to microglial cells [Collo et al., 1997], but in subsequent studies P2X7 expression was also detected in neuroglial cells and neurons [Sperlágh and Illes, 2014]. The presence of P2X7 in neurons has a wide acceptance among researchers, but is also a matter of ongoing debate [Illes et al., 2017], [Kaczmarek-Hajek et al., 2018], [Miras-Portugal et al., 2017]. Several functional studies argue for the expression of P2X7 in neurons, which has recently been reviewed by Miras-Portugal et al. and Sperlágh et al. [Miras-Portugal et al., 2017], [Sperlágh and Illes, 2014]. P2X7 mRNA was indeed detected in neurons and P2X7 protein was found in neuronal cell culture and neuronal tissues [Ohishi et al., 2016], [Yu et al., 2008]. However, the major drawback in the analysis of protein expression is the lack of specific P2X7 antibodies. As a consequence, P2X7 localization determined in a large part of studies is questionable [Anderson and Nedergaard, 2006], [Jager and Vaegter, 2016], [Sim et al., 2004].

### 1.3.3. Signaling

Due to the high ATP concentration which is needed to activate the receptor, P2X7 should be silent under most physiological conditions and only active under pathological conditions, e.g. when ATP gets massively released from injured or dying cells. The best described function of P2X7 is the release of the proinflammatory cytokine interleukin (IL)-1 $\beta$ , for example after activation of the innate immune system due to injuries or infections (Figure 3). Toll-like receptors (TLRs) on immune cells recognize pathogen-associated molecular patterns (PAMPs) from invading microorganisms, which leads to the synthesis of pro-IL-1 $\beta$ . This invasion also leads to the release of danger/damage associated molecular patterns (DAMPs) from surrounding cells [Vénéreau et al., 2015]. One of these DAMPs is extracellular ATP, which acts on P2X7 leading to the activation of the NOD-like receptor pyrin domain-containing (NLRP)-3 inflammasome and subsequent release of mature IL-1 $\beta$  [Ferrari et al., 1997]. The NLRP3 inflammasome consists of a NOD-like receptor (NLR) subunit, an adaptor molecule named apoptosis-associated speck-like protein containing a CARD (ASC), and

the cysteine protease (pro-)caspase-1. Caspase-1 is responsible for the conversion of the inactive precursor of IL-1 $\beta$  to the active inflammatory cytokine. The dependency on P2X7 was shown in macrophages from *P2rx7*<sup>-/-</sup> mice, which were not able to produce and secrete the mature form of IL-1 $\beta$  in response to ATP [Solle et al., 2001]. The exact mechanism of NLRP3 inflammasome activation is still unclear, but a common step of different NLRP3 activators is the decrease in intracellular K<sup>+</sup> concentration [Muñoz-Planillo et al., 2013]. How each of these activators leads to a drop in K<sup>+</sup> is still obscure, but the current understanding is that extracellular ATP acting on P2X7 allows the efflux of cytosolic K<sup>+</sup> balanced by Na<sup>+</sup> and Ca<sup>2+</sup> influx, which leads to the activation of the inflammasome [Giuliani et al., 2017]. Downstream of the potassium efflux, NIMA-related kinase (NEK) 7 was recently identified as an additional component of the inflammasome complex that regulates NLRP3 oligomerization and activation [He et al., 2016]. It has also been shown that P2X7 directly interacts with the NLR subunits and the adaptor protein ASC of the inflammasome [Franceschini et al., 2015], [Minkiewicz et al., 2013], [Silverman et al., 2009]. This is described in more detail in section 1.3.4.7. Since IL-1 $\beta$  does not follow the endoplasmic reticulum (ER)-Golgi route for secretion, several different release mechanisms have been suggested in which P2X7 might play a pivotal role [Di Virgilio et al., 2017]. The secretion mechanism might be dependent upon the strength of the inflammatory stimulus and might escalate from lysosomal exocytosis, microvesicle shedding, and exosomal release to a terminal, pro-inflammatory form of cell death called pyroptosis [Lopez-Castejon and Brough, 2011]. Recently two independent research groups identified gasdermin D as the key substrate for the inflammatory caspases, which upon its cleavage leads to pyroptosis [Kayagaki et al., 2015], [Shi et al., 2015]. In addition to the release of IL-1 $\beta$ , P2X7 activation is also associated with secretion of other cytokines, like IL-1 $\alpha$  [Dagvadorj et al., 2015], [Pelegriin et al., 2008], IL-1RA [Wilson et al., 2004], IL-6 [Shieh et al., 2014], IL-18 [Mehta et al., 2001], and IL-36 $\alpha$  [Martin et al., 2009]. Other known P2X7-dependent signaling pathways involve membrane-related changes (e.g. actin-tubulin rearrangements, phosphatidylserine (PS) translocation, membrane blebbing), the formation of reactive oxygen species (ROS), prostaglandin release, glutamate efflux, activation of transcription factors, cell proliferation, and phagocytosis. For further details the reader is referred to recent publications reviewing P2X7 signaling and its role in inflammation [Bartlett et al., 2014], [Di Virgilio et al., 2017].

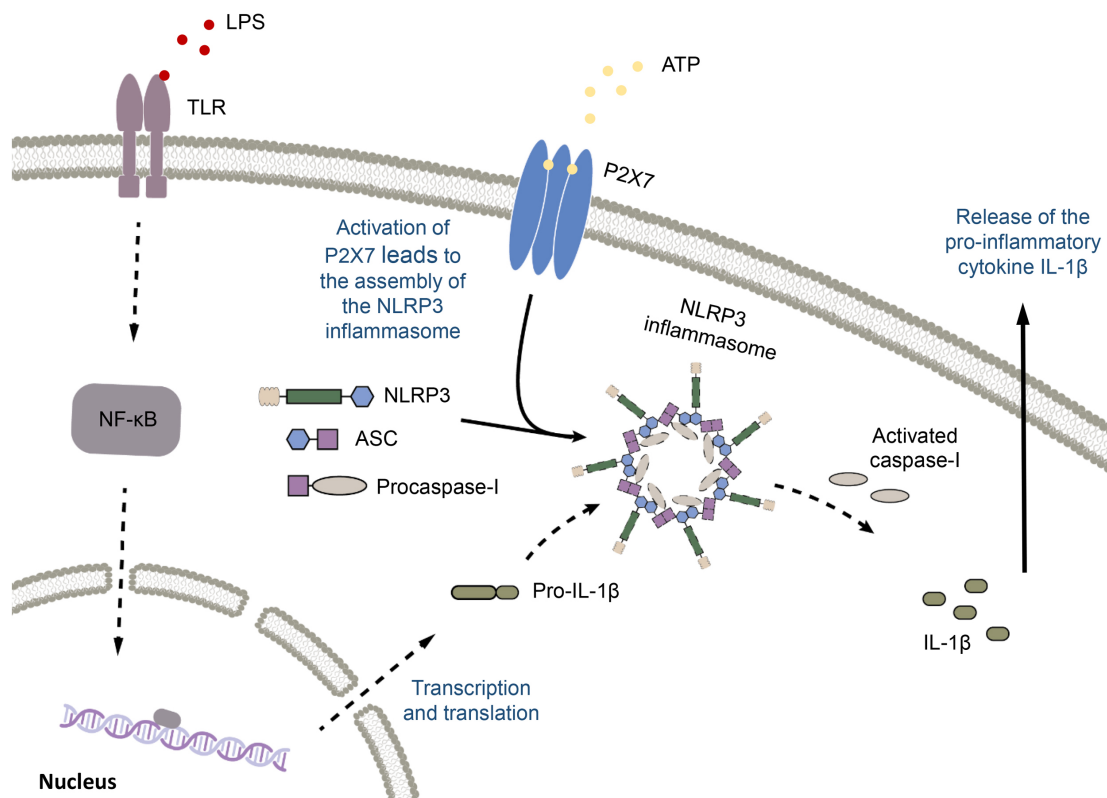


Figure 3 – **Role of P2X7 in the maturation and release of the pro-inflammatory cytokine IL-1 $\beta$ :** Toll-like receptors (TLRs) recognize PAMPs like lipopolysaccharide (LPS) which results in the activation of NF- $\kappa$ B and a subsequent transcription and translation of the IL-1 $\beta$  gene. Extracellular ATP acts on the P2X7 receptor and triggers the assembly and activation of the NLRP3-inflammasome via efflux of K<sup>+</sup>. The activated form of the inflammasome allows maturation of IL-1 $\beta$  via caspase-1. The pro-inflammatory cytokine is then released via secretory lysosomes, plasma membrane microvesicles, exosomes, or pyroptosis.

### 1.3.4. Interaction partners

In recent years over 50 different proteins have been identified to physically interact with the P2X7 receptor (table 16). The majority of the interacting proteins are collected on a P2X7 interactome database together with the most relevant information about the nature of their interaction and the respective references (<http://www.p2x7.co.uk>). Different screening approaches like immunoprecipitation followed by mass-spectrometry analysis [Gu et al., 2009], [Kim et al., 2001], [Li et al., 2017], yeast two-hybrid [Wang et al., 2011], [Wilson et al., 2002] and peptide array [Wu et al., 2007] were used to identify novel interacting proteins. In addition, several speculated candidates for a possible physical interaction were analyzed using immunoprecipitation followed by immunoblotting (table 16). For the majority of these proteins, the interaction domains and the physiological consequences of this interaction are only poorly described. One should also bear in mind that some of the proteins are frequently found as contaminants in approaches that rely on affinity purification coupled with mass spectrometry (MS), since they tend to interact with the solid-phase support or the affinity tag instead of the actual bait protein (marked with asterisks in table 16) [Mellacheruvu et al., 2013]. Furthermore, a majority of the data originate from heterologous expression systems in which P2X7 is not naturally occurring (e.g. human embryonic kidney (HEK) 293 cells). However, some of the identified proteins were studied in more detail and selected proteins are briefly described in the following sections.

Protein name	Method	Cell sytem	Reference
Actin, cytoplasmic 1 (Beta-actin)*	IP-MS/WB	HEK293, THP-1	[Kim et al., 2001], [Gu et al., 2009]
Alpha-actinin 4*	IP-MS/WB	HEK293	[Kim et al., 2001]
Alpha-synuclein	IP-WB	BV2	[Jiang et al., 2015]
Anoctamin-6	IP-WB	HEK293	[Ousingsawat et al., 2015]
ASC	IP-WB	Primary neurons, astrocytes	[Silverman et al., 2009], [Minkiewicz et al., 2013]
Beta-adrenergic receptor kinase 2	IP-WB	CaSKI, HEK293	[Feng et al., 2005]
Beta-arrestin 2	IP-WB	CaSKI, HEK293	[Feng et al., 2005]
Biglycan	IP-WB	Peritoneal macrophages	[Babelova et al., 2009]
Calmodulin*	IP-WB	HEK293	[Roger et al., 2008], [Roger et al., 2010]
CASK	Y2H		[Wang et al., 2011]
Caveolin-1	PD/IP-WB nPAGE	E10, HL-1	[Barth et al., 2008], [Weinhold et al., 2010], [Pfleger et al., 2012]
Caveolin-3	nPAGE	HL-1	[Pfleger et al., 2012]
CD14	IP-WB	HEK293	[Dagvadorj et al., 2015]
CD44	IP-WB	CHO-K1	[Moura et al., 2015]

Clathrin	IP-WB	CaSKI, HEK293	[Feng et al., 2005]
Cytoplasmic FMR1-interacting protein	IP-MS	Prefrontal cortex (mouse)	[Li et al., 2017]
Cytoplasmic protein NCK1	Peptide array		[Wu et al., 2007]
Dynamin-1	IP-WB	CaSKI, HEK293	[Feng et al., 2005]
E3 ubiquitin-protein ligase TRIM21*	IP-MS	THP-1, HEK293	[Gu et al., 2009]
Ephrin-B3	Y2H		[Wang et al., 2011]
Epithelial membrane protein 1/2/3	Y2H, PD/IP-WB	HEK293	[Wilson et al., 2002]
Growth factor receptor-bound protein 2	Peptide array		[Wu et al., 2007]
Heat shock 70 kDa protein 1A/1B*	IP-MS/WB	HEK293	[Kim et al., 2001], [Gu et al., 2009]
Heat shock cognate 71 kDa protein*	IP-MS/WB	HEK293	[Kim et al., 2001]
Heat shock protein HSP 90-beta*	IP-MS/WB	HEK293, peritoneal macrophages, PC12	[Kim et al., 2001], [Adinolfi et al., 2003], [Gu et al., 2009], [Franco et al., 2013]
Integrin $\beta$ -2	IP-MS/WB	HEK293	[Kim et al., 2001]
IP6 kinase	IP-MS	THP-1	[Gu et al., 2009]
Laminin subunit alpha-3	IP-MS/WB	HEK293	[Kim et al., 2001]
MAGUK p55 subfamily member 3	IP-MS/WB	HEK293	[Kim et al., 2001]
MyD88	IP-WB	HEK293	[Liu et al., 2011]
Myosin-9*	IP-MS/WB	THP-1	[Gu et al., 2009]
Myosin regulatory light chain 12A/B*	IP-MS	THP-1	[Gu et al., 2009]
Neutrophil defensin 1	PD-WB	HEK293	[Chen et al., 2014]
Nitric oxide synthase, brain	IP-WB	Brain	[Pereira et al., 2013]
NLRP 2	IP-WB	Astrocytes	[Minkiewicz et al., 2013]
NLRP 3	IP-WB	N13 microglia	[Franceschini et al., 2015]
Nucleoprotein TPR	IP-MS	HEK293	[Gu et al., 2009]
Nucleoside diphosphate kinase B	IP-MS	HEK293	[Gu et al., 2009]
P2X4 receptor	PD/IP-WB nPAGE	HEK293, BMDM, E10, tsA 201, primary gingival epithelial cells	[Guo et al., 2007], [Boumechache et al., 2009], [Weinhold et al., 2010], [Antonio et al., 2011], [Hung et al., 2013], [Pérez-Flores et al., 2015]
Pannexin-1	PD/IP-WB	HEK293, J774 cells, primary neurons, N2a cells, HPDL cells	[Pelegri and Surprenant, 2006], [Iglesias et al., 2008], [Silverman et al., 2009], [Li et al., 2011], [Poornima et al., 2012], [Kanjanamekanant et al., 2014], [Boyce and Swayne, 2017]
Phosphatidylinositol 4-kinase $\alpha$	IP-MS/WB	HEK293	[Kim et al., 2001]
PMP-22	Y2H, PD/IP-WB	HEK293	[Wilson et al., 2002]
Protein kinase C $\gamma$ type	IP-WB	RBA-2	[Hung et al., 2005]
Protein-tyrosine phosphatase 1C	IP-MS	THP-1	[Gu et al., 2009]
Protein-tyrosine phosphatase $\beta$	IP-MS	HEK293	[Kim et al., 2001]
Supervillin	IP-MS/WB	HEK293	[Kim et al., 2001]

TLR 2/4	IP-WB	Peritoneal macrophages	[Babelova et al., 2009]
Transmembrane 9 superfamily member 1	Y2H		[Wang et al., 2011]
Tubulin $\beta$ chain*	IP-MS	HEK293	[Gu et al., 2009]
Tyrosine-protein kinase ABL1	Peptide array		[Wu et al., 2007]
Tyrosine-protein kinase Fyn	IP-WB	OPC (rat)	[Feng et al., 2015]
Unconventional myosin-Va	IP-MS/WB	HEK293	[Gu et al., 2009]

Table 2 – Identified interaction partners of P2X7. Data taken and adapted from <http://www.p2x7.co.uk> (12/2018). Asterisks indicate proteins that are frequently found as contaminants in MS-based approaches [Mellacheruvu et al., 2013]. PD = pull down, IP = immunoprecipitation, WB = western blot, MS = mass spectrometry, nPAGE = native PAGE, Y2H = yeast two-hybrid.

### 1.3.4.1. Heat shock protein HSP 90

In two independent mass spectrometry-based screening approaches heat shock protein (HSP) 90 was identified to physically interact with the P2X7 receptor in HEK293 cells [Gu et al., 2009], [Kim et al., 2001]. As part of a proposed P2X7 signaling complex, HSP90 was subsequently shown to be tyrosin phosphorylated in HEK293 cells and rat peritoneal macrophages [Adinolfi et al., 2003]. An increase in phosphorylation was associated with decreased currents and membrane blebbing, which exposes phosphorylated HSP90 as a negative regulator of P2X7 receptor function [Adinolfi et al., 2003]. Nitration of HSP90, in contrast, leads to apoptosis mediated by P2X7-dependent activation of the Fas pathway in PC12 cells. The nitrated protein may either activate the receptor or fail to repress receptor function [Franco et al., 2013]. In a more recent study with HEK293 cells, it was proposed that HSP90 regulates P2X7 function and facilitates currents by interacting with the cysteine-rich domain in the C-terminus [Migita et al., 2016]. In muscle cells, HSP90 is required for P2X7 pore formation and involved in P2X7-dependent autophagic death of dystrophic muscles [Young et al., 2015] and in a mouse model of subarachnoid hemorrhage it was shown that HSP90 mediates inflammation via the P2X7/NLRP3 inflammasome pathway [Zuo et al., 2018].

#### 1.3.4.2. Pannexin-1

Pannexin-1 belongs to the pannexin family of channel-forming glycoproteins and has been reported to mediate the release of ATP [Chekeni et al., 2010]. In several co-precipitation experiments it could be shown that pannexin-1 physically interacts with the P2X7 receptor [Boyce and Swayne, 2017], [Iglesias et al., 2008], [Kanjanamekanant et al., 2014], [Li et al., 2011], [Pelegriin and Surprenant, 2006], [Poornima et al., 2012], [Silverman et al., 2009]. Pannexin-1 was initially thought to be recruited as an accessory protein for the formation of the P2X7 macropore and also to be involved in inflammasome activation and P2X7-mediated cell death [Hung et al., 2013], [Iglesias et al., 2008], [Locovei et al., 2007], [Pelegriin and Surprenant, 2006]. However, this mechanism is controversial and more recent studies could show that Pannexin-1 is not essential for P2X7 pore-formation, caspase-1 activation, secretion of the pro-inflammatory cytokines IL-1 $\beta$  and IL-18, and the ATP-induced cell death [Alberto et al., 2013], [Hanley et al., 2012], [Qu et al., 2011]. The uptake of large molecular dyes is rather an intrinsic property of P2X7 that does not require progressive channel-to-pore transition or an accessory pore-forming protein and has recently been reviewed by Di Virgilio et al. [Di Virgilio et al., 2018], [Harkat et al., 2017], [Karasawa et al., 2017], [Pippel et al., 2017]. However, there is evidence for a functional crosstalk of both proteins. Pannexin-1 serves as an ATP release channel and might potentiate P2X7 signaling [Chekeni et al., 2010], [Isakson and Thompson, 2014]. On the other hand, extracellular ATP can inhibit pannexin-1 channels and stimulate pannexin-1 internalization via P2X7 activation in a clathrin-independent manner [Boyce et al., 2015], [Boyce and Swayne, 2017], [Qiu and Dahl, 2008].

#### 1.3.4.3. Calmodulin

A novel calmodulin binding motif was identified in the C-terminus of rat P2X7. The specific binding of calmodulin to this region could be shown by co-immunoprecipitation and mutagenesis in HEK293 cells [Roger et al., 2008]. Interestingly, this binding motif is absent in human and mouse P2X7. Indeed, an interaction of calmodulin with the human receptor could not be detected in HEK293 cells [Roger et al., 2010]. The binding of calmodulin facilitates and pro-

longs calcium entry and is proposed to play a role in cytoskeletal rearrangements and membrane blebbing [Roger et al., 2008].

#### **1.3.4.4. Caveolins**

In the mouse alveolar epithelial cell line E10, P2X7 was found in association with lipid rafts, where caveolin-1 is highly expressed [Barth et al., 2007]. Immunostainings of both proteins in E10 cells indicated a partial co-localization and the physical interaction of both proteins was shown in a subsequent study via co-precipitation [Barth et al., 2007], [Barth et al., 2008]. Using nPAGE, P2X7 was found in the same protein complex with caveolin-1 in E10 lung alveolar epithelial cells and mouse atrium cells, where caveolin-3 was also detected [Weinhold et al., 2010], [Pfleger et al., 2012]. Interestingly, knockout or short hairpin RNA (shRNA)-mediated downregulation of caveolin-1 significantly reduced P2X7 protein expression and also affected its subcellular localization in E10 cells [Barth et al., 2007]. Respectively, also the expression and localization of caveolin-1 was influenced by shRNA-mediated P2X7 knockdown [Weinhold et al., 2010]. The exact physiological function of this interaction is so far not completely understood, but it is assumed that the association with lipid rafts might contribute to the targeting of the receptor to the plasma membrane, caveolae-mediated internalization and functional regulation of P2X7 channel activity [Barth and Kasper, 2009].

#### **1.3.4.5. Myosin-9**

The non-muscle myosin-9 was not only shown to co-precipitate with P2X7, but also to co-localize in the plasma membrane and membranes of intracellular organelles in a human monocytic cell line (THP-1 cells). The close association was confirmed by Förster resonance energy transfer (FRET) experiments in HEK293 cells [Gu et al., 2009]. It was proposed that P2X7 is anchored in the membrane by myosin-9 and that activation of P2X7 via extracellular ATP leads to dissociation of the myosin-P2X7 complex and the formation of the large pore and membrane blebbing. The integrity of this complex was proposed to be required to regulate P2X7-mediated phagocytosis [Gu et al., 2010].

#### 1.3.4.6. Proteins involved in P2X7 receptor internalization

Other studies showed evidence for the direct interaction of proteins involved in P2X7 receptor internalization, degradation, and recycling. Feng et al. described a pathway in which activation of P2X7 leads to its phosphorylation via G-protein-coupled receptor kinase (GRK) 3 followed by  $\beta$ -arrestin-2-mediated internalization into clathrin-coated endosomes, which is regulated by the GTPase dynamin. Via co-immunoprecipitation in CaSki and HEK293 cells, all of these proteins were shown to directly interact with the P2X7 receptor [Feng et al., 2005].

#### 1.3.4.7. Proteins involved in P2X7-mediated interleukin secretion

Bacterial LPS is a commonly known PAMP that activates innate immune responses. LPS is usually recognized by TLR4. However, also P2X7 harbors a potential LPS binding motif in its intracellular C-terminal domain [Denlinger et al., 2001]. Therefore, binding of LPS to this domain might require internalization. In a recent study, CD14 was identified as a possible co-receptor of P2X7 in the lung that allows internalization and binding of LPS to P2X7 [Dagvadorj et al., 2015]. This study showed that both proteins physically interact in transfected HEK293 cells, whereby LPS stimulation increased the amount of co-precipitated CD14 or P2X7 protein. The authors proposed that a possible outcome of the interaction upon LPS activation is necrosis of alveolar macrophages and the release of pro-IL-1 $\alpha$ . This may induce tight junction opening of endothelial cells via IL-1 receptor and myeloid differentiation primary response 88 (MyD88) signaling to allow neutrophils to infiltrate the lungs. This might represent the basic mechanism of early inflammation in LPS-induced acute lung injury (ALI) [Dagvadorj et al., 2015]. Interestingly, in HEK293 cells P2X7 was also shown to directly interact with MyD88 via its C-terminus to activate NF- $\kappa$ B [Liu et al., 2011].

The best-described role of P2X7 is the activation of the inflammasome and subsequent release of mature IL-1 $\beta$ . It is therefore not surprising that also proteins involved in this pathway were found to directly interact with P2X7. A physical interaction of P2X7 was detected with the NLR subunits and the adaptor molecule ASC of the inflammasome complex [Franceschini et al., 2015], [Minkiewicz et al., 2013], [Silverman et al., 2009]. The identity of the NLR family member varies across different cell types. The NLRP1 inflammasome is found in

neurons, where P2X7 could be co-immunoprecipitated using an anti-ASC antibody [Silverman et al., 2009]. Astrocytes express a NLRP2 inflammasome and P2X7 was co-precipitated from astrocyte lysates using an ASC, as well as a NLRP2 antibody [Minkiewicz et al., 2013]. Finally, P2X7 was also found to directly interact with the NLRP3 inflammasome via the NLRP3 scaffold protein in N13 mouse microglia [Franceschini et al., 2015]. In addition, a mutual relationship in messenger RNA (mRNA) and protein expression was detected and both proteins co-localize at discrete sites in the subplasmalemmal cytoplasm [Franceschini et al., 2015].

Binding of PAMPs to TLRs is one initial step that is required for this P2X7-mediated innate immune response, since it activates gene transcription of pro-IL-1 $\beta$ . However, there are also endogenous mechanisms that trigger inflammation in absence of infections. Biglycan, a proteoglycan of the extracellular matrix, can stimulate the expression of NLRP3 and pro-IL-1 $\beta$  mRNA and activate caspase-1, leading to the release of mature IL-1 $\beta$  [Babelova et al., 2009]. Via co-precipitation it was shown that biglycan directly interacts with the P2X4 and P2X7 receptors in peritoneal macrophages. Interestingly, in the presence of biglycan the TLRs 2 and 4 were co-immunoprecipitated using P2X4 or P2X7 antibodies, indicating that biglycan might serve as a linker between P2X receptors and TLRs [Babelova et al., 2009].

#### **1.3.4.8. Anoctamin channels**

Anoctamin channels are calcium-activated Cl<sup>-</sup> channels and are co-expressed with P2X7 in various cell types. Since a P2X7-mediated increase in anion conductance has been observed in different studies, researchers asked the question if P2X7 activation might lead to a subsequent activation of members of the transmembrane protein (TMEM) 16/anoctamin family, either functionally through an increase in cytosolic Ca<sup>2+</sup> or physically via a direct interaction [Stolz et al., 2015]. A functional interaction could be shown for anoctamin-1 in *X. laevis* and *A. mexicanum* oocytes, but not for anoctamin-6 [Stolz et al., 2015]. However, in the same year another group could show that stimulation of P2X7 activates anoctamin-6 in *X. laevis* oocytes, transfected HEK293 cells, and also in mouse macrophages [Ousingsawat et al., 2015]. In addition, P2X7 and anoctamin-6 were co-immunoprecipitated in HEK293 cells, overexpressing both proteins. The authors described a role of anoctamin-6 in several cellular responses downstream

of P2X7 like cell shrinkage, membrane blebbing, phospholipid scrambling and apoptosis.

#### **1.3.4.9. P2X4 receptor**

Within the P2X receptor family P2X4 shows the highest amino acid sequence similarity compared to P2X7 (59% coverly and 47% identity within the human proteins) and therefore represents the most closely related subtype. Furthermore, both genes are located in immediate proximity on the same chromosome and are thought to have originated from the same ancestral gene as a result of gene duplication [Hou and Cao, 2016]. The encoded proteins are co-expressed in various cell types, particularly in microglia [Xiang and Burnstock, 2005], macrophages [Bowler et al., 2003], [Guo et al., 2007] and epithelial cells [Ma et al., 2006]. Both receptors can also be linked to similar physiological and pathophysiological functions, especially in immune response and inflammatory processes. In the recent years, there was a number of studies arguing for and against a physical or tight functional interaction between both subtypes. However, the existence of a physical interaction is still not clear.

#### **Evidence for functional interaction**

In early studies, it was shown that epithelial ciliated cells have a combination of P2X4 and P2X7 electrophysiological properties and this raised the question if there might be a functional interaction [Ma et al., 2006]. This potential functional interaction was further described in patch-clamp recordings from HEK293 cells, where a formation of heterotrimeric complexes was suggested [Guo et al., 2007]. The influence of co-expression of P2X4 on P2X7 currents was also shown in another study with heterologously expressed receptors [Casas-Pruneda et al., 2009]. However, in a more recent study conducted in *X. laevis* oocytes, there was no evidence for a functional interaction [Schneider et al., 2017]. Conflicting results were also obtained in studies regarding the influence of the P2X4 subtype on the non-selective pore formation of P2X7. A decreasing and decelerating effect of P2X4 on ethidium bromide uptake was described in HEK293 cells and stands in contrast to other studies conducted in macrophages [Casas-Pruneda et al., 2009]. While P2X4 knock-down via shRNA in mouse macrophage RAW264.7 cells did not affect P2X7 pore formation, a complete knock-out of P2X4 led to a significantly

reduced YO-PRO-1 uptake in macrophages and argues for a positive effect of P2X4 on pore formation [Kawano et al., 2012b], [Pérez-Flores et al., 2015].

### **Mutual expression**

A mutual influence on mRNA and protein levels of both subtypes was also described in the literature. While mRNA levels were significantly reduced in kidneys via knockout of the respective other subunit, a downregulation via shRNA of one subtype resulted in an increase of protein level of the other in alveolar epithelial cells [Craigie et al., 2013], [Weinhold et al., 2010]. However, in other studies on immune cells a shRNA-mediated downregulation of P2X4 did not affect P2X7 protein expression [Kawano et al., 2012b], [Sakaki et al., 2013]. Interestingly, co-expression of P2X4 with P2X7 increased surface expression of P2X4 [Guo et al., 2007].

### **Signaling**

The mutual influence on protein expression, current kinetics, and pore formation might also influence cellular signaling, since both receptors are also involved in the same inflammatory signaling cascades. For example, both receptors are involved in ROS production and the secretion of mature IL-1 $\beta$  and IL-18 through the activation of the NLRP3 inflammasome [Babelova et al., 2009], [Hung et al., 2013], [Kawano et al., 2012a]. The expression of P2X4 does not affect pro-IL-1 $\beta$  synthesis but the maturation and release of the cytokine, which is mediated by P2X7 activation [Pérez-Flores et al., 2015]. A rapid initial P2X4-mediated Ca<sup>2+</sup> influx might be required to initiate this cascade [Sakaki et al., 2013]. Both receptors play also a role within the phagosome [Kuehnel et al., 2009], [Qureshi et al., 2007]. Especially for the P2X7-mediated autophagy a direct involvement of P2X4 was shown [Kawano et al., 2012a]. In addition, influence of P2X4 in P2X7 signaling was described for P2X7-mediated cell death of macrophages [Kawano et al., 2012b].

### **Localization**

Although both receptors are expressed in the same cell types and seem to be involved in the same signaling pathways, the two receptor subtypes show a distinctly different subcellular localization, which has been studied in various cell systems. In recombinant systems and also primary cells the P2X4

subtype was mostly found intracellularly, co-localizing with lysosomal markers [Bobanovic et al., 2002], [Guo et al., 2007], [Qureshi et al., 2007]. P2X4 signal was also detected in the early endosome (EE) of neurons heterologously expressing green fluorescent protein (GFP) tagged P2X4 [Bobanovic et al., 2002] but not in the EE of primary macrophages, microglia, or vascular endothelial cells [Qureshi et al., 2007]. P2X7, in contrast, is localized at the plasma membrane and only to some extent intracellularly. In transfected normal rat kidney (NRK) cells the intracellular P2X7 signal was overlapping with a marker for the ER [Guo et al., 2007]. The spatial proximity to each other is of special interest, since it forms the basis for a possible physical interaction. However, in co-transfected NRK cells only small parts of P2X4 and P2X7 signals were overlapping at the plasma membrane [Guo et al., 2007]. Nevertheless, overlapping signal was also seen in recombinant human kidney cells and the close proximity within the transfected cells was further confirmed via *in situ* proximity ligation assays [Antonio et al., 2011]. Due to lack of specific antibodies that allow co-immunostainings in native tissue, this could so far only been shown in recombinant systems with tagged proteins. FRET experiments with fluorophore-conjugated receptors in HEK293 cells and *X. laevis* oocytes also showed evidence for a tight spatial proximity, at least in over-expression systems [Pérez-Flores et al., 2015], [Schneider et al., 2017].

### **Evidence for physical interaction**

The physical interaction and the potential presence of both subtypes in the same protein complex was investigated by nPAGE, cross-linking, and co-precipitation experiments. In the first interaction studies on P2X subunits, a co-assembly of P2X7 with one of the other subtypes was excluded and also nPAGE data from different rat tissues argued against an interaction [Nicke, 2008], [Torres et al., 1999]. However, different co-immunoprecipitation studies showed that P2X7 can be co-precipitated with P2X4 in transfected HEK293 and tsA 201 cells, as well as mouse bone marrow-derived macrophages, alveolar and gingival epithelial cells [Antonio et al., 2011], [Boumechache et al., 2009], [Guo et al., 2007], [Hung et al., 2013], [Pérez-Flores et al., 2015], [Weinhold et al., 2010]. While P2X4 was not detected upon immunoprecipitation of P2X7 in alveolar epithelial cells, it was co-precipitated in recombinant kidney cells with a P2X7 antibody and nickel nitrilotriacetic acid (Ni-NTA) purification of His-tagged P2X7 [Antonio et al., 2011], [Weinhold et al., 2010]. Although it was first assumed that

the physical interaction takes place in form of heterotrimers, subsequent cross-linking and nPAGE experiments, as well as atomic force microscopy showed that the predominant assembly state is in form of interacting homotrimers [Antonio et al., 2011], [Boumechache et al., 2009].

## 1.4. Preliminary work and aim of the study

The P2X7 receptor is involved in a number of different diseases including viral, bacterial and fungal infections, inflammatory diseases, cancer, and neurodegenerative disorders [Savio et al., 2018]. Due to its low sensitivity to ATP, P2X7 signaling is thought to be silent under physiological conditions and only activated in a pathological state. Therefore, it represents a promising target for the treatment of those diseases. Despite its importance as a promising drug target, the localization of P2X7 and the proteins that are involved in P2X7 signaling as well as its function under physiological conditions are still unclear. Although there is a large interest in P2X7 and a couple of potential interaction partners have already been identified, many questions remain still unresolved.

### **Preliminary work**

To answer these questions, a P2X7 bacterial artificial chromosome (BAC) transgenic mouse model was previously generated in which the P2X7 receptor is fused via a strep-heptahistidyl-linker to the reporter protein enhanced green fluorescent protein (EGFP) (Figure 4) [Kaczmarek-Hajek et al., 2018]. This BAC transgenic approach should allow P2X7-EGFP expression under its endogenous promoter at near physiological or moderate over-expression levels.

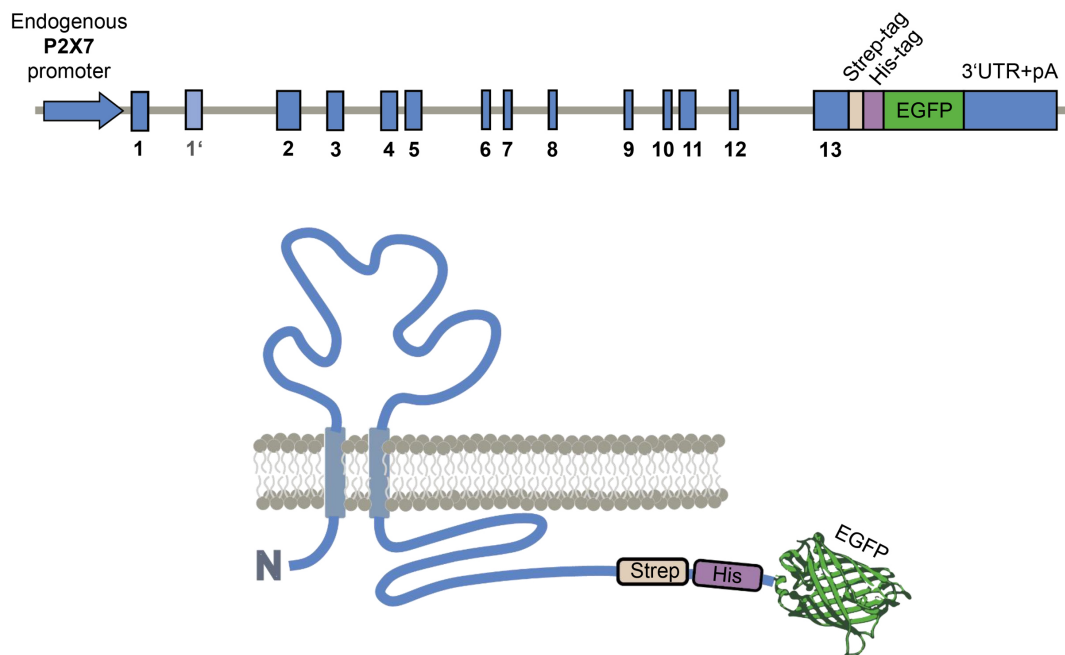


Figure 4 – **The P2X7-EGFP BAC transgenic mouse model:** Scheme of the BAC construct containing the full-length *P2rx7* with the Strep-His-EGFP cassette inserted upstream of the stop codon into exon 13 of mouse *P2rx7*. This results in expression of the P2X7-EGFP fusion protein under the endogenous *P2rx7* promoter.

### Aim of the study

The major aim of this study was to use the P2X7-EGFP BAC transgenic mouse model to identify novel interaction partners of P2X7. In addition to EGFP, a Strep-tagII-Gly-7xHis-Gly linker was inserted to provide further tools for the isolation of the fusion construct from complex mouse tissue via affinity purification. By precipitating the P2X7-EGFP fusion protein from native mouse tissue, co-precipitated proteins that physically interact with the receptor can be identified by liquid chromatography tandem mass spectrometry (LC-MS/MS). To verify that the transgenic protein is correctly folded and transported to the plasma membrane, and is forming a functional ion channel, the transgenic lines were first characterized in detail. This forms the basis for using the mouse model as a tool for interaction studies and the analysis of P2X7 protein expression and function. The second aim of this thesis was to clarify the cell type-specific protein expression of P2X7. Since the commercially available antibodies lack selectivity and are therefore not well suited for protein expression studies via immunofluorescence analysis, we aimed to use the BAC transgenic mice for the visualization of functional EGFP-tagged P2X7 receptors *in vivo*. This is especially of great value for

the ongoing debate about neuronal protein expression of P2X7 (section 1.3.2) and its involvement in central nervous system (CNS) pathology. The aim was to contribute to an in depth analysis of P2X7 expression in the nervous system via biochemical and microscopic approaches.

The third aim was to use the transgenic mice to investigate the postulated interaction of P2X4 and P2X7 subunits (section 1.3.4.9). The interaction of both subunits is a long discussed question and the existence of a physical interaction or heteromerization in native tissue remains unclear. This might be of great significance for the understanding of their role in immune function and their involvement in inflammatory diseases. Co-stainings of both subtypes in native tissue were hardly possible, since suitable antibody combinations were missing. The P2X7-EGFP BAC transgenic mice could help to overcome these limitations. In addition, co-precipitation analysis via the introduced affinity tags can help to detect if both P2X subtypes can physically interact under native conditions.

## 2. Materials and Methods

### 2.1. Materials

#### 2.1.1. Mouse lines

Designation	Reference	Information
P2X7-EGFP(FVB/N-Tg(RP24-114E20P2X7-StrepHis-EGFP)Ani)	[Kaczmarek-Hajek et al., 2018]	Lines: 46, 59 (also in BL/6N), 61
P2X7451P-EGFP(FVB/N-Tg(RP24-114E20P2X7451P-StrepHis-EGFP)Ani)	[Kaczmarek-Hajek et al., 2018]	Lines: 15, 17 (also in BL/6N)
B6-P2rx7 <sup>tm1a</sup> (EUCOMM)Wtsi	European Mutant Mouse Archive	
Gt(ROSA)-26Sor <sup>tm1</sup> (FLP1) <sup>Dym</sup>	[Farley et al., 2000]	FLPe deleter
Tg(EIIa-cre)C5379Lmgd	[Lakso et al., 1996]	EIIa-Cre mouse
B6-Cx3cr1 <sup>tm1.1</sup> (cre) <sup>Jung</sup>	[Yona et al., 2013]	Cx3cr-1-Cre mouse
B6- Cnp <sup>tm1</sup> (cre) <sup>Kan</sup>	[Lappe-Siefke et al., 2003]	CNP-Cre mouse
P2rx4 <sup>-/-</sup>	[Sim et al., 2006]	Gift from Prof. Dr. Mederos y Schnitzler

Table 3 – Mouse lines used in this study.

### 2.1.2. Chemicals and materials

All chemicals were purchased from Carl Roth GmbH and Co. KG or Sigma-Aldrich if not stated differently.

Name	Supplier
4',6-diamidino-2-phenylindole (DAPI)	Carl Roth
Amersham Hybond-N+ nylon membrane	GE Healthcare
Ampicilin	Carl Roth
Collagenase type IIa	Serva
cOmplete™ EDTA-free Protease Inhibitor Cocktail	Roche
Cy5 conjugated NHS-Ester	GE Healthcare
Disuccinimidyl suberate (DSS)	Thermo Fisher
Deuterated disuccinimidyl suberate (DSS-d4)	ProteoChem
Fetal bovine serum	Thermo Fisher
Gel Loading Dye, Purple (6X)	New England Biolabs
Gentamicine	Carl Roth
GFP-Trap®_A	Chromotek
Goat serum	Thermo Fisher
Immobilon-FL PVDF membrane	Merck
Isoflurane (IsoFlo®)	Abbot
Ketamine	Medistar
LightCycler 480 multiwell plate 96	Roche
Ni-NTA Agarose	Qiagen
PefaBlock	Fluka
Penicillin-Streptomycin (100x)	Sigma-Aldrich
Percoll® solution	GE Healthcare
PermaFluor mounting medium	Thermo Fisher
Phosphoimager plates	Molecular Dynamics
Precision Plus Protein™ All Blue Standards	Bio-Rad
Quick-Load® Purple 2-Log DNA Ladder	New England Biolabs
Rat serum	Thermo Fisher
RD680 conjugated NHS-Ester	LI-COR
Roti®-GelStain	Carl Roth
Tissue-Tek® O.C.T.™ compound	Sakura
Xylazine (Xylarium®)	Ecuphar N.V.

Table 4 – Chemicals and materials.

### 2.1.3. Commercial kits and solutions

Name	Supplier
Gibson Assembly <sup>®</sup> master mix	New England Biolabs
InstantBlue <sup>™</sup> Coomassie protein stain	Expedeon
LightCycler 480 SYBR green I master	Roche
mMESSAGE mMACHINE <sup>®</sup> T7/SP6 transcription kit	Thermo Fisher
NucleoSpin <sup>®</sup> gel and PCR clean-up kit	Macherey-Nagel
Plasmid miniprep kit I, peqGold	VWR Peqlab
QuantiNova reverse transcription kit	Qiagen
Random primed labeling kit	Roche
RNeasy plus mini kit	Qiagen
SapphireAmp <sup>®</sup> fast PCR master mix	Takara Clontech

Table 5 – Commercial kits and solutions.

### 2.1.4. Buffers and media

#### 2.1.4.1. Buffers and media for molecular biology

Name	Composition
Tail lysis buffer	100 mM Tris/HCl; 5 mM EDTA 200 mM NaCl; 0.2% SDS
SOC medium	2% (w/v) tryptone; 0.5% (w/v) yeast extract 10 mM NaCl; 2.5 mM KCl 10 mM MgCl <sub>2</sub> ; 10 mM MgSO <sub>4</sub> 20 mM glucose
TAE buffer	40 mM Tris; 20 mM Acetic acid; 1 mM EDTA

Table 6 – Buffers and media for molecular biology.

2.1.4.2. Buffers for *X. laevis* oocytes

Name	Composition
ND96 Ringer's solution	96 mM NaCl; 2 mM KCl 1 mM MgCl <sub>2</sub> ; 1 mM CaCl <sub>2</sub> 5 mM HEPES, pH 7.4
Ca <sup>2+</sup> -free Ringer's solution	96 mM NaCl; 2 mM KCl 2 mM MgCl <sub>2</sub> 5 mM HEPES, pH 7.4

Table 7 – Buffers for *X. laevis* oocytes.

## 2.1.4.3. Buffers for biochemical applications

Name	Composition
Homogenization buffer (mouse tissue)	0.1 M sodium phosphate buffer, pH 8.0 0.4 mM Pefablock <sup>®</sup> SC cOmplete <sup>™</sup> , EDTA-free (1 tablet/15 ml)
Solubilization buffer (mouse tissue)	Homogenization buffer + 1% (v/v) NP40
GFP-Trap washing buffer	Solubilization buffer + 500 mM NaCl
Ni-NTA washing buffer	20% (v/v) solubilization buffer 80% (v/v) 0.1 M sodium phosphate buffer 20-40 mM imidazole
Native elution buffer	20 mM Tris/HCl 100 mM imidazole 10 mM EDTA; pH 7.4
Cross-linking buffer I	0.1 M sodium phosphate buffer, pH 8.0 0.2 M DSS
Cross-linking buffer II	0.1 M sodium phosphate buffer, pH 8.0 1 M DSS 0.5% NP40
SDS sample buffer (5x)	0.3 M Tris/HCl; pH 6.8 5% (w/v) SDS 50% (v/v) glycerol 0.1% bromphenol blue
SDS-PAGE running buffer	25 mM Tris; 192 mM glycine 0.1% SDS
4x Stacking gel buffer	0.4% (w/v) SDS; 0.5M Tris-HCl, pH 6.8
4x Separation gel buffer	0.4% (w/v) SDS; 1.5M Tris-HCl, pH 8.8
Western blot transfer buffer (10x)	250 mM Tris; 1.92 M Glycin 7 mM SDS
Odyssey <sup>®</sup> blocking buffer (TBS)	supplied by LI-COR
Western blot blocking buffer	50% (v/v) Odyssey <sup>®</sup> blocking buffer (TBS) 50% (v/v) TBS

TBS (10x)	1.4 M NaCl; 200 mM Tris/HCl, pH 7.4
TBS-T	TBS + 0.05% (v/v) Tween-20

Table 8 – Buffers for biochemical applications.

#### 2.1.4.4. Buffers and media for immunohistochemistry

Name	Composition
PBS	137 mM NaCl; 27 mM KCl 10 mM Na <sub>2</sub> HPO <sub>4</sub> ; 1.8 mM KH <sub>2</sub> PO <sub>4</sub> , pH 7.4
Immunostaining blocking solution	PBS supplemented with 0.2% Triton X-100 and 5% goat serum
Immunostaining blocking solution (adherent cells)	PBS supplemented with 4% bovine serum albumin and 4% goat serum

Table 9 – Buffers and media for immunohistochemistry.

#### 2.1.4.5. Buffers and media for FACS analysis and cell culture

Name	Composition
Ammonium-chloride-potassium erythrocyte lysis buffer	150 mM NH <sub>4</sub> Cl; 10 mM KHCO <sub>3</sub> ; 0.1 mM EDTA, pH 7.4
Cell culture medium	DMEM supplemented with 10% (v/v) (heat-inactivated) fetal bovine serum and Penicillin-Streptomycin
DMEM	supplied by Sigma-Aldrich
FACS buffer	PBS supplemented with 0.2% BSA and 1 mM EDTA
HBSS	supplied by Thermo Fisher
RPMI	supplied by Thermo Fisher

Table 10 – Buffers and media for FACS analysis and cell culture.

## 2.1.5. Antibodies

### Primary antibodies:

Antibody	Supplier	Identifier	Dilution
Aquaporin-5, rb pAb	Alomone	Cat.# AQP-005, RRID: AB_2039736	IF 1:100
CD68, rat FA-11	AbD Serotec	Cat.# MCA1957, RRID: AB_322219	IF 1:200
GFAP, ms GA5	Millipore	Cat.# MAB360, RRID: AB_11212597	IF 1:200
GFP, rat 3H9	Chromotek	Cat.# 3h9-100, RRID: AB_10773374	WB 1:1000
GFP, chk pAb	Thermo Fisher	Cat.# A10262, RRID: AB_2534023	IF 1:400
GFP, rb pAb	Abcam	Cat.# ab6556, RRID: AB_305564	IF 1:2000
GlutSynth, ms GS-6	Millipore	Cat.# MAB302, RRID: AB_2110656	IF 1:500
Iba1, rb pAb	WAKO	Cat.# 019-19741, RRID: AB_839504	IF 1:500
ICAM-1 (CD54), ham 3E2B	Thermo Fisher	Cat.# MA5405, RRID: AB_223595	IF 1:50
Integrin $\beta$ -2 (CD18), rat M18/2	Abcam	Cat.# ab119830, RRID: AB_10902855	IF 1:300
MPZ, rb pAb	Abcam	Cat.# ab31851, RRID: AB_2144668	IF 1:200
NeuN, ms A60	Millipore	Cat.# MAB377, RRID: AB_2298772	IF 1:500
P2X4, rb pAb	Alomone	Cat.# APR-002, RRID: AB_2040058	WB 1:1000 IF 1:200
P2X7 C-term, rb pAb	Synaptic Systems	Cat.# 177003, RRID: AB_887755	WB 1:1500 IF 1:500
P2X7 ECD, 7E2-rbIgG	Nolte lab	Nanobody rbIgG fusion construct	IF 0.1 $\mu$ g/ml
Pecam-1 (CD31), rat MEC13.3	BioLegend	Cat.# 102501, RRID: AB_312908	IF 1:100
S100 $\beta$ , rb pAb	Synaptic Systems	Cat.# 287003, RRID: AB_2620024	IF 1:500
TH, rb pAb	Millipore	Cat.# AB152, RRID: AB_390204	IF 1:200
Vinculin, ms hVin-1	Sigma-Aldrich	Cat.# V9131, RRID: AB_477629	WB 1:10000

Table 11 – Primary antibodies used in this study. rb = rabbit, ms = mouse, ham = hamster, pAb = polyclonal antibody IF = immunofluorescence, WB = western blot

**Secondary antibodies:**

Antibody	Supplier	Identifier	Dilution
800CW gt anti-ms	LI-COR	Cat.# 925-32210, RRID: AB_2687825	WB 1:15000
800CW gt anti-rb	LI-COR	Cat.# 926-32211, RRID: AB_621843	WB 1:15000
680RD dk anti-rb	LI-COR	Cat.# 925-68073, RRID: AB_2716687	WB 1:15000
680RD gt anti-rat	LI-COR	Cat.# 925-68076, RRID: AB_10956590	WB 1:15000
A488 gt anti-rb	Thermo Fisher	Cat.# A11008, RRID: AB_143165	IF 1:400
A488 gt anti-chk	Thermo Fisher	Cat.# A11039, RRID: AB_2534096	IF 1:400
A594 gt anti-ms	Thermo Fisher	Cat.# A11032, RRID: AB_2534091	IF 1:400
A594 gt anti-rat	Thermo Fisher	Cat.# A11007, RRID: AB_10561522	IF 1:400
A594 gt anti-rb	Thermo Fisher	Cat.# A11037, RRID: AB_2534095	IF 1:400
A647 gt anti-ham	BioLegend	Cat.# 405510, RRID: AB_2566695	IF 1:400

Table 12 – Secondary antibodies used in this study. gt = goat, rb = rabbit, ms = mouse, ham = hamster, IF = immunofluorescence, WB = western blot

**2.1.6. Enzymes**

Enzyme	Supplier
PNGase F	New England Biolabs
Endoglycosidase H	New England Biolabs
DpnI	New England Biolabs
BglII	New England Biolabs
Trypsin EDTA solution	Sigma-Aldrich

Table 13 – Enzymes used in this study.

### 2.1.7. Oligonucleotides

All oligonucleotides were purchased from Metabion AG.

Name	Sequence	Application
Cnp-fwd	gcc ttc aaa ctg tcc atc tc	Genotyping
Cnp-rev	ccc agc cct ttt att acc ac	Genotyping
Cx3cr-fwd	cct cta aga ctc acg tgg acc tg	Genotyping
Cx3cr-rev(wt)	gac ttc cga gtt gcg gag cac	Genotyping
Cx3cr-spec1	gcc gcc cac gac cgg caa ac	Genotyping
mX7-fwd	ctg gca act atc cat ttt cc	Genotyping
mX7-rev	gtg tga gtg aat gag atc gtg	Genotyping
X7Ex13-fwd	ggt tct tag cag gct taa cag ca	Genotyping
X7BAC5-rev	atg ggg gtg ttc tgc tgg tag t	Genotyping
mP2X4_GA-fwd	caa act ggg gca cag ctg act cga ggg ggg gc	Gibson assembly
mP2X4_GA-rev	gtg gct cca ggc act ctg gtc cgt ctc tcc g	Gibson assembly
mP2X7_GA-fwd	cat gga cga gct gta caa gtg act cga ggg ggg gc	Gibson assembly
mP2X7_GA-rev	gtg gct cca ggc act gta ggg ata ctt gaa gcc act	Gibson assembly
EGFP_GA-fwd	cgg aga gac gga cca gag tgc ctg gag cca ccc g	Gibson assembly
EGFP_GA-rev	ctc acc cac cat ccc atg gtg atg gtg atg gtg c	Gibson assembly
T7_seq	taa tac gac tca cta tag gg	Sequencing
SP6_seq	att tag gtg aca cta tag	Sequencing
mP2X4_seq1	act tca ccc tct tgg taa ag	Sequencing
mP2X4_seq2	atg tgg aag act acg agc ag	Sequencing
mP2X7_seq1	cga gat cta ctg gga ttg c	Sequencing
mP2X7_seq2	agg atc cgg aag gag ttc	Sequencing
P2X7_qPCR-fwd	ctg gtt ttc ggc act gga	qRT-PCR
P2X7_qPCR-rev	cca aag tag gac agg gtg ga	qRT-PCR
P2X4_qPCR-fwd	cca aca ctt ctc agc ttg gat	qRT-PCR
P2X4_qPCR-rev	tgg tca tga tga aga ggg agt	qRT-PCR
PPIA_qPCR-fwd	agg gtg gtg act tta cac gc	qRT-PCR
PPIA_qPCR-rev	ctt gcc atc cag cca ttc ag	qRT-PCR
RPLP0_qPCR-fwd	gga ccg cct ggt tct cct at	qRT-PCR
RPLP0_qPCR-rev	acg atg tca ctc caa cga gg	qRT-PCR

Table 14 – Oligonucleotides used in this study.

### 2.1.8. Special equipment

Device	Manufacturer
Odyssey <sup>®</sup> FC imaging system	LI-COR
NanoDrop <sup>™</sup> 2000c	Thermo Fisher Scientific
LightCycler <sup>®</sup> 480 system	Roche
Precellys <sup>®</sup> 24 homogenizer	Bertin Instruments
Typhoon <sup>™</sup> Trio	GE Healthcare
Mini Trans-Blot <sup>®</sup> cell	Bio-Rad
Trans-Blot <sup>®</sup> SD Semi-Dry Transfer Cell	Bio-Rad
Ultimate <sup>™</sup> 3000 nanoLC system	Thermo Fisher Scientific
Q Exactive <sup>™</sup> HF mass spectrometer	Thermo Fisher Scientific
FACSCelesta <sup>™</sup> flow cytometer	BD Biosciences
CM1900 Cryostat	Leica
LSM 880 with Airyscan	Zeiss

Table 15 – Special equipment used for this study.

## 2.2. Methods

### 2.2.1. Animal breeding and experiments

Mice were from the Max Planck Institute of Experimental Medicine in Göttingen or the Walther Straub Institute of Pharmacology and Toxicology in Munich and housed in standard conditions (22°C, 12 h light-dark cycle, water/food *ad libitum*). All mouse breedings, handling, and experimental procedures were performed in accordance with German guidelines and were approved by the government of Upper Bavaria (transcardial perfusion (55.2-1-54-2532-59-2016)) and Lower Saxony (generation of BAC transgenic mice, transcardial perfusion (33.9-42502-04-12/0863)). Tail biopsies were taken at weaning, at the age of 3-4 weeks and used for genotyping according to the indicated protocols (2.2.2.3). The genotype of the P2X7-EGFP lines was double checked by fluorescence scanning of brain samples using a Typhoon<sup>™</sup> scanner.

## 2.2.2. Molecular biology

### 2.2.2.1. Gibson assembly

For the generation of the desired plasmid DNA constructs, multiple different DNA fragments were assembled according to the Gibson assembly protocol [Gibson et al., 2009]. Polymerase chain reaction (PCR) was used to generate linear double-stranded DNA fragments with overlapping ends. For the specific primers used in the reaction mixture refer to section 2.1.7. The PCR product was afterwards checked for the correct size by agarose gel electrophoresis and incubated with DpnI (60 min at 37°C) to remove the bacteria-derived plasmid templates. The linearized fragments were subsequently purified using the NucleoSpin® PCR clean-up kit. The obtained overlapping DNA fragments were then combined in the actual assembly reaction using the Gibson Assembly® master mix according to the manufacturer's protocol. During this one-step isothermal reaction (60 min at 50°C), the exonuclease creates single-stranded 3' ends which allow annealing of the complementary overhangs, the DNA polymerase fills the gaps between the annealed fragments, and the ligase joins the DNA molecules to form the recombinant DNA construct. By using a plasmid vector-derived fragment as a backbone and DNA that codes for the respective receptor, affinity tags, and/or a reporter protein as an insert, the desired plasmid DNA constructs were generated and transformed into competent *E.coli* cells.

### 2.2.2.2. Heat shock transformation

To obtain large quantities of the DNA constructs, competent *E.coli* DH5 $\alpha$  cells were transformed with the plasmid vector via heat shock. 2-5  $\mu$ l of DNA was added to 50  $\mu$ l of competent *E.coli* DH5 $\alpha$  cells and incubated for 30 min on ice, followed by a heat shock at 42°C for 60 sec. 950  $\mu$ l of super optimal broth with catabolite repression (SOC) medium was subsequently added to the cells and incubated for one hour at 37°C shaking at 850 revolutions per minute (rpm). Cells were plated on lysogeny broth (LB) agar containing 100  $\mu$ g/ml ampicillin as a selection antibiotic and cultivated overnight at 37°C.

### 2.2.2.3. Polymerase chain reaction

PCR is a standard procedure for the enzymatic amplification of desired DNA fragments and well described in the literature. The method was used according to common protocols and therefore only special applications are mentioned in the following paragraphs.

#### **Genotyping:**

Tail biopsies from 3-4 week old mice were digested overnight shaking at 56°C in 200  $\mu$ l tail lysis buffer containing proteinase K (20  $\mu$ g/ml). The lysate was centrifuged at 13000 rpm for 10 min at room temperature (RT) and the DNA was subsequently precipitated by adding 500  $\mu$ l of 2-propanol to the supernatant. After centrifugation at 13000 rpm for 5 min at RT, the DNA pellet was washed with 200  $\mu$ l 70% EtOH and afterwards resuspended in 20  $\mu$ l milli-Q<sup>®</sup> H<sub>2</sub>O for 40 min at 56°C. A 1:10 dilution of the isolated DNA was used for the genotyping of the mice via PCR. The following primer combination were used for genotyping:

- **P2X7-EGFP line**

Primer: X7Ex13-fwd + X7BAC5-rev

Expected product: 1284 base pairs (bp)

- **P2rx7-tm1c/tm1d line**

Primer: mX7-fwd + mX7-rev

Expected products: 1257 bp for tm1c; 415 bp for tm1d

- **Cx3cr Cre line**

Primer: Cx3cr-fwd + Cx3cr-rev(wt) + Cx3cr-spec1

Expected product: 304 bp

- **Cnp Cre line**

Primer: Cnp-fwd + Cnp-rev

Expected product: 683 bp

**Real-time quantitative reverse transcription PCR (qRT-PCR) :**

Total mRNA was isolated from 20-30 mg mouse tissue using the RNeasy plus mini kit. Complementary DNA (cDNA) was afterwards synthesized with the QuantiNova reverse transcription kit following the manufacturer's instructions. The quantitative PCR was carried out in the LightCycler<sup>®</sup> 480 System using LightCycler<sup>®</sup> 480 SYBR green I master and LightCycler<sup>®</sup> 480 multiwell plates. Primers were designed to span an exon-exon junction using Roche's Universal ProbeLibrary (refer to section 2.1.7). Relative mRNA levels were calculated by the  $\Delta C_t$ -method using ribosomal protein lateral stalk subunit P0 (RPLP0) and peptidylprolyl isomerase A (PPIA) as a reference [Schmittgen and Livak, 2008]:

$$\begin{aligned}\text{Relative mRNA level} &= 2^{-\Delta C_t}; \\ \Delta C_t &= C_t(\text{target}) - C_t(\text{reference}); \\ C_t &= \text{cycle threshold}\end{aligned}$$

**Colony-PCR:**

Transformation of the correct plasmid DNA was verified by colony-PCR. Single *E. coli* colonies were picked from LB agar plates and resuspended in 10  $\mu\text{l}$  milli-Q<sup>®</sup> H<sub>2</sub>O. 2  $\mu\text{l}$  of this suspension was used for the PCR with specific primers (refer to section 2.1.7) and the SapphireAmp PCR master mix. Agarose gel electrophoresis was used to screen for colonies with the correct size of the amplified PCR product.

**2.2.2.4. Plasmid DNA preparation**

Plasmid DNA was isolated from overnight *E. coli* cultures cultivated in LB media containing 100  $\mu\text{g}/\text{ml}$  ampicillin. The DNA was extracted and purified using peqGold plasmid miniprep kit I. PCR or enzymatic digestion followed by agarose gel electrophoresis and subsequent DNA sequencing conducted by eurofins genomics confirmed the correctness of the plasmid DNA.

**2.2.2.5. Agarose gel electrophoresis**

Agarose gel electrophoresis was used to determine the size of PCR products, linearized plasmid DNA, or synthesized complementary RNA (cRNA). Briefly,

agarose was boiled in tris-acetate-EDTA (TAE) buffer, supplemented with Roti®-GelStain (8  $\mu$ l / 100 ml Agarose) and transferred into the casting chamber. DNA or RNA samples were supplemented with gel loading dye and loaded in the chambers of the solidified agarose gel and a voltage of 100-120 V was applied for 30-90 min. A molecular weight marker was used for size comparison. For documentation, the nucleic acid fragments were visualized in the 600 nm channel of an Odyssey® Fc imaging system.

#### 2.2.2.6. Quantification of nucleic acid samples

To assess nucleic acid sample concentration and purity, the optical density at 260/280 nm was measured using a NanoDrop™ 2000c UV-Vis spectrophotometer. 1.5  $\mu$ l of sample DNA or RNA was loaded on the photometer and concentration was calculated in comparison to the blank solution (milli-Q® H<sub>2</sub>O).

#### 2.2.2.7. *In-vitro* cRNA synthesis

For cRNA synthesis, 10  $\mu$ g of plasmid DNA was digested with 2  $\mu$ l restriction enzyme in the supplied reaction buffer for 2 hrs at 37°C. The linearization was verified by agarose gel electrophoresis. The linearized DNA was purified with the Qiagen clean up kit and subsequently used for *in-vitro* synthesis of cRNA using the mMESSAGING mMACHINE® T7/SP6 transcription kit. RNA concentration was measured using the NanoDrop™ 2000c and afterwards adjusted to 0.5  $\mu$ g/ $\mu$ l and stored in aliquots at -80°C.

#### 2.2.2.8. Southern blot analysis

Southern blot analysis was conducted by Dr. Volker Eulenburg as described [Kaczmarek-Hajek et al., 2018]. Briefly, the genomic DNA was isolated from mouse tail biopsies and subsequently digested with BglII. After separation in an 0.8% agarose gel, the DNA was transferred onto nylon membrane via capillary transfer. DNA was immobilized by UV irradiation (1500  $\mu$ J/cm<sup>2</sup>) and hybridized to a <sup>32</sup>P labeled probe corresponding to a 645 bp fragment 2.6 kilobases (kb) downstream of the *P2rx7* stop codon using the random primed labeling kit. Hybridization signals were specifically detected at 5277 bp for the transgenic *P2rx7*

and at 4561 bp for the endogenous *P2rx7* via autoradiographic analysis with phosphoimager plates. The intensity ratios were used to determine the number of inserted BAC copies.

### 2.2.3. Protein biochemical methods

#### 2.2.3.1. *X. laevis* oocytes as expression system

*X. laevis* oocytes were provided by the Max Planck Institute of Experimental Medicine in Göttingen. Ovarian lobes were sent via express mail in cooling packs and used on the day after the surgery. The lobes were dissected in small pieces and incubated for 105 min at 16°C in sterile filtered ND96, supplemented with 500  $\mu$ l/ml gentamicine and 1 mg/ml collagenase type IIA. The separated single oocytes were then incubated for 15 min at RT in Ca<sup>2+</sup>-free Ringer's solution. The defolliculated oocytes were afterwards transferred into sterile filtered ND96 solution (supplemented with 500  $\mu$ l/ml gentamicine) and stage V-VI oocytes were selected for injection using a stereo microscope. Injection needles were made from borosilicate capillaries using a micropipette puller and filled with RNase-free mineral oil. After mounting of the injection needles on a Nanoject II injector, they were filled with the cRNA solution. Selected oocytes were injected with 25 ng cRNA at the interface between animal and vegetal pole and incubated for 2-3 days at 16°C in ND96, supplemented with 500  $\mu$ l/ml gentamicine.

#### 2.2.3.2. Protein extraction from *X. laevis* oocytes

Two or three days after injection 6-12 *X. laevis* oocytes were homogenized with a pipette in 0.1 M sodium phosphate buffer (PB) supplemented with Pefabloc SC and 1% NP40 (20  $\mu$ l buffer / oocyte). After 15 min incubation on ice, the supernatant was cleared by two steps of centrifugation for 15 min at 15000 x g and 4°C. The so obtained protein extract was used for further experiments.

#### 2.2.3.3. Protein extraction from mouse tissue

Mice were euthanized by a prolonged CO<sub>2</sub> exposure or cervical dislocation. The different mouse tissues were dissected and either used directly in the experi-

ment or shock frozen in liquid nitrogen and stored at  $-80^{\circ}\text{C}$  until usage. For the extraction of proteins, the tissue was milled in a Precellys<sup>®</sup> 24 homogenizer in homogenization buffer using 2.8 mm ceramic beads. Cell fragments, nuclei, and organelles were pelleted by centrifugation at  $1000 \times g$  and  $4^{\circ}\text{C}$  for 15 min. The supernatant, comprising membrane fragments and soluble proteins, was subsequently centrifuged at  $21000 \times g$  and  $4^{\circ}\text{C}$  for 60 min to obtain a crude pelleted membrane fraction. Membrane proteins were extracted by resuspension in solubilization buffer and incubation for 15 min at  $4^{\circ}\text{C}$ . The protein extract was afterwards cleared from insoluble fragments by centrifugation at  $21000 \times g$  and  $4^{\circ}\text{C}$  for 15 min to obtain the supernatant with solubilized membrane proteins.

#### **2.2.3.4. Glycosylation analysis**

Glycosylation is a co- and post-translational enzymatic modification, which is essential for the correct folding, stability, and membrane trafficking of proteins. It takes place in the ER and the Golgi apparatus. For the analysis of the glycosylation status, protein extracts were treated with two different endoglycosidases. 10-30  $\mu\text{l}$  aliquots of membrane extract or purified protein were supplemented with reducing 5x sample buffer and incubated for 30 min at  $37^{\circ}\text{C}$  with 10 IUB miliunits endoglycosidase H (Endo H) or 20 IUB miliunits PNGase F to differentiate between core glycosylations that were attached in the ER and complex glycoylations from the Golgi apparatus.

#### **2.2.3.5. Purification of affinity-tagged proteins**

The 7xHis and EGFP-tagged proteins were purified from membrane extracts using Ni-NTA or anti-GFP nanobodies coupled agarose beads (GFP-Trap<sup>®</sup>\_A). 30-50  $\mu\text{l}$  beads were three times washed with 300-500  $\mu\text{l}$  GFP-Trap washing buffer or Ni-NTA washing buffer, before they were incubated for 30 min at  $4^{\circ}\text{C}$  with the protein extract on an end-over-end rotator. After additional washing in the same manner, the bound proteins were eluted from the beads. While proteins that were purified using Ni-NTA beads could be eluted in their native conformation using native elution buffer, the purification via nanobodies needed harsh conditions to destroy the strong nanobody-antigen interactions. Therefore, beads were treated for 2 min with 0.2 M glycine (pH 2.5) and afterwards neutralized with 1/10 volume 1 M Tris (pH 10.5) as recommended by the manufacturer. As an alternative,

the protein can also be eluted with 5x SDS sample buffer at 90°C for 10 min. Both elution methods lead to denaturation of the proteins and loss of EGFP fluorescence.

#### **2.2.3.6. Fluorescent labeling of proteins**

To visualize enriched proteins after the purification process, all proteins that were bound to the agarose beads were labeled with a fluorescent dye before they were eluted from the beads. The agarose beads were incubated with Cy5/RD680 coupled mono-reactive N-hydroxysuccinimide (NHS) ester (50  $\mu\text{g}/\mu\text{l}$  in 0.1 M PB, pH 8.0) for 30 min on ice. Beads were afterwards washed three times with 500  $\mu\text{l}$  0.1 M PB (pH 8.0) and the fluorescently labeled proteins were eluted as described above.

#### **2.2.3.7. Protein cross-linking**

Homogenized tissue, membrane fractions, or solubilized proteins were cross-linked using disuccinimidyl suberate (DSS). Tenfold stock solutions of DSS were prepared in dimethyl sulfoxide (DMSO) directly before use and then added to the aqueous cross-linking reaction. The protein samples were incubated with 0.2 mM, 1 mM, or 2 mM DSS for 30 min at RT. Unreacted NHS esters were afterwards quenched by the addition of 100 mM Tris (10 min at RT) to the buffer solution.

#### ***In-situ* cross-linking:**

Mice were euthanized using CO<sub>2</sub> and subsequently transcardially perfused with 25 ml 0.1 M PB (pH 8.0). For that, a 27 G butterfly needle (0.4 x 10 mm) was inserted into the left ventricle of the heart. Then 25 ml of cross-linking buffer I was perfused. In a second step, 2 ml of cross-linking solution II was injected transcardially and afterwards 1.5 ml of the same solution into the trachea. For the intratracheal application a blunt ended 21 G needle (0.8 x 40 mm) was used and fixed with surgical threads to avoid leakage of the cross-linking solution. The actual cross-linking reaction took place for 30 min at RT. The lung was afterwards isolated, shock frozen in liquid nitrogen, and stored at -80°C until usage.

### **2.2.3.8. Sample preparation for LC-MS/MS analysis**

Three cross-linked lungs were milled in 500  $\mu$ l homogenization buffer supplemented with 100 mM Tris (3x 15 sec at 4500 rpm) using a Precellys<sup>®</sup> 24 homogenizer. After centrifugation at 1000 x g for 15 min at 4°C, the supernatant was transferred into a new tube. The pellet was resuspended in 400  $\mu$ l homogenization buffer and additionally homogenized as described before. After centrifugation (1000 x g for 15 min at 4°C) both supernatants were combined in one tube, supplemented with NP40 (final concentration: 1% v/v), and incubated for 15 min on ice. The mixture was cleared from insoluble debris by centrifugation at 21000 x g for 30 min at 4°C and the supernatant was used for purification of the P2X7-EGFP fusion protein.

Briefly, GFP-Trap<sup>®</sup> agarose beads were washed three times with 0.1 M PB (pH 8.0) supplemented with 1% NP40 before they were incubated with the protein extract for 2 h at 4°C on an end-over-end rotator. For the purification of 1500  $\mu$ l of protein extract obtained from three lungs, 60  $\mu$ l of GFP-Trap slurry was used. Beads were afterwards transferred into mini spin columns and washed eight times with 500  $\mu$ l GFP-Trap washing buffer followed by three washing steps with 0.1 M PB (pH 8.0). The beads were then centrifuged for 4 min at 1000 x g and 4°C to remove all remaining buffer. For the elution of the proteins, the spin columns were incubated for 2 min with 40  $\mu$ l of 0.2 M glycine (pH 2.5), placed on a new 1.5 ml reaction tube containing 4  $\mu$ l of 1 M Tris (pH 10.5) and centrifuged for 2 min at 1000 x g at 4°C. The whole eluate was loaded on a SDS gel for colloidal coomassie staining and subsequent LC-MS/MS analysis.

### **2.2.3.9. SDS-PAGE**

Proteins were separated according to their molecular weight by sodium dodecylsulfate polyacrylamide gel electrophoresis (SDS-PAGE). The samples were incubated with 5x SDS sample buffer, supplemented with 100 mM dithiothreitol (DTT), for 10 minutes at 40°C and loaded on the gel. Separation took place in SDS-PAGE running buffer at 100 V for the stacking gel and 130 V for the separation gel. After the separation of the proteins, the gel was analyzed on a Typhoon<sup>™</sup> fluorescence scanner and afterwards either stained with colloidal coomassie staining solution or used for western blot analysis.

### **2.2.3.10. Western blot analysis**

After the separation in the SDS gel, the proteins were transferred onto a Immobilon-FL polyvinylidene difluoride (PVDF) membrane and analyzed with specific antibodies. For that, the PVDF membrane was plunged in methanol and afterwards equilibrated for 10 min in western blot transfer buffer. Transfer of proteins took place at 100 V and 350 mA for 60 min in a tank blot system or at 15 V and 3 mA/cm<sup>2</sup> for 60 min in a semi-dry blotting system. Free binding sites of the membrane were blocked by incubation with western blot blocking buffer for 60 min at RT. For the immunological detection of proteins, the membrane was incubated with the specific first antibodies diluted in western blot blocking buffer for 60 min at RT or overnight at 4°C. For dilution ratios refer to section 2.1.5. After washing three times for 5 min with TBS-T, the membrane was incubated with the according fluorescent dye conjugated secondary antibodies diluted in TBS-T for 60 min at RT. The membrane was again washed three times for 5 min with TBS-T and finally rinsed with TBS before detecting signals by using the Odyssey<sup>®</sup> Fc imaging system.

### **2.2.3.11. LC-MS/MS analysis**

The MS analysis was done in collaboration with the Protein Analysis Unit of the Biomedical Center Munich (Prof Dr. Axel Imhof) and conducted by Dr. Andreas Schmidt. Excised gel lanes were cut into small cubes to increase the surface and subsequently washed with 100 mM ammonium bicarbonate (ambic) and destained with 50 mM ambic containing 50% acetonitrile (ACN). Disulfide bonds were reduced with 5 mM DTT in 100 mM ambic at 56°C for 35 min and free sulfhydryl groups were alkylated with 15 mM iodoacetamide to prevent formation of undesired disulfide bonds. Next, gel bands were dried and 0.2 µg trypsin in 100 mM ambic were applied to enzymatically cleave the proteins into oligopeptides suitable for LC-MS/MS analysis. The gel pieces were incubated for 12 hrs at 37°C while shaking vigorously. After completing the protein digestion, the supernatants containing the oligopeptides were separated from the gel pieces and stored in a separate Eppendorf vial. Peptides retained in the acrylamide gel were recovered by washing the gel pieces with 0.1% formic acid (FA), 30% ACN containing 0.1% FA, and 70% ACN containing 0.1% FA. After each washing step

the supernatants were taken off and combined with the supernatant of the protein digestion. Finally, the peptide solution was acidified using 10% trifluoroacetic acid (TFA) to reach pH 2-3 and subsequently dried in a SpeedVac centrifuge. To remove salt and buffer compounds, C18 stage tips with 3 discs of Empore C18 filters (3M) were prepared, washed with 50  $\mu$ l of 100% Methanol, 50  $\mu$ l of elution solvent (70% ACN, 29.9% H<sub>2</sub>O 0.1% FA), and three times 70  $\mu$ l 0.1% TFA. The dried peptide fractions were resuspended in 0.1% TFA and slowly passed through the stage tips to allow peptide binding to the hydrophobic surface. Remaining salt was removed by washing twice with 50  $\mu$ l of 0.1% FA. Finally, peptides were eluted from the C18 discs using two times 70  $\mu$ l of elution solvent. The peptide fractions were again dried under vacuum using the SpeedVac and redissolved in 6  $\mu$ l of 0.1% FA for LC-MS/MS analysis. For reversed phase high performance liquid chromatography (HPLC) separation of peptides on an Ultimate 3000 nanoLC system, 5  $\mu$ l of the solution were loaded onto the analytical column (120 x 0.075 mm, in house packed with ReprosilC18-AQ, 2.4  $\mu$ m, *Dr. Maisch GmbH*), washed for 5 min at 300 nl/min at 3% ACN containing 0.1% FA and subsequently separated applying a linear gradient from 3% ACN to 40% ACN over 50 min. Eluting peptides were ionized in a nanoESI source and on line detected on an QExactive HF mass spectrometer. The mass spectrometer was operated in a TOP10 method in positive ionization mode, detecting eluting peptide ions in the m/z range from 375 to 1600 and performing MS/MS analysis of up to 10 precursor ions. Peptide ion masses were acquired at a resolution of 60000 (at 200 m/z). higher-energy collision-induced dissociation (HCD) MS/MS spectra were acquired at a resolution of 15000 (at 200 m/z). All mass spectra were internally calibrated to lock masses from ambient siloxanes. Precursors were selected based on their intensity from all signals with a charge state from 2+ to 5+, isolated in a 2 m/z window and fragmented using a normalized collision energy of 27%. To prevent repeated fragmentation of the same peptide ion, dynamic exclusion was set to 20 sec.

**Database search parameters:**

All MS raw data were searched against a combined forward/reversed protein database of *m. musculus* (Uniprot, 12/2017) by the Andromeda search engine within the MaxQuant (v1.5.3.12 and v1.6.0.16) software suit [Cox et al., 2011]. For peptide masses the mass accuracy was set to 15 parts per million (ppm) for the first search and 4 ppm for the main search, for fragment ions an ac-

curacy of 25 ppm was applied. Peptides with maximal 2 missed cleavages by Trypsin/P, a minimal score of 10 for unmodified peptides and 35 for peptides carrying post-translational modifications were considered. Carbamidomethylation of cysteine was set as fixed modification. Putative variable modifications were oxidation (M), acetylation (Protein N-term), and phosphorylation (STY). Modifications by the crosslinking reagents were selected with regard to the experimental set-up: glutarate\_XL (K), glutarate\_monolink (K), suberate\_XL (K), suberate\_monolink (K). These peptide spectrum matches were filtered for 5% false discovery rate (FDR) and the resulting protein hits were again filtered for 5% detection of reversed sequences. MS raw data were converted into mascot generic files (mgf) by the proteome discoverer software (v2.2) and searched for protein-protein crosslinks and monolinks using an in house software crossfinder (v1.3) against a database consisting of P2X7 and the 5 most enriched proteins identified in the sample [Forné et al., 2012].

### **Statistical analysis of interacting proteins:**

For statistical analysis of potential interaction partners of P2X7, the MaxQuant file of three biological replicates was loaded into the Perseus software (v1.5.8.5). Proteins were filtered for contaminants, proteins 'only identified by site', and reverse identifications. Intensities were transformed by calculating the logarithm to the base 2 and afterwards grouped according to replicates. The data were then again filtered to have a minimum of 3 valid values in at least one group. Missing values were afterwards imputed from normal distribution. A two-sample t-test was used to identify potential interactors. The minimal fold change (s0) was set to 2 and the FDR to 0.01. The results were also visualized in form of a volcano plot. The t-test difference was plotted against the negative logarithm of the p-value. Proteins with a minimum of 5 unique peptides in each biological replicate were chosen as bona fide candidates for interactors of P2X7.

### **2.2.4. Flow cytometry**

Fluorescence-activated cell sorting (FACS) analysis was performed by Dr. Björn Rissiek as described [Kaczmarek-Hajek et al., 2018]. 8-12 week old mice were sacrificed and a single cell suspension was prepared from their brains by digestion with collagenase for 30 min at 37°C in a shaking water bath. The suspension

was filtered through a 70  $\mu\text{m}$  cell strainer and subsequently centrifuged for 5 min at 300 x g. The pellet was afterwards resuspended in 33% Percoll<sup>®</sup> solution and centrifuged for 20 min at 300 x g. To remove erythrocytes, the pellet was incubated on ice with 1 ml ammonium-chloride-potassium erythrocyte lysis buffer for 1 min. The cells were washed in 10 ml FACS buffer and resuspended in 100  $\mu\text{l}$  of the same buffer, before they were incubated with microglial specific antibodies (anti-CD11b-perCP and anti-CD45-PE-Cy7) in the presence of normal rat serum and anti-CD16/CD32 antibody for Fc-blocking. The stained cells were then washed twice with FACS buffer and resuspended in 200  $\mu\text{l}$  RPMI medium. After the addition of 4',6-diamidino-2-phenylindole (DAPI) (1.5  $\mu\text{M}$ ), the cells were incubated in the pre- or absence of ATP (1 mM) for 15 min at 37°C. DAPI uptake of CD11b+CD45low microglial cells was measured with FACSCelesta<sup>™</sup> flow cytometer.

## **2.2.5. Immunohistochemistry**

### **2.2.5.1. Immunostaining of lung and DRG cryosections**

Mice were euthanized using CO<sub>2</sub> or isoflurane and subsequently transcardially perfused with phosphate-buffered saline (PBS) (pH 7.4) followed by 4% paraformaldehyde (PFA)/PBS. Lungs were afterwards post-fixed overnight in 4% PFA/PBS at RT and washed for 1-3 days in 0.1 M PB (pH 7.4) before they were transferred into 18% sucrose in PBS (pH 7.4) for cryoprotection (24 hrs at RT). Lungs were afterwards embedded in Tissue-Tek<sup>®</sup> O.C.T.<sup>™</sup> Compound using plastic cryomolds and stored at -20°C for short term and -80°C for long term storage. For immunofluorescence staining, the frozen lungs were cut into 10  $\mu\text{m}$  sections using a CM1900 cryostat. Cryostat sections were dried for 30 min at RT, then washed for 10 min in PBS and blocked for 30 min at RT using immunostaining blocking solution. The tissue sections were subsequently incubated with primary antibodies for 16-24 hrs at 4°C. After washing (3 x 5 min, PBS), the fluorescent-dye conjugated secondary antibodies were added for 60 min at RT. All antibodies were diluted in blocking solution. For dilution rates refer to section 2.1.5. After washing as above, the slices were incubated with DAPI (1 mg/l) for 1-3 min and additionally washed before the coverslips were mounted using PermaFluor mounting medium. For the immunostaining of dorsal root ganglions (DRGs), mice were euthanized using isoflurane and dissected to prepare thoracic and lumbar DRGs.

DRGs were fixed in 4% PFA/PBS overnight at 4°C, embedded in Tissue-Tek® O.C.T.™ Compound and sectioned into 10  $\mu\text{m}$  slices. Preparation and sectioning of the DRGs was conducted by Heinz Janser. The obtained sections were post-fixed for 10 min in 4% PFA/PBS and incubated for 30 min in 0.1 M glycine/PBS. After treatment of the slices with 10 mM sodium citrate (pH 6.0, >95°C) for 1 min, they were incubated with immunostaining blocking solution (0.1% Triton X-100) and stained as described above. All mounted slides were stored at 4°C in the dark and images were obtained by confocal laser scanning microscopy using a LSM 880.

### **2.2.5.2. Free floating immunostaining of brain slices**

Mice were anesthetized with 100 mg/kg ketamine and 20 mg/kg xylazine and subsequently transcardially perfused with PBS (pH 7.4), followed by 4% PFA/PBS. Brains were post-fixed (4% PFA/PBS overnight at 4°C) and afterwards transferred into cryoprotection solution (30% sucrose/PBS for 24 hrs at 4°C) and embedded in Tissue-Tek® O.C.T.™ Compound. The brains were then cut into 40  $\mu\text{m}$  sections, washed (3 x 10 min at RT, PBS) and blocked in immunostaining blocking solution (60 min at RT). For immunostaining, the slices were incubated with the primary antibodies (16-24 hrs at 4°C), followed by the fluorescence conjugated secondary antibodies (60 min at RT) and DAPI (1 mg/ml DAPI/PBS, 1-3 min at RT). Between each step, the brain slices were washed (3 x 5 min with PBS at RT) while gently shaking. All antibodies were diluted in immunostaining blocking solution. After a final washing step (3 x 5 min at RT, PBS), the sections were mounted on object slides with PermaFluor mounting medium.

### **Intra-amygdala kainic acid-induced status epilepticus:**

The procedures of kainic acid-induced status epilepticus were undertaken by Dr. Tobias Engel at the Royal College of Surgeons in Ireland (RSCI) as described [Jimenez-Pacheco et al., 2013], [Kaczmarek-Hajek et al., 2018]. In short, 8-12 week old mice (bred at the RSCI) were anesthetized with isoflurane and maintained normothermic via a feedback-controlled heat blanket. Mice were then placed in a stereotaxic frame and a guide cannula was affixed for kainic acid injection (coordinates from Bregma; AP = -0.94 mm, L = -2.85 mm). Status epilepticus was induced via injection of 0.3  $\mu\text{g}$  kainic acid in 0.2  $\mu\text{l}$  PBS into

the basolateral amygdala. Control mice received 0.2  $\mu$ l vehicle. 40 min after injections, mice received intraperitoneal lorazepam (6 mg/kg) to curtail seizures. 24 hrs after lorazepam injection, mice were killed and perfused with PFA (4% PFA/PBS). The brains were post-fixed (4% PFA/PBS overnight at 4°C), embedded in 2% agarose, and cut into 30  $\mu$ m sections using a vibratome. Brain sections were stored in ethylene glycol at -20°C.

### **2.2.5.3. Immunostaining of adherent cells**

Cells plated on coverslips were fixed with 3.7% PFA/PBS for 10 min at RT and afterwards washed twice with PBS. After the permeabilization of the cells with 0.5% Triton X-100/PBS, they were blocked with immunostaining blocking solution for adherent cells (60 min at RT). Fluorescent labeling of the cells was achieved by incubation with the primary antibodies (16-24 hrs at 4°C), fluorescence conjugated secondary antibodies (60 min at RT) and DAPI staining solution (1 mg/ml DAPI/PBS, 1-3 min at RT). After each labeling step the cells were washed in 0.1% bovine serum albumin (BSA)/PBS (3 x 5 min at RT) and finally rinsed in mill-Q<sup>®</sup> H<sub>2</sub>O before they were mounted on object slides with PermaFluor mounting medium. All antibodies were diluted in 2% BSA/PBS according to section 2.1.5.

### **2.2.6. Isolation and cultivation of primary cells**

#### **2.2.6.1. Cells in the bronchoalveolar lavage fluid**

Mice were euthanized using CO<sub>2</sub> and bronchoalveolar lavage fluid (BALF) was collected as described [Sun et al., 2017]. In short, a blunt end 22G needle was inserted into the trachea and 0.8 ml of PBS was four times slowly injected and aspirated. The recovered lavage fluid was transferred into a new 1.5 ml tube. This step was repeated three times. The BALF was centrifuged at 800 x g for 10 min at 4°C and the cells were resuspended in 200  $\mu$ l PBS and combined. The combined fluid was again centrifuged at 800 x g for 10 min at 4°C and the bronchoalveolar lavage cells were then resuspended in 200  $\mu$ l ammonium-chloride-potassium erythrocyte lysis buffer. After 10 min, lysis was stopped by the addition of 1 ml PBS. The solution was then centrifuged at 800 x g for 10 min

at 4°C and the cell pellet was resuspended in 400  $\mu$ l PBS.  $10^5$  cells were plated on poly-L-lysine coated cover slips and used for immunofluorescence stainings.

### **2.2.6.2. Isolation of peritoneal macrophages**

Mice were euthanized using isoflurane and subsequently 5 ml of ice cold Hanks' balanced salt solution (HBSS) was injected into the peritoneal cavity using a 27 G needle. The peritoneum was then gently massaged to detach the cells and afterwards, as much fluid as possible was collected and transferred into a 50 ml falcon. This step was repeated twice in order to increase the yield. The collected cell suspension was centrifuged at 800 x g for 10 min at 4°C and cells were resuspended in 2-5 ml cell culture medium.  $10^5$  cells were plated on poly-L-lysine coated cover slips and cultured overnight at 37°C (95% O<sub>2</sub>, 5% CO<sub>2</sub>) before they were used for immunofluorescence stainings.

### **2.2.6.3. Primary microglia culture**

P4-P6 mouse pups were decapitated and brains transferred into ice cold Dulbecco's modified Eagle's medium (DMEM) supplemented with 1% Pen/Strep. Cerebelli and olfactory bulbs were removed and the genotype of the pups was checked for GFP fluorescence using a Typhoon<sup>TM</sup> scanner. The tissue from five pups was transferred into 5 ml of preheated trypsin ethylenediaminetetraacetic acid (EDTA) solution, minced into small pieces and incubated for 15 min at 37°C in a water bath. Afterwards, trypsin digestion was stopped by adding 20 ml of cell culture medium. Cells were pelleted by centrifugation at 800 x g for 3 min, resuspended in 5 ml cell culture medium and triturated with a 1 ml pipet tip. After adding additional 15 ml of preheated cell culture medium, cells were counted in a hemocytometer and  $7 \times 10^6$  cells were plated in T75 flasks. Seeded flasks were transferred into a cell culture incubator at 37°C (95% O<sub>2</sub>, 5% CO<sub>2</sub>) and medium was changed every 2-3 days. After 14 days, microglia were split from astrocytes by shaking the flask for 3-4 hrs at 300 rpm and tapping vigorously on the bench top. The supernatant, containing the floating microglia, was centrifuged at 1500 rpm for 5 min and cells were resuspended in 1 ml cell culture medium and afterwards plated on poly-L-lysine coated cover slips. Microglia were used for subsequent experiments on the following day.

## 3. Results

### 3.1. Characterization of the P2X7-EGFP BAC transgenic mouse model

#### 3.1.1. Protein expression levels and stability of expression

The P2X7-EGFP BAC transgenic mouse model in which the P2X7 receptor is fused via a strep-heptahistidyl-linker to the reporter protein EGFP was previously generated (for details refer to [Kaczmarek-Hajek et al., 2018]). The BAC transgenic approach should allow P2X7-EGFP overexpression under the control of its endogenous promoter at near physiological or moderate over-expression levels. Five P2X7-EGFP BAC transgenic mouse lines were selected for the initial characterization: three P2X7(451L)-EGFP constructs (Line 59, 46 and 61) and two lines with a putative gain of function polymorphic P2X7(451P)-EGFP construct (Line 15 and 17) [Adriouch et al., 2002] [Sorge et al., 2013]. All of them efficiently express the EGFP-tagged fusion protein, which can be visualized by direct EGFP fluorescence in the SDS polyacrylamide gel after electrophoresis. To analyze the protein expression levels of the different BAC transgenic mouse lines, equivalent amounts of membrane extracts from transgenic mouse cerebra were loaded on a gel and after electrophoresis, the fluorescence intensity of P2X7-EGFP was analyzed using a Typhoon<sup>TM</sup> fluorescence scanner. Comparison of the EGFP signal intensities of the samples from the five BAC transgenic mouse lines indicated that each line expresses different quantities of the P2X7-EGFP fusion construct. The protein expression levels correlated well with the number of integrated BAC copies determined by Dr. Volker Eulenburg via southern blot analysis (4-15 integrated BAC copies), which demonstrates that the majority of the integrated copies is functional and leads to the expression of the actual fusion protein (Figure 5). The highest protein expression was detected in lines 17 and 61, while line 59 showed the lowest expression levels. Mice from line 61 developed

significant motor deficits and fluorescence *in situ* hybridization (FISH) analysis (ChromBios GmbH, Nussdorf) revealed a partial trisomy. Therefore, line 17 was used to conduct most of the subsequent experiments.

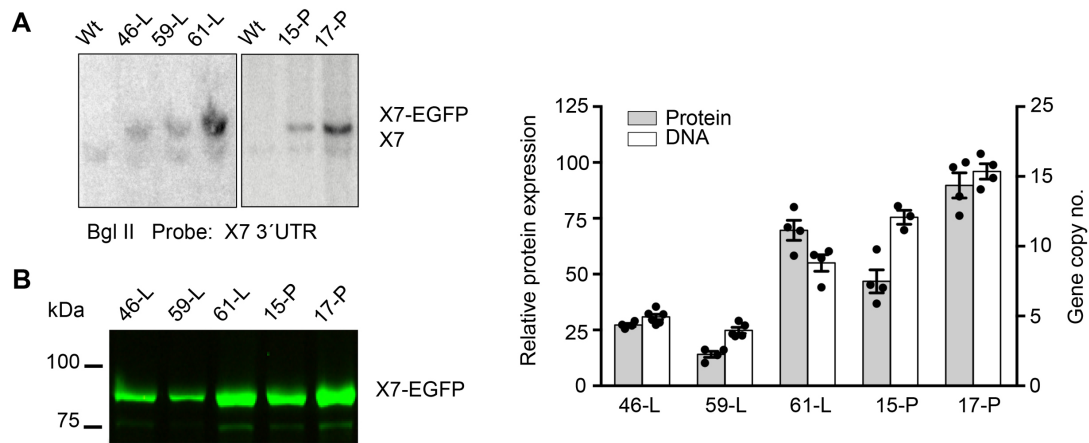


Figure 5 – **Comparison of the number of integrated BAC copies and protein expression levels of the five different transgenic mouse lines:** (A) Southern blot analysis conducted by Dr. Volker Eulenburg (transgenic *P2rx7*, 5277 bp; endogenous *P2rx7*, 4561 bp). (B) Representative acrylamide gel after electrophoresis: 60  $\mu$ g total protein of membrane extracts (1% NP40) from transgenic mouse cerebra were loaded and analyzed by direct EGFP fluorescence on a Typhoon<sup>TM</sup> scanner. Protein expression levels correlated well with the number of integrated BAC copies. Data from 3-6 individual mice are shown as mean  $\pm$ SEM.

To ensure a stable integration of the BAC construct into the chromosome of the mice, the expression of the protein was analyzed across successive generations as described above. The comparison of samples from mice of the second filial with those from mice of the sixth generation revealed no alteration in protein expression levels. Furthermore, no significant differences in the samples from transgenic mice with different gender or age (10 weeks compared to 57 weeks) were detected (Figure 6).

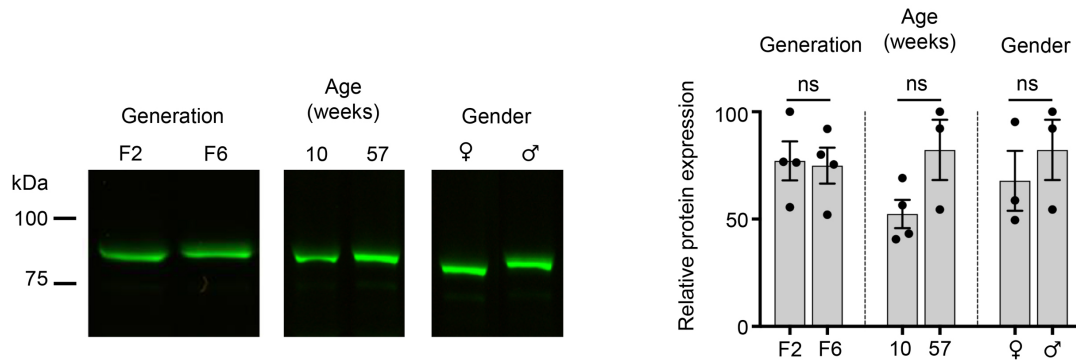


Figure 6 – **Comparison of P2X7-EGFP expression of animals from different generations, with different age and gender:** 50  $\mu$ g total protein from brain extracts from BAC transgenic mice were loaded on SDS polyacrylamide gels and the direct EGFP fluorescence was quantified on a Typhoon™ scanner. Representative gels are shown and data from 3-4 individual mice of line 59 are presented as mean  $\pm$ SD. Significance was analyzed using Student's t-test.

### 3.1.2. Influence on endogenous P2X7 expression

Although the chosen BAC approach should allow P2X7-EGFP expression at physiological or moderate overexpression levels, it cannot be excluded that the altered P2X7 expression might influence the protein expression of the endogenous receptor. The overexpression of EGFP-tagged P2X7 could promote endogenous P2X7 expression, leading to an overall higher P2X7 protein level or in contrast, it can have a negative impact and lead to a decreased expression of the endogenous receptor resulting in an overall lower P2X7 protein level than expected. To analyze the influence of the transgenic P2X7 on the endogenous expression, crude membrane extracts from transgenic (tg) and wild type (wt) mouse cerebella were separated by electrophoresis and the expression of both receptor forms were quantified by measuring the signal intensity (normalized to vinculin signal) after immunoblotting with a P2X7 specific antibody. This quantitative western blot analysis showed that the expression level of the endogenous protein is not altered between samples from tg or wt mice, indicating that overexpression does not significantly affect protein synthesis of the endogenous P2X7 receptor (Figure 7).

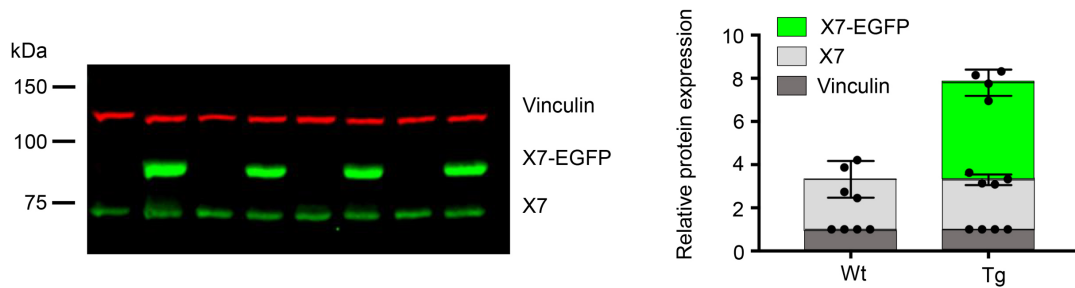


Figure 7 – **Influence of P2X7-EGFP overexpression on the endogenous protein:** 50  $\mu$ g total protein from brain extracts of tg (L17) and wt mice were loaded on the gel and after separation immunoblotted with a P2X7-specific antibody (green). Vinculin was used as a loading control (red). Signal intensity of the fluorescent dye-coupled secondary antibodies was quantified using a LI-COR Odyssey<sup>®</sup> FC imaging system. P2X7 signal was normalized to the loading control. Data from four individual animals are presented as mean  $\pm$ SD. In two independent experiments, no significant difference of endogenous P2X7 expression between tg and wt animals was found using Student's t-test.

### 3.1.3. Protein expression pattern

To demonstrate that the transgenic P2X7-EGFP is regulated by the endogenous P2X7 promoter and shows the same tissue-specific expression as the endogenous protein, expression levels and patterns of both proteins were compared. Therefore, proteins from different brain regions were extracted, separated via SDS-PAGE, and immunoblotted with a P2X7-specific antibody. Quantitative analysis of the signal intensity of endogenous and transgenic P2X7 expression showed that there is no significant difference in the protein ratios (Figure 8). Furthermore, immunofluorescence analysis of P2X7 protein expression indicated that the transgenic protein mirrors the endogenous expression pattern with an overall higher intensity in different tissues (refer to section 3.2).

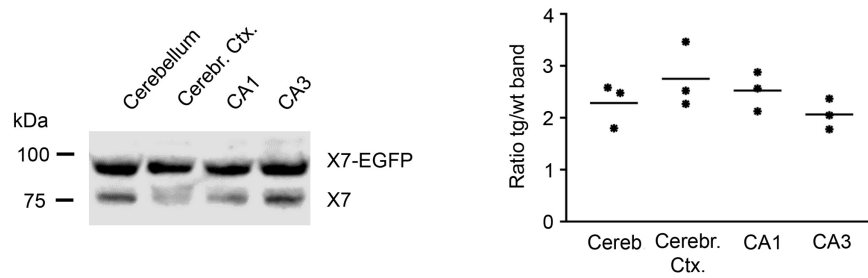
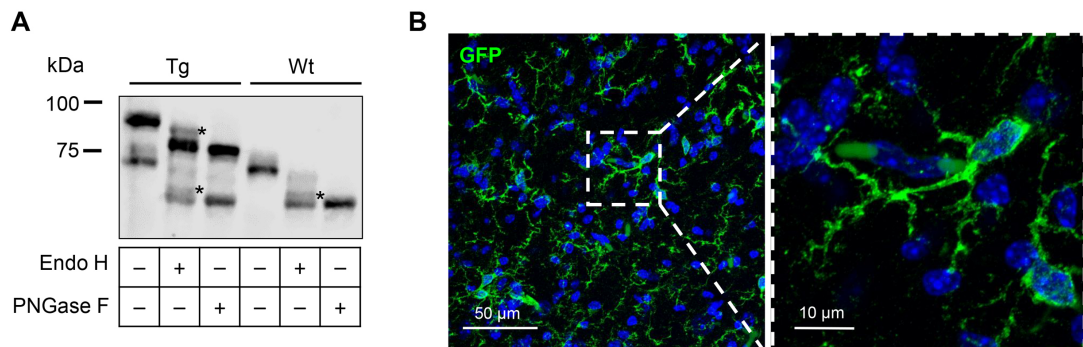


Figure 8 – **Ratios of transgenic and wild type P2X7 protein in different brain regions:** 75 $\mu$ g total protein extract from the indicated regions of tg (L17) brains were separated by SDS-PAGE and immunoblotted with a P2X7-specific antibody. The signal of the fluorescent secondary antibodies was quantified in a LI-COR Odyssey<sup>®</sup> FC imaging system. A representative western blot is shown and data are presented as means from three animals. Cereb. = Cerebellum, Cerebr. Ctx. = Cerebral cortex.

### 3.1.4. Plasma membrane targeting

To determine if the EGFP-tag has a negative impact on folding, on its exiting pathway from the ER, and membrane transport of the P2X7-EGFP fusion construct, protein trafficking was monitored by glycosylation analysis. The use of two deglycosylating enzymes with different cleavage specificity allows examination of the glycosylation status of the proteins. PNGase F hydrolyses all N-linked glycans at the site where they are attached to asparagine. Endo H, in contrast, only cleaves between two N-acetylglucosamines of oligomannose and hybrid glycans. More complex glycans, which are attached in the Golgi apparatus, cannot be hydrolyzed. Therefore, proteins with complex glycan modifications that occur in or downstream of the Golgi apparatus are to a certain degree resistant to Endo H treatment. Glycosylation analysis of endogenous and transgenic P2X7 from membrane extracts of mouse cerebrum revealed that similar to the endogenous receptor, P2X7-EGFP is to a great extent Endo H resistant, indicating a complex glycosylation of the transgenic protein (Figure 9 A). Treatment with PNGase F showed the size of the completely deglycosylated form. To further validate correct trafficking and localization of the fusion construct, confocal laser scanning microscopy was used. Immunostaining with a GFP-specific antibody of brain slices revealed that the receptor can be specifically found in the long and ramified extensions of microglia, indicating specific transport of the protein to subcellular regions (Figure 9 B). Cell type identity was determined by co-

stainings with anti-ionized calcium-binding adapter molecule 1 (Iba1) antibody (data not shown).



**Figure 9 – Glycosylation status and membrane targeting of P2X7-EGFP:** (A) Glycosylation analysis of endogenous and transgenic P2X7. Total protein, extracted from spinal cord of tg (L17) and wt mice, was treated with Endo H (10 IUB miliunits) or PNGase F (20 IUB miliunits) and compared to the untreated sample. P2X7 protein was detected via immunoblotting with a P2X7-specific antibody. Asterisks indicate protein with complex glycosylation, resistant to Endo H treatment. In  $n > 5$  experiments with different organs, no difference in glycosylation between transgenic and endogenous protein was observed. (B) Immunostainings with anti-GFP antibody of brain cryosections. P2X7-EGFP is located at the plasma membrane and specifically found in the long and ramified extensions of microglia, indicating efficient plasma membrane targeting of the transgenic protein.

### 3.1.5. Receptor assembly

In addition to the visualization of the P2X7 receptor, the EGFP tag can also be used to purify the transgenic receptor from complex protein mixtures like membrane extracts. A Strep- and His-tag were inserted as a linker between EGFP and the P2X7 C-terminus to extend the purification strategies and to minimize interference of EGFP with the C-terminus. Purification of the receptor using Strep-Tactin columns revealed poor binding and yielded low amounts of purified protein. However, purification of the transgenic receptor via the His- or EGFP-tag showed an efficient enrichment. While the receptor is eluted from Ni<sup>2+</sup>-NTA agarose beads under native conditions by competitive displacement with a high imidazole concentration, elution from GFP-Trap<sup>®</sup> beads requires harsh conditions (SDS, 90°C or 0.2 M glycine pH 2.0) to dissociate the nanobody-antigen binding. This treatment also destroys the EGFP fluorescence and structure as seen by a size shift of the protein in the SDS polyacrylamide gel. Purification of the transgenic receptor via His- and/or EGFP-tag demonstrated co-purification of the endogenous P2X7 subunit, confirming their co-assembly (Figure 10 A). Fluorescent labeling of all enriched proteins with a Cy5-conjugated NHS-ester showed that the transgenic as well as the endogenous P2X7 subunits are significantly increased, while several other proteins bind unspecifically to the agarose beads and thus appear in the eluates of both the tg and the wt sample. A tandem purification protocol via Ni-NTA agarose beads followed by immunoprecipitation via GFP-Trap<sup>®</sup> allowed recovery of highly pure transgenic and endogenous P2X7 subunits (Figure 10 B).

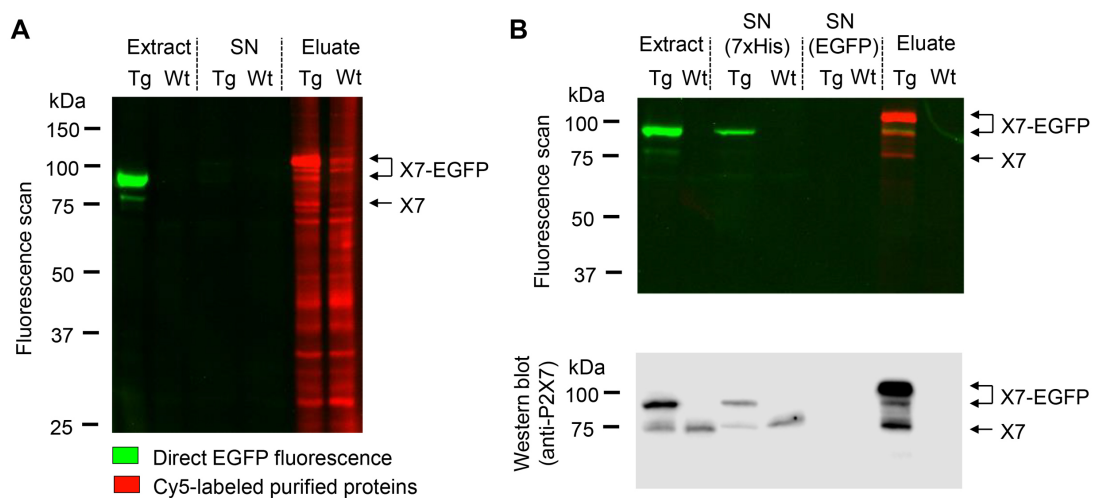


**Figure 10 – Purification of the transgenic protein via its His- and/or GFP-tag:** The P2X7-EGFP fusion protein was purified from brain extracts using an anti-GFP nanobody coupled to agarose beads (GFP-Trap<sup>®</sup>) (A) or a tandem purification protocol via Ni-NTA agarose beads followed by immunoprecipitation via GFP-Trap<sup>®</sup> (B). All proteins bound to the beads were labeled with Cy5 dye and subsequently separated via SDS-PAGE and analyzed with a Typhoon<sup>™</sup> scanner. Western blot analysis with a P2X7-specific antibody confirmed that the enriched proteins are transgenic and endogenous P2X7 subtypes. SN = supernatant

### 3.1.6. Receptor function

To demonstrate that the overexpressed P2X7-EGFP forms a functional ion channel, the transgenic mice were mated with *P2rx7*<sup>-/-</sup> mice to obtain ‘rescue mice’, which express the transgenic but not the endogenous P2X7 receptor. Since *P2rx7*<sup>-/-</sup> mice have a C57BL/6 background, the transgenic P2X7-EGFP FVB/N mice were crossed into C57BL/6 for at least 8 generations before mating. Western blot analysis with a P2X7-specific antibody on tail tips and ear punches had to be performed to confirm successful breeding, since deletion of the endogenous *P2rx7* gene could not be confirmed by PCR in the presence of the transgene. Further western blot analysis of cerebral membrane extracts confirmed the deletion of the endogenous P2X7 in the ‘rescue mice’ (Figure 11 A). Flow cytometry of microglia isolated from these mice showed that the EGFP-tagged receptor can fully rescue the ATP-induced DAPI uptake, which is absent in cells from *P2rx7*<sup>-/-</sup> mice, confirming the formation of a functional channel (Figure 11 B). FACS analysis was conducted by Dr. Björn Rissiek (University Medical Center Hamburg-Eppendorf).

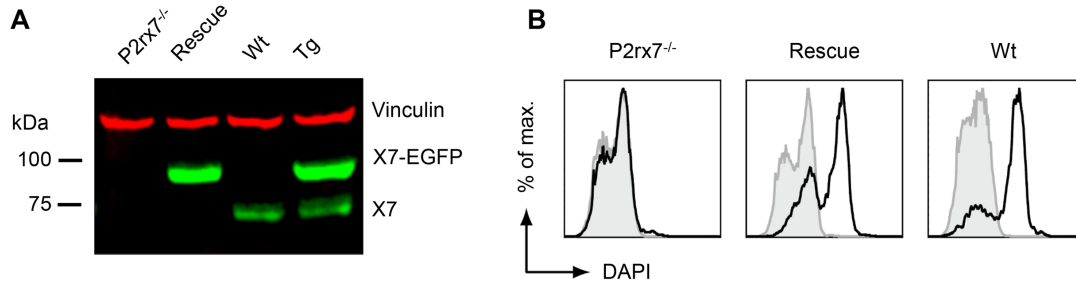


Figure 11 – **Functionality of the transgenic P2X7-EGFP:** (A) ‘Rescue mice’ were obtained by crossing the P2X7-EGFP transgene into the *P2rx7*<sup>-/-</sup> background. Immunoblotting of brain extracts with a P2X7-specific antibody confirmed the deletion of the endogenous receptor in this mouse line. (B) DAPI uptake of microglia from ‘rescue mice’ in comparison to microglia from wt and *P2rx7*<sup>-/-</sup> mice was investigated by FACS analysis. Microglia from ‘rescue mice’ regained the ATP-induced (1 mM) DAPI uptake. FACS analysis was conducted by Dr. Björn Rissiek (University Medical Center Hamburg-Eppendorf). A representative result is shown (n = 3 animals).

## 3.2. Localisation of P2X7 protein in the nervous system

### 3.2.1. Central nervous system

Previous experiments in our lab indicated that microglia and oligodendrocytes are the dominating cell types in the brain expressing the P2X7 receptor, while no expression of P2X7 was detected in neurons [Kaczmarek-Hajek et al., 2018]. To further verify this expression pattern, microglial and oligodendroglial cell-specific *P2rx7*<sup>-/-</sup> mice were generated by mating *P2rx7*<sup>fl/fl</sup> mice with *Cx3cr1*<sup>tm1.1(cre)Jung</sup> and *Cnp*<sup>tm1(cre)Kan</sup> lines [Lappe-Siefke et al., 2003], [Yona et al., 2013]. Quantitative western blot analysis of protein extracts from brain samples from these mice revealed that the *Cx3cr1*-Cre-positive and *Cnp*-Cre-positive mice show  $51.5 \pm 4.5\%$  and  $60.4 \pm 2.9\%$  reduction in P2X7 protein expression respectively (Figure 12). This correlated well with data obtained from quantitative analysis of the respective cell type by co-immunostainings with cell-specific marker proteins of brain sections from P2X7-EGFP transgenic mice [Kaczmarek-Hajek et al., 2018]. This verifies that microglia and oligodendrocytes are the dominant cell types in the brain expressing P2X7.

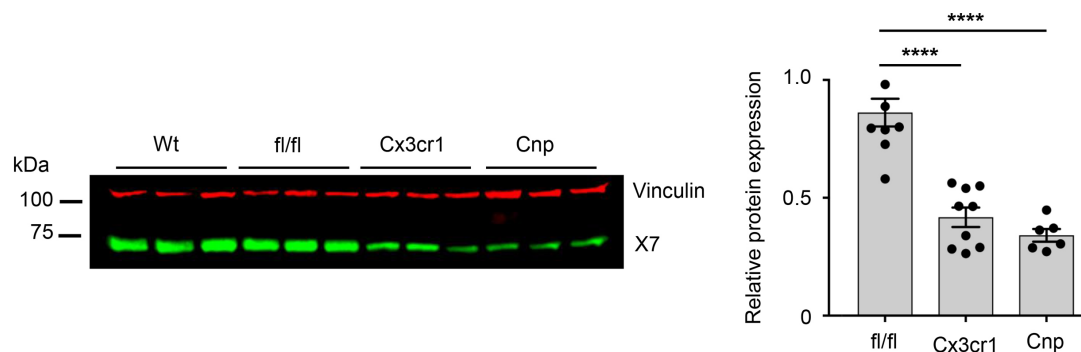


Figure 12 – **Reduction of P2X7 protein expression in cell type-specific knockout mice (CNP-cre and Cx3cr1-cre):** 75  $\mu$ g total protein from cerebrum extracts were immunoblotted with a P2X7-specific antibody (green). Vinculin served as a loading control (red). Fluorescence intensity was quantified using a LI-COR Odyssey<sup>®</sup> FC imaging system and normalized to the P2X7 expression in wt animals. A representative western blot is shown and data are presented as mean  $\pm$ SEM from 6 - 9 animals, from three independent experiments. Significance compared to *P2rx7*<sup>fl/fl</sup> was analyzed using two-tailed unpaired Student's t-test. \*\*\*\* = significant reduction of P2X7 protein expression ( $p < 0.0001$ )

Further analysis of brain sections revealed strong EGFP signal in the cerebellar cortex, hypothalamus, and components of the basal ganglia (pallidum and substantia nigra) (Figure 13 A, left side). Since P2X7 expression was described in immortalized dopaminergic neurons derived from substantia nigra [Jun et al., 2007], the existence of neuronal P2X7-EGFP in basal ganglia was analyzed. Co-stainings with marker for neurons (NeuN-immunopositive cells) and dopaminergic neurons (tyrosine hydroxylase (TH)-immunopositive cells) were performed. In agreement with previous studies on cerebellum and hippocampus in which no neuronal expression in the molecular layers was observed [Kaczmarek-Hajek et al., 2018], also no P2X7-EGFP expression was detected in neurons of the basal ganglia (caudoputamen (CPu), pallidum (Pal), or substantia nigra (SN)), as well as in the hypothalamus (Hy) (Figure 13 B/C). Instead, most of the EGFP-positive cells showed co-labeling with a marker for microglia (Iba1-immunopositive cells) (Figure 13 D). The strong EGFP signal in the cerebellar cortex revealed the expression of P2X7 in this region in Bergmann glia cells (S100 $\beta$ -immunopositive cells) [Kaczmarek-Hajek et al., 2018].

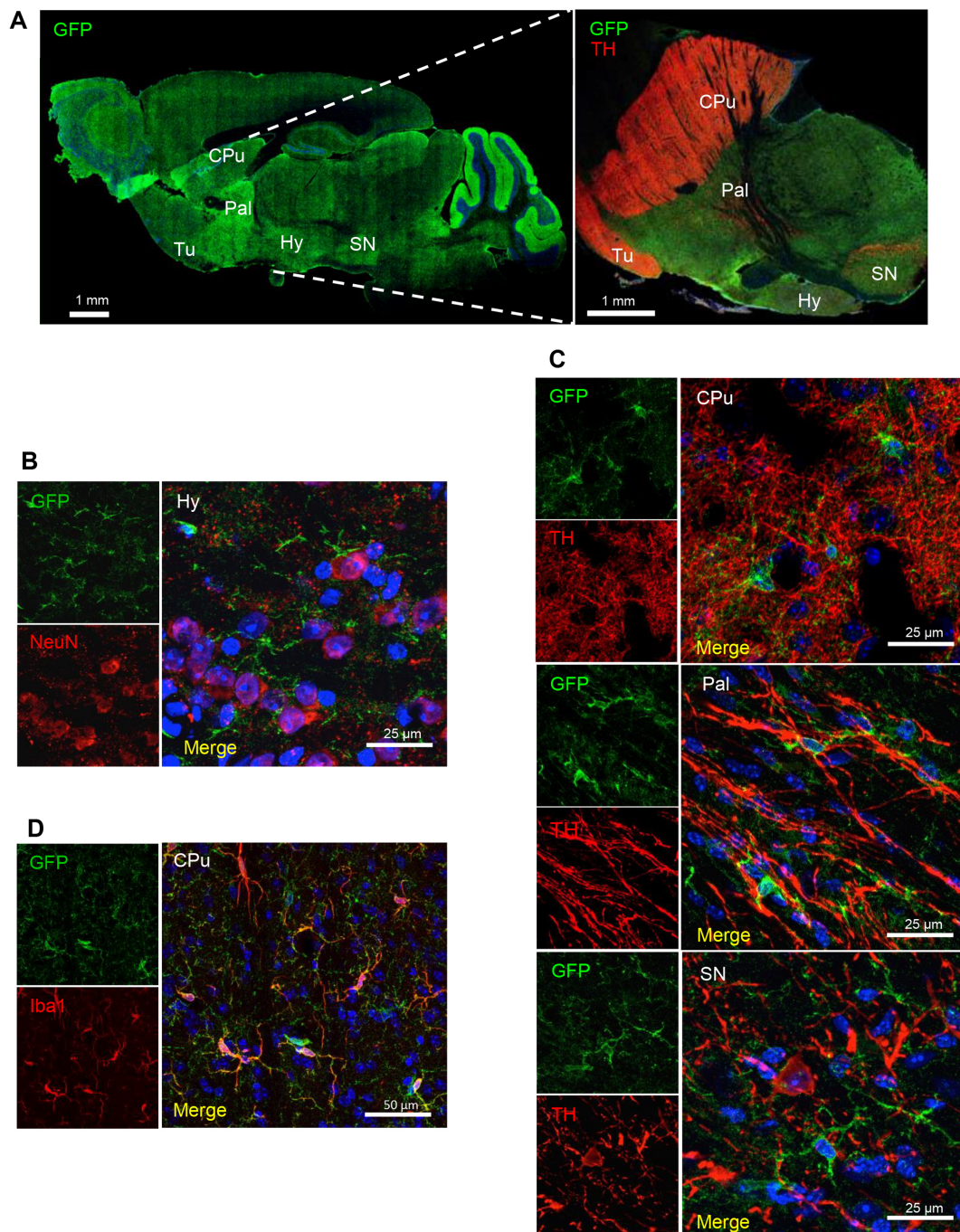


Figure 13 – **Co-staining of EGFP with cell type-specific markers in hypothalamus (Hy), caudoputamen (CPu), pallidum (Pal) and substantia nigra (SN):** (A) Tile-scan of EGFP-stained sagittal sections of a transgenic (L17) mouse brain as an overview to identify regions shown in B-D. In addition, a tile-scan of a co-staining with TH is shown to indicate the dopaminergic neurons. B-D show detailed views of the indicated regions. (B) Co-staining with neuronal marker (NeuN). (C) Co-staining with marker for dopaminergic neurons (TH). (D) Co-staining with marker for microglia (Iba1). DAPI staining is shown in blue. Tu = Olfactory tubercle.

Since increased P2X7 protein expression was detected upon ATP stimulation in neuronal cell culture [Ohishi et al., 2016] and astroglial P2X7 expression has been described [Salas et al., 2013], it was tested if a pathological or damaging conditions (e.g. neuroinflammation or tissue damage) could induce neuronal or astroglial protein expression. Therefore, a model of unilateral intra-amygdala kainic acid-induced status epilepticus was used to analyze P2X7-EGFP expression during CNS injury. However, no neuronal or astroglial P2X7-EGFP expression was observed in the CA3 region of the hippocampus 24 hrs after induction of status epilepticus, although a clear activation of microglia by the change in their morphology from a ramified to an amoeboid state and neuronal damage in the CA3 region was detected, as described [Engel et al., 2012]. P2X7-EGFP signal was clearly overlapping with a marker for microglia (Iba1-immunopositive cells), but not with markers for neurons (NeuN-immunopositive cells) and astroglial cells (GFAP- or S100 $\beta$ -immunopositive cells) (Figure 14).

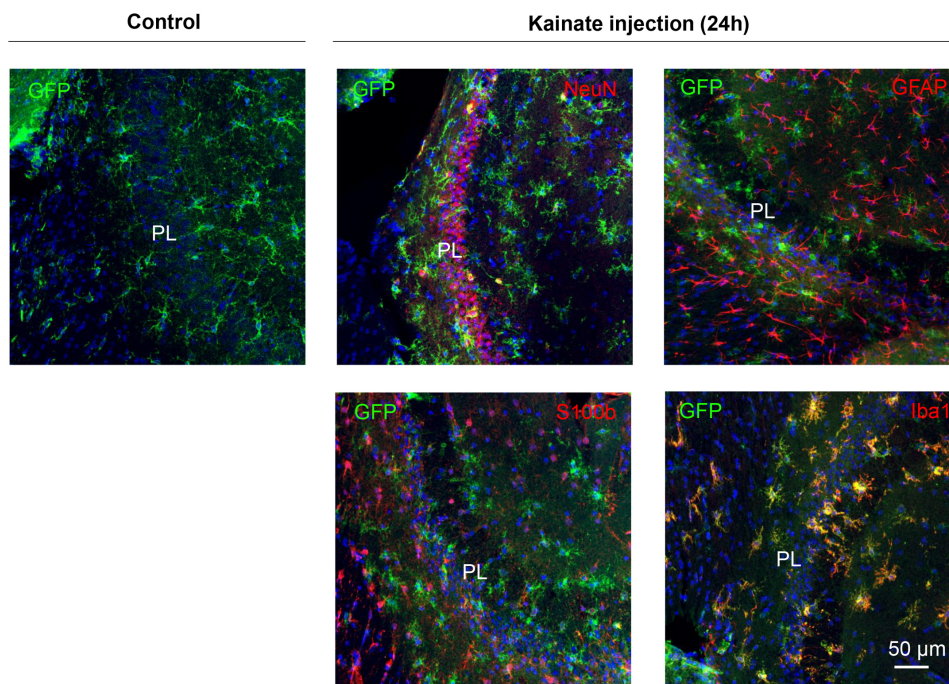


Figure 14 – **Expression of P2X7-EGFP after kainic acid-induced status epilepticus:** Co-labeling of P2X7-EGFP with marker proteins for neurons (NeuN), astrocytes (GFAP; S100 $\beta$ ), and microglia (Iba1) in the CA3 region of the hippocampus 24 hrs after induction of status epilepticus. P2X7-EGFP signal was detected in microglia but not in neurons or astrocytes. Induction of status epilepticus led to a change in microglia morphology, indicating their activation. Microglia from control-injected transgenic mice were non-activated (Upper left). DAPI was used as a nuclear counterstain (blue). PL = Pyramidal cell layer

### 3.2.2. Peripheral nervous system

To test for neuronal expression of P2X7 in the peripheral nervous system, stainings of cryosections from DRGs were performed. Also here, no co-staining of EGFP with neuronal markers (NeuN-immunopositive cells) was observed (Figure 15 A). To confirm these results in wt mice, additional stainings of DRGs were performed with a novel P2X7-specific nanobody-based heavy chain antibody (7E2-rabbit-IgG) [Danquah et al., 2016], which also revealed no neuronal expression of P2X7 (Figure 15 A). Instead, a clear signal was detected in the cells surrounding the large sensory neurons. To determine the identity of this cell type, co-stainings with the satellite cell marker glutamine synthetase (GS) were performed. Indeed, most but not all of the GS-immunopositive cells were also EGFP-positive (Figure 15 B), which is in agreement with previous findings [Zhang et al., 2005], [Chen et al., 2012b]. In addition, P2X7 expression in cells surrounding the neurons that were not satellite glial cells was detected. To see if the EGFP-positive but GS-negative cells represent myelinating Schwann cells, myelin protein zero (MPZ) was used as a marker for co-stainings. However, no co-labeling was detected (Figure 15 B). The exact identity of these cells has to be further analyzed in additional studies but there is no evidence for neuronal expression of P2X7 in DRGs.

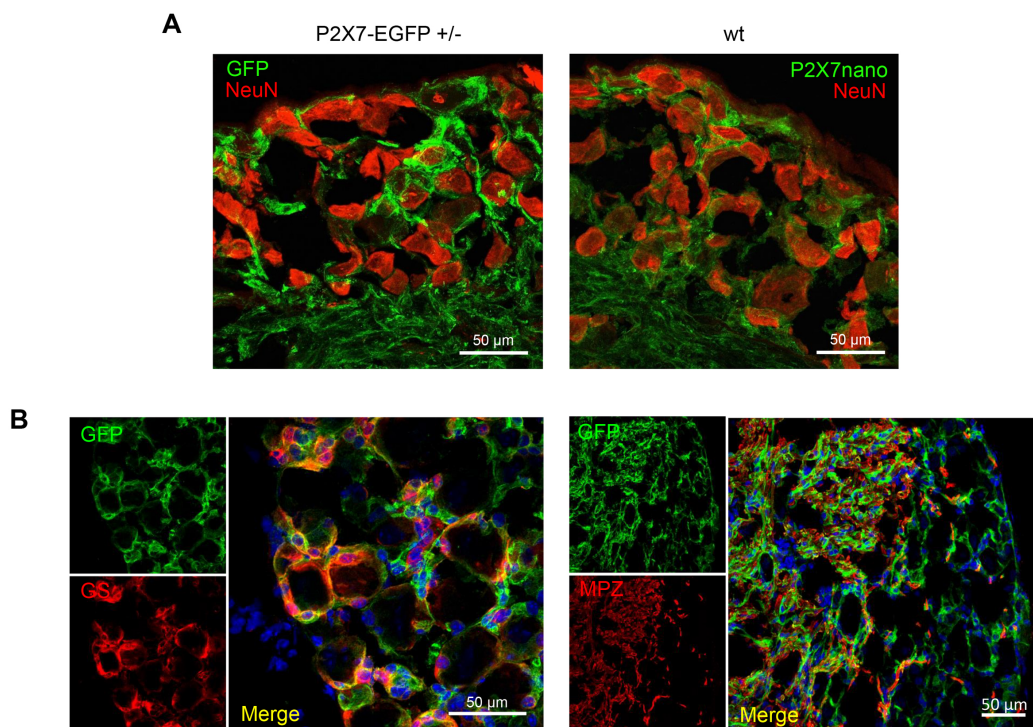


Figure 15 – **Localization of P2X7 in dorsal root ganglia:** (A) Co-staining of anti-GFP or anti-P2X7 nanobody-based heavy chain antibody with neuronal marker (NeuN). (B) The signal of the EGFP-positive cells surrounding the sensory neurons is partially overlapping with a marker for satellite glia cells (GS). No co-staining with the Schwann cell marker MPZ was observed, but cells were closely associated. DAPI staining is shown in blue.

### 3.3. Interaction and interrelation of P2X4 and P2X7 subunits

#### 3.3.1. Localization of P2X4 and P2X7 subunits

Among the other P2X receptor subtypes, P2X4 shares the highest sequence similarity with P2X7. Their encoding genes are adjoining on the same chromosome and are thought to have arisen by gene duplication. Thus, a number of studies arguing for and against a mutual interrelation, a physical interaction, or heteromeric assembly of P2X7 and P2X4 were published in recent years (refer to section 1.3.4.9). Both subtypes are highly expressed in the lung, in particular in pulmonary epithelial cells and macrophages and have been shown to contribute to the secretion of lung surfactant [Miklavc et al., 2013], [Mishra et al., 2011] and to enhanced inflammation in the pulmonary tissue under pathological conditions. Accordingly, it was shown that both receptors are involved in a variety of respiratory diseases, like asthma, ALI, and chronic obstructive pulmonary disease (COPD) [Burnstock et al., 2012], [Savio et al., 2018], [Zech et al., 2016]. Since the P2X4 and P2X7 subtypes share common functions and are expressed to a large extent in the same cell types, it was investigated how they are expressed in native lung tissue and if both subtypes co-localize in the same cell.

Immunostainings of lung sections with the P2X7-specific nanobody-based heavy chain antibody (7E2-rabbit-IgG) showed that P2X7 signal is found along the lung alveoli with strong signal in single cells located at the interphases between alveoli and bronchioles or pulmonary blood vessels, which most likely represent immune cells (Figure 16 A). The same expression pattern was observed in lung sections from wt mice but with a lower signal intensity. This further confirms that the transgene mirrors the endogenous expression pattern but with an overall higher expression level compared to the wt. Staining of sections from *P2rx7<sup>-/-</sup>* mice validated the specificity of the used nanobody. Furthermore, signal of the P2X7 nanobody-based antibody is overlapping with the signal of the anti-GFP antibody, demonstrating that both antibodies recognize the P2X7-EGFP fusion construct with a high specificity (Figure 16 B). Co-stainings with cell type-specific markers showed that the EGFP-positive cells at the alveoli represent mostly alveolar type (AT) I cells (aquaporin-5 (AQP5)-immunopositive cells) (Figure 16 C, left). However, since alveoli are tightly packed with different cell types and single cells are hardly to distinguish, P2X7 protein expression in other cell types

like microvascular endothelial cells and fibroblasts cannot be excluded. The single cells with a more intense anti-GFP labeling at the interphases were identified as interstitial macrophages (Iba1-immunopositive cells) (Figure 16 C, right).

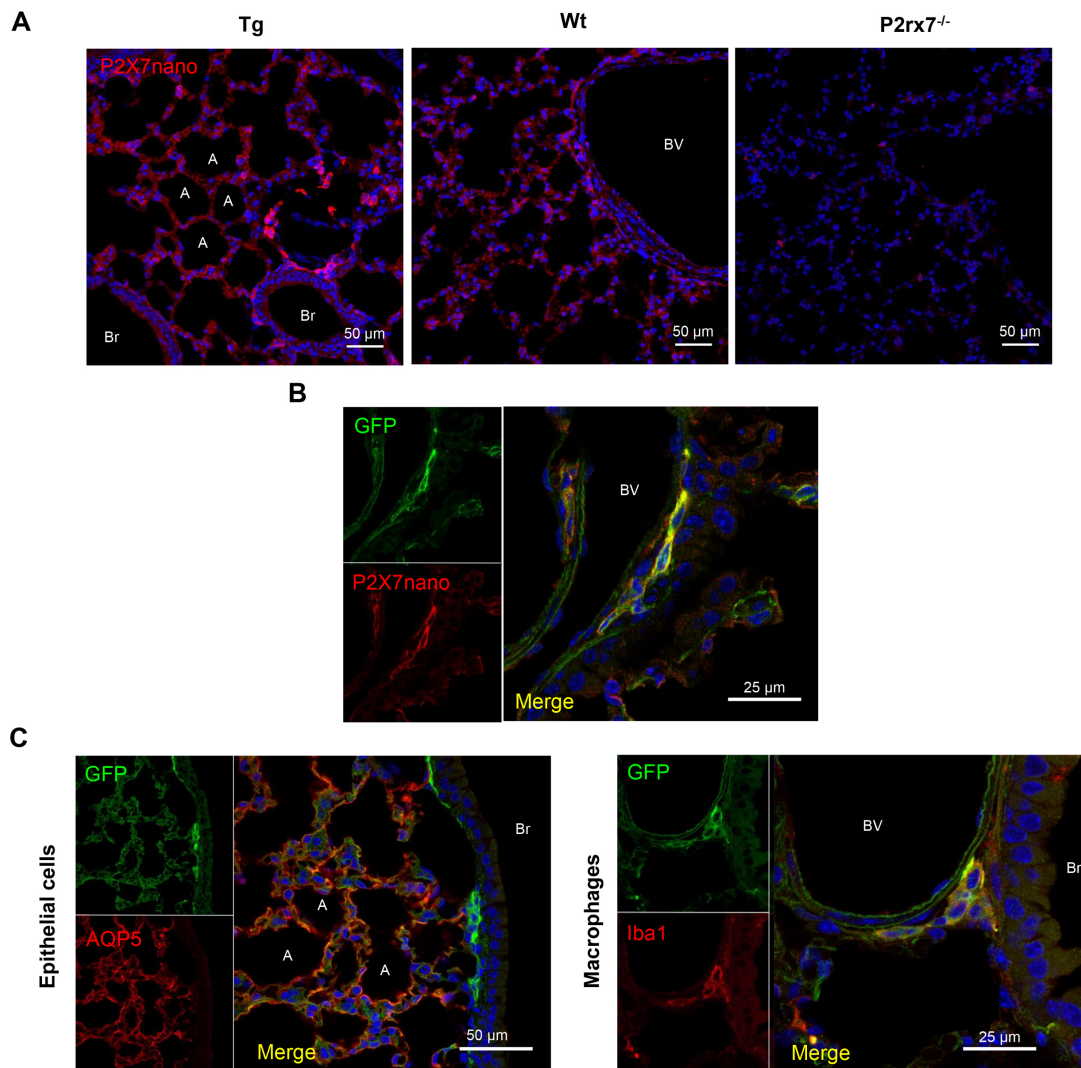


Figure 16 – **Cell type-specific P2X7 protein expression in the lung:** (A) Immunostaining with P2X7 nanobody-based antibody of lung cryosections from tg, wt, and *P2rx7*<sup>-/-</sup> mice. (B) Co-stainings with anti-P2X7 nanobody and anti-GFP antibody showing specificity of both antibodies. (C) The majority of EGFP-positive cells are also positive for AQP5, a marker for ATI cells. Single cells at bronchioles or pulmonary blood vessels with high EGFP expression represent macrophages (Iba1-immunopositive cells). Nuclear DAPI staining is shown in blue. A = Alveolus, Br = Bronchiole, BV = Blood vessel.

Co-stainings of the P2X4 and P2X7 subtypes in native tissue have previously been difficult due to the lack of suitable antibody combinations. However, the novel BAC transgenic mouse model now allows the use of EGFP to localize P2X7 protein expression. In lung sections of transgenic mice the two subtypes showed a distinctly different expression in the alveolar epithelium. While P2X7-EGFP is consistently expressed among the respiratory epithelium, the P2X4 signal was only detected in single cells at crossing points between the alveoli, which most likely represent ATII cells (Figure 17 A, left). This finding is in agreement with a recently described role of P2X4 in the modulation of lung surfactant secretion [Miklavc et al., 2013]. Lung surfactant is stored in lamellar bodies and their exocytosis results in a local, fusion-activated  $\text{Ca}^{2+}$  entry (FACE). This FACE is mediated by P2X4 receptors located on lamellar bodies and has been shown to facilitate surfactant release [Miklavc et al., 2011].

Most, but not all of the cells with a particular high P2X7-EGFP expression also showed expression of the P2X4 subtype (Figure 17 A, right), confirming the co-expression of both in macrophages [Bowler et al., 2003]. Although both subtypes are partly co-expressed in the described cell types, they showed a clear difference in their subcellular localization. While P2X7-EGFP signal was mostly localized at the cell membrane and to some extent in cytosolic regions, P2X4 showed almost complete intracellular expression. Fluorescence signals were mainly detected in structures around the nucleus, but not at the plasma membrane. To confirm our results from native lung tissue, we performed additional immunostainings in two other phagocytic cell types, which express the P2X4 and P2X7 subtypes: isolated peritoneal macrophages and microglia from brains of animals at postnatal day 4-7 (P4-7). Again, both subtypes showed a clear difference in their expression, with no detection of P2X4 signal at the plasma membrane (Figure 17 B and C). Instead, P2X4 signal was overlapping with the lysosome marker protein CD68 (Figure 17 B). This is in agreement with previous findings, where P2X4 signal was overlapping with the signal of lysosome-associated membrane glycoprotein 1 (LAMP-1) in macrophages, microglia, endothelial cells, and HEK293 cells [Guo et al., 2007], [Qureshi et al., 2007].

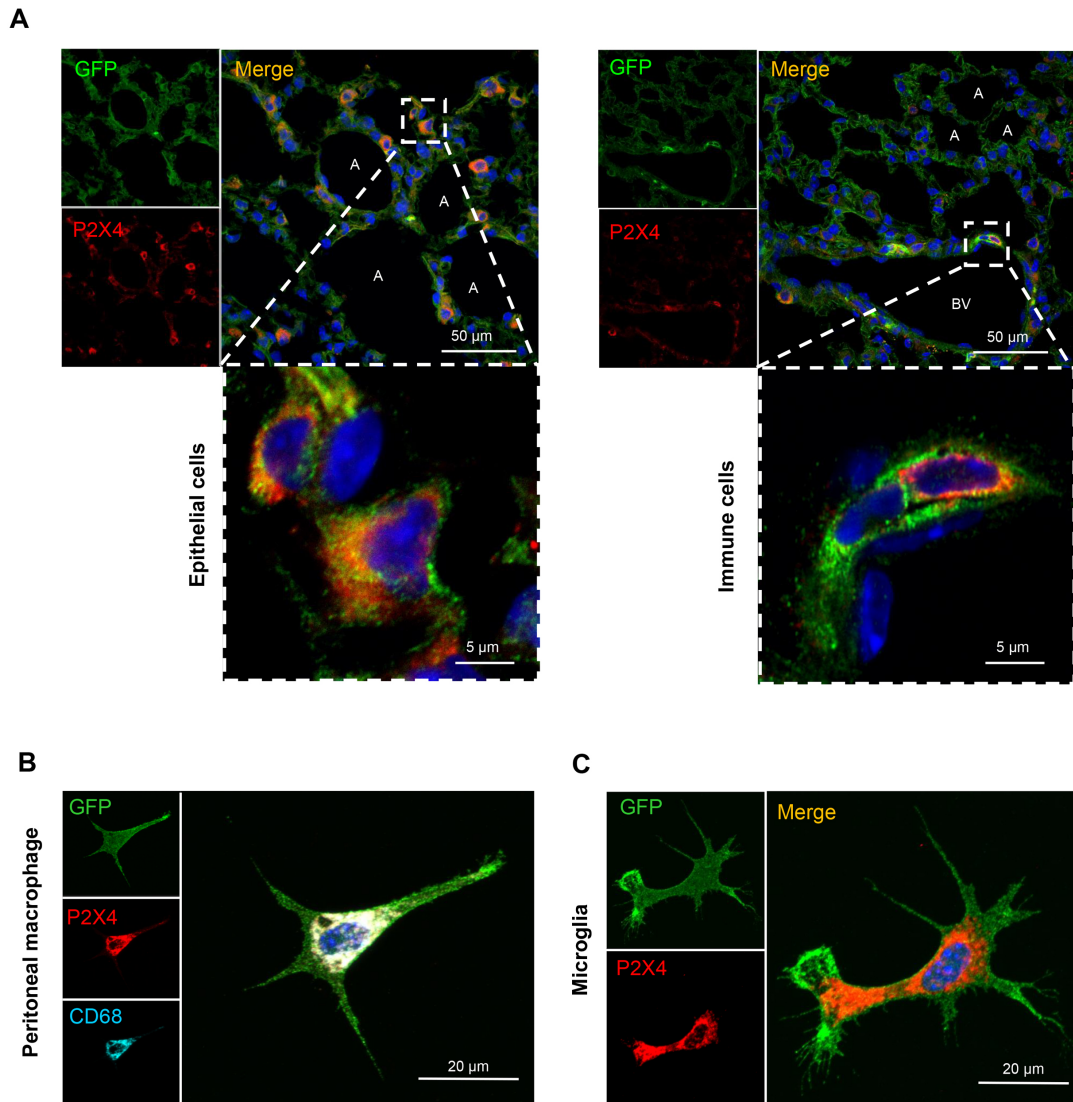


Figure 17 – **Subcellular localization of P2X4 and P2X7 protein:** Confocal images showing subcellular distribution of P2X4 and P2X7 receptors. Cryosections ( $10\ \mu\text{m}$ ) of lung tissue (A) or primary cells (B and C) from transgenic mice were immunostained with anti-GFP (green) and anti-P2X4 (red) antibodies. Detail images of isolated cells show peritoneal macrophages (B) co-labeled with the lysosome marker CD68 (cyan) or cultured primary microglia from brains of transgenic mice at postnatal day 4-7 (C). DAPI staining is shown in blue. A = Alveolus, BV = Blood vessel.

### 3.3.2. Mutual interrelation

In previous studies, the cross-talk between the P2X4 and the P2X7 receptor has been analyzed at mRNA and protein expression levels to show their mutual interaction. Data from mouse kidney showed a significant reduction of P2X4 and P2X7 mRNA levels via the knockout of the respective other subunit [Craigie et al., 2013]. Therefore, the question was addressed if overexpression of P2X7 in the BAC transgenic mouse model or the genetic ablation of one of both subtypes influences mRNA levels of the respective other subunit in lung tissue. Although a slight trend in the data was observed, the mRNA level of each P2X subunit was not significantly altered by P2X7-EGFP overexpression or genetic ablation of the other P2X receptor (Figure 18 A). In contrast to the qRT-PCR data, a previous study that focused on protein expression showed a reverse relationship: in an alveolar epithelial cell line, downregulation of one receptor subtype via shRNA resulted in an increase in protein expression of the other [Weinhold et al., 2010]. We therefore also analyzed if any mutual interrelation on the level of protein expression can be observed in the mouse models. In lung tissue, neither the depletion of P2X7 protein, nor the overexpression of P2X7 in the BAC transgenic mice had a significant influence on P2X4 protein levels. Furthermore, no change in P2X7 protein expression in *P2rx4*<sup>-/-</sup> mice was detected (Figure 18 B).

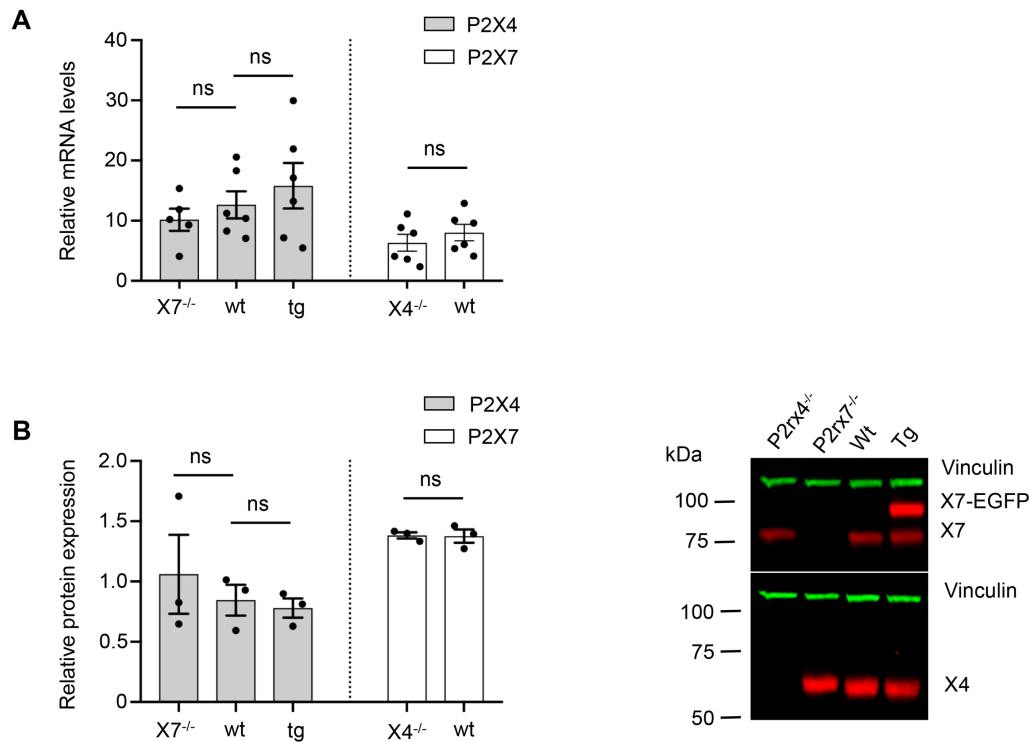


Figure 18 – **Mutual interrelation of P2X4 and P2X7 expression:** (A) Total RNA was isolated from 20-30 mg lung tissue and after reverse transcription quantified in a LightCycler<sup>®</sup> 480 system. RPLP0 and PPIA were used as reference genes to calculate relative P2X4 and P2X7 mRNA levels. No significant changes in P2X4 mRNA levels were observed in samples of P2X7-EGFP transgenic or *P2rx7*<sup>-/-</sup> animals compared to wt samples (grey bars). In addition, no significant alteration in P2X7 mRNA level was detected in samples of *P2rx4*<sup>-/-</sup> animals (white bars). (B) 50  $\mu$ g total protein of membrane extracts from lung tissue was separated by SDS-PAGE and immunoblotted with a P2X4- or P2X7-specific antibody (red). Protein levels were quantified via fluorescence intensity of the secondary antibodies and vinculin was used as a loading control for normalization (green). Protein expression of each P2X subtype was not significantly altered by P2X7-EGFP overexpression or genetic ablation of the respective other P2X receptor. Data are presented as mean  $\pm$ SEM from three to five animals. Significance was analyzed using Student's t-test.

### 3.3.3. Physical interaction

A physical interaction between P2X4 and P2X7 receptor has been shown before in recombinant expression systems and in macrophages [Antonio et al., 2011], [Pérez-Flores et al., 2015], [Schneider et al., 2017]. To further examine this, pull-down experiments were performed using the EGFP-tagged P2X7 receptor as a bait. Results from experiments conducted with heterologous expressed proteins in *X. laevis* oocytes were compared with those from native transgenic mouse tissue. Parts of this work were carried out by Stella Schieferstein during her master thesis under my supervision.

Plasmid DNA constructs for synthesis of untagged mouse P2X4 and P2X7 cRNA for the injection into *X. laevis* oocytes were already available in the lab. The EGFP-tagged P2X7 construct was designed according to the fusion protein expressed in the P2X7-EGFP transgenic mouse line. Therefore, the cDNA coding for the Gly-Strep-tagII-7xHis-Gly linker sequence and EGFP were inserted into the plasmid coding for P2X7 via Gibson assembly. Colony-PCR and subsequent sequencing verified the correct insertion. Three days after cRNA injection, the oocytes were used for the actual pull-down experiments. These experiments showed that while P2X4 is co-purified with P2X7-EGFP in the heterologous system (Figure 19 A), there is no evidence for a physical interaction in the native lung tissue (Figure 19 B). To exclude that this interaction gets lost due to the choice of detergent, the same pull-down experiment were performed with membrane extracts from lung tissue using three different non-denaturing detergents (NP40, n-dodecyl  $\beta$ -D-maltoside, and digitonin). However, we did not detect any interaction (not shown), suggesting that the interaction in recombinant systems is an artifact, possibly due to aggregation of overexpressed protein.

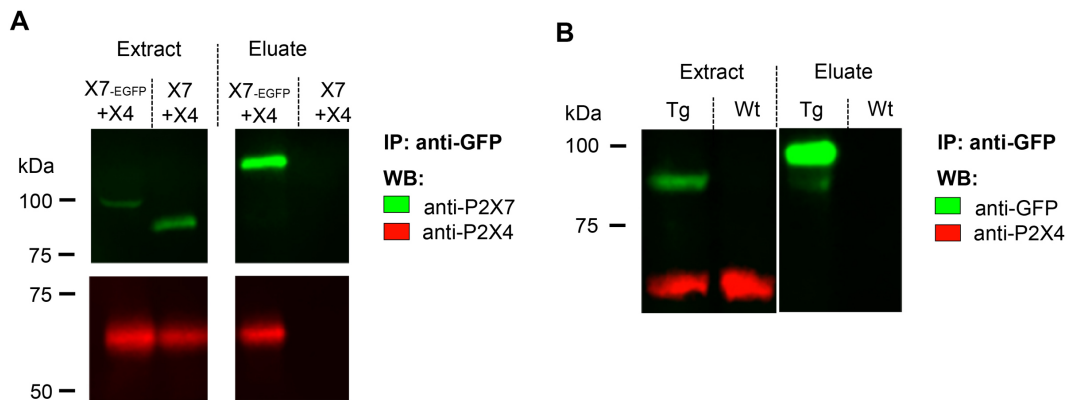


Figure 19 – **Physical interaction of P2X4 and P2X7 receptors:** (A) P2X4 was co-expressed with P2X7-EGFP or untagged P2X7 as control in *X. laevis* oocytes. After immunoprecipitation of P2X7-EGFP via anti-GFP nanobody the gel was immunoblotted with anti-P2X7 and anti-P2X4 antibodies. (B) Immunoprecipitation of P2X7-EGFP from native lung tissue. Anti-GFP and anti-P2X4 antibodies were used for immunoblotting. Samples from wt animals served as a negative control. Parts of these experiments were conducted by Stella Schieferstein during her master thesis under my supervision.

### 3.4. Identification of novel interaction partners of P2X7

#### 3.4.1. Co-immunoprecipitation experiments

Although P2X7 is a promising drug target, the molecular basis of interactions with other proteins or signaling pathways is not well described so far. Therefore, the BAC transgenic mouse model was used to identify novel P2X7 interaction partners and confirm previously proposed interactions. In a first approach, the transgenic P2X7-EGFP receptor was used to identify novel interaction partners by purification and subsequent MS analysis. However, four biological replicates of purified protein samples from brain extracts analyzed by LC-MS/MS revealed no reproducible and significant protein enrichment in samples of transgenic animals. Further control analysis of the purification process by labeling of all enriched proteins with a fluorescent dye and separation by SDS-PAGE showed that in each replicate some proteins were enriched but varied between purification replicates (Figure 20). A possible explanation is that these interactions are very labile and/or transient and the interactors are lost during the multi-step purification

process. Since detergents are necessary to solubilize the receptors prior to the purification process, the protein interactions within the protein complex are likely to become destabilized and interactors might get lost during the purification process.

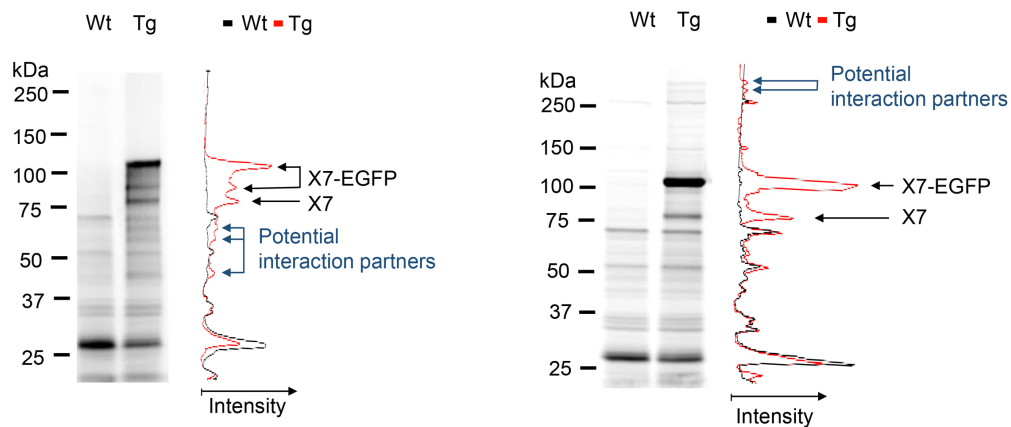


Figure 20 – **Immunoprecipitation of P2X7-EGFP reveals variable enrichment of potential interaction partners:** P2X7-EGFP was immunoprecipitated using anti-GFP nanobody (GFP-Trap<sup>®</sup>). All purified proteins were labeled with Cy5-conjugated NHS-ester and separated by SDS-PAGE. Intensities of the fluorescence signal were plotted next to the gel (wt lane: black, tg lane: red). Peaks in the tg lane that are absent in the wt lane, represent enriched proteins. P2X7-EGFP, endogenous P2X7, and potential interaction partners are marked with arrows. Two representative co-immunoprecipitation experiments are shown.

### 3.4.2. Protein cross-linking of membrane extracts

To overcome the problem with weak and transient protein-protein interactions, we decided for an approach in which protein complexes get covalently fixed via a chemical cross-linker prior to the purification process. Formaldehyde and glutaraldehyde are commonly known as fixatives in histological analysis and have also been used for interaction studies before [Klockenbusch and Kast, 2010], [Subbotin and Chait, 2014]. The major advantages of formaldehyde are: (I) it is a very small compound with a relatively short spacer arm and therefore cross-links only proteins that are in very close proximity, (II) it has a high membrane permeability and does not require the use of organic solvents like DMSO, and (III) it has a very fast reaction time [Sutherland et al., 2008]. Glutaraldehyde on the other hand has a longer spacer arm and a slower diffusion rate but shows

similar chemical reactivity. Both substances were tested for their efficiency in cross-linking of P2X7 complexes. At concentrations between 0.05 - 4% and reaction times from 5 to 60 min, either no band for cross-linked P2X7 complexes were observed or large protein aggregates were formed, which could not get resolved by SDS-PAGE. One major drawback of formaldehyde and glutaraldehyde is the unspecific reactivity. Formaldehyde is not only used for protein-protein, but also for protein-DNA interaction studies since it reacts not only with amino groups but also with imino groups of the DNA. In contrast, bi-functional NHS esters show specificity toward primary amines and are to date the reagents that are most widely used for protein cross-linking studies. NHS esters react with strong nucleophiles, like the  $\epsilon$ -amino group in the sidechain of lysines, to form an amide bond. They also form, to a minor extent, covalent bonds with serine, threonine, and tyrosine residues by reacting with their hydroxyl groups. However, only around 25% of the cross-linked peptides are products from reactive hydroxyl groups of the mentioned amino acids, while the remaining 75% are assigned to lysine [Kalkhof and Sinz, 2008]. We chose the bi-functional NHS ester DSS, since it is membrane permeable and has a medium spacer length. Initial cross-linking experiments with DSS conducted in membrane extracts from brain samples showed that endogenous and transgenic P2X7 can be efficiently cross-linked to obtain covalently fixed P2X7 dimers, trimers, and higher complexes. Using 0.2 mM DSS, the different dimer and trimer combinations of endogenous and transgenic P2X7 can be resolved by SDS-PAGE, while with 2 mM DSS a single broad band at higher molecular weight was obtained (Figure 21 A). Most likely this band contains a mixture of P2X7 dimers and trimers, as well as covalently bound interacting proteins.

### 3.4.3. Optimization of the cross-linking protocol to allow *in-situ* cross-linking of lung tissue

The initial experiments demonstrated that DSS is able to quantitatively cross-link P2X7 complexes in membrane extracts and preserves the complex during the purification process, thus enabling the use of more stringent purification conditions. However, at this stage the receptor was already separated from the plasma membrane and some interactions might have been lost already. Therefore, the protocol was further optimized to allow cross-linking at a stage as close as possible to *in vivo* conditions. Previous cross-linking studies were largely performed

on purified proteins. A small number of cross-linking studies have also been successfully performed *in vivo*, by adding cross-linking reagents directly to cultured cells [Vasilescu et al., 2004], [Tardiff et al., 2007] or in the tissue via transcatheter perfusion [Schmitt-Ulms et al., 2004]. However, these studies used formaldehyde as the classical reagent for *in vivo* cross-linking due to its high membrane permeability. Only recently, the first cross-linking studies were performed without formaldehyde and more advanced cross-linking reagents *in vivo* with HEK293 cells [Kaake et al., 2014] and in heart tissue by dissecting the tissue into 1 mm<sup>3</sup> cubes, prior to the cross-linking process [Chavez et al., 2018].

By using 0.2 mM DSS, cross-linking of P2X7-EGFP complexes was also possible in isolated membrane fractions, homogenized tissue, and even in intact lung tissue when applied by transcatheter perfusion (Figure 21). In contrast, other tested tissues like brain, spleen, or liver revealed poor yields of cross-linked protein after transcatheter perfusion (not shown). However, when concentrations above 1 mM DSS were used in samples where the receptor was still integrated into the plasma membrane, such as homogenized tissue, yields of cross-linked P2X7 complexes were very low. The reason is most likely that the P2X7 complexes were fixed to larger cellular complexes or structures, e.g. cytoskeleton, and could not be extracted. To overcome this problem, detergent was added to the cross-linking solution for tissue homogenates. Addition of 0.05 - 1% NP40 revealed that 0.1% NP40 was sufficient to significantly increase the amount of cross-linked and purified P2X7 complexes (Figure 22 A). Next, conditions for *in-situ* cross-linking via perfusion of the lung were optimized. The best results were obtained when a protocol was used in which the concentration of cross-linker was increased from 0.2 mM to 1 mM in two sequential perfusion steps. The sacrificed mouse was first transcatheterally perfused with phosphate buffer to remove blood cells. Next, 0.2 mM of DSS was perfused. In this initial cross-linking reaction, small amounts of proteins get already covalently fixed and should preserve the basic structure of the protein complex. In a third step, 1 mM cross-linker was injected together with the detergent to allow a slow distribution into the tissue. In this step, the concentration of the cross-linker and the concentration of detergent gradually increases and the P2X7 complexes get quantitatively cross-linked while being solubilized. In a last step, the same cross-linker/detergent mixture was also injected through the trachea to allow the cross-linker to reach the cells from the alveolar side in addition to the vascular side (Figure 22 B). For details refer to section 2.2.3.7. As

seen in figure 22 B, a high yield of cross-linked complex could be extracted and purified and was used for protein-protein interaction analysis by MS.

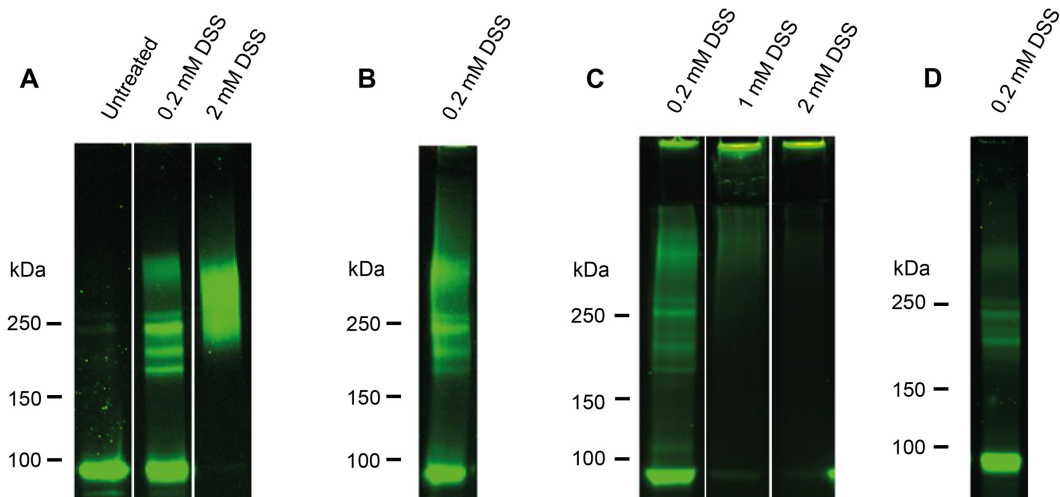


**Figure 21 – P2X7 cross-linking with DSS in protein extract, homogenate and tissue samples:** Different samples were treated with DSS as indicated. After cross-linking, P2X7-EGFP was purified via its polyhistidine-tag, separated by SDS-PAGE and analyzed by direct EGFP fluorescence on a Typhoon™ scanner. (A) Cross-linking of protein extracts from brain samples of transgenic mice. Covalently fixed dimers and trimers of endogenous and transgenic P2X7 can be resolved in samples treated with low concentration of DSS (0.2 mM). Treatment with higher concentrations of cross-linker (2 mM) led to an accumulation of different high molecular weight complexes, most likely consisting of P2X7 dimers, trimers and covalently bound interacting proteins. (B) The detergent-free homogenated membrane, in which proteins are still integrated into the plasma membrane, was treated with 2 mM DSS, leading to incomplete cross-linking. (C) Detergent-free, non-fractionated tissue homogenate treated with different DSS concentrations. While treatment with low DSS concentrations (0.2 mM) resulted in small amounts of cross-linked P2X7 receptors, a higher DSS concentration ( $\geq 1$  mM) led to the formation of insoluble protein-membrane aggregates. (D) Cross-linking of transgenic lung tissue via transcatheter perfusion with 2 mM DSS. With the exception of (D), all experiments were performed with brain samples of transgenic mice.

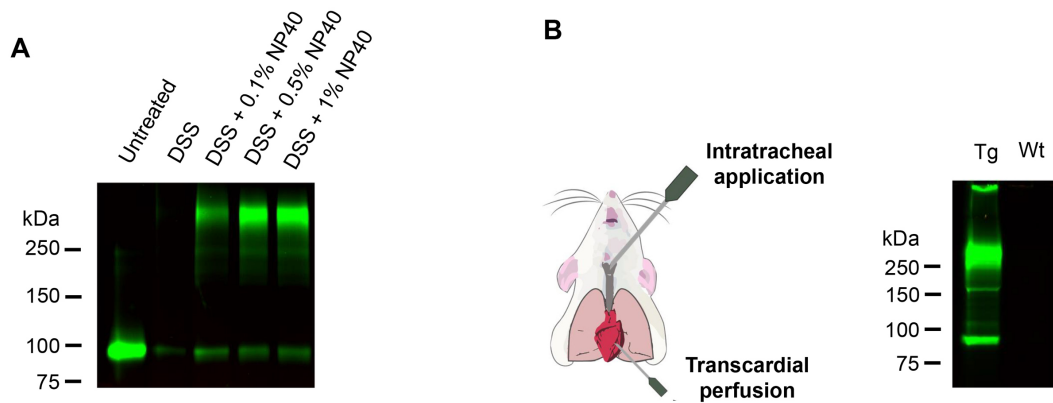


Figure 22 – **Optimization of cross-linking conditions for *in-situ* cross-linking of lung tissue:** (A) Tissue homogenates were treated with the indicated concentrations of DSS and detergent (NP40). (B) Proteins were cross-linked via transcardial perfusion and intratracheal application of DSS (for more details refer to section 2.2.3.7). After purification of P2X7-EGFP via its polyhistidine-tag, the samples were separated by SDS-PAGE and analyzed on a Typhoon™ scanner.

#### 3.4.4. Optimization of the purification protocol

Identification of proteins by LC-MS/MS analysis usually requires an amount of 10 - 20 ng of protein. This protein amount should produce a colloidal coomassie stainable band in the SDS acrylamide gel. By using a known concentration of purified GFP as a standard to compare fluorescence signals in the gel, it was estimated that lungs from 3-5 animals are necessary to get a clear band. In a first approach, protein extracted from lungs from five perfused animals was used to purify the transgenic P2X7 via its GFP tag, using nanobodies against GFP coupled to agarose beads (GFP-Trap®). The purification process was monitored by SDS-PAGE to judge how efficiently the GFP-Trap® nanobodies bind the cross-linked P2X7-EGFP complex and how much unbound protein can be found in the supernatant. The fluorescence scan of the SDS acrylamide gel showed that only a very small amount of protein was found in the supernatant and most of it was immobilized at the agarose beads (Figure 23 A), which indicates that the modification of the proteins by the cross-linking reagent does not disturb the recognition of EGFP by the nanobodies.

In previous experiments, different conditions for the elution of the bound proteins have already been tested. Elution with SDS sample buffer at 90°C resulted in a higher yield of total protein, but the recommended elution with 0.2 mM glycine (pH 2.5) produced higher purity with still sufficient amount of recovered pro-

tein. The reason for this could be that the elution with glycine (pH 2.5) destroys the antigen-nanobody interaction more specifically due to the low pH that leads to conformational changes in the nanobody molecule, while the SDS buffer also releases a lot of proteins bound unspecifically to the agarose beads. Therefore, glycine was used to elute the cross-linked protein complexes. As expected, a high yield of cross-linked P2X7-EGFP complex was obtained as visualized via the fluorescence scan of the SDS acrylamide gel. However, subsequent coomassie staining of the same gel revealed a high background of unspecific protein bands present in both wt and tg samples (Figure 23 B). The reason for this is probably the high density of the proteins in the extract from the whole lung tissue. Different conditions for protein extraction and washing of the bound proteins were tested and the best results were obtained using a protocol in which the proteins were extracted with 1% NP-40, the beads were washed in spin columns with a buffer containing 1% NP-40 and 150 mM NaCl, and proteins were eluted with 0.2 mM glycine (pH 2.5) (for details refer to section 2.2.3.8). This protocol yielded highly pure cross-linked P2X7 complexes enriched in the tg sample that could be visualized as a distinct band in the coomassie stained acrylamide gel and was used for analysis of interaction partners by LC-MS/MS (Figure 23 C).

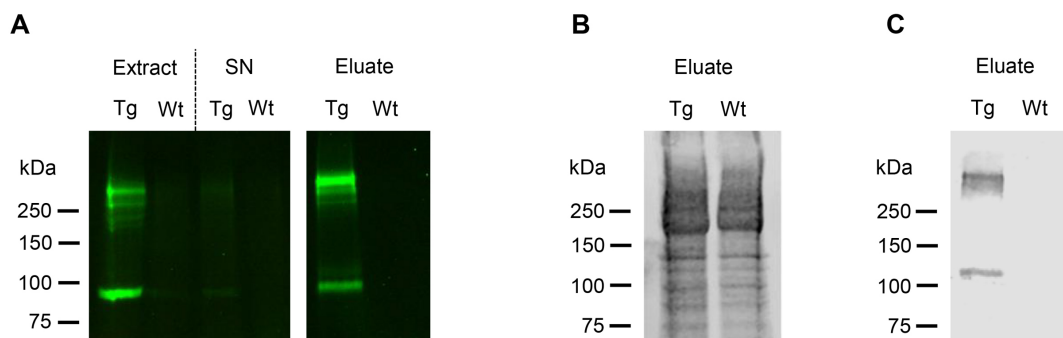


Figure 23 – **Optimization of purification conditions:** (A) After *in situ* cross-linking via transcatheter perfusion and intratracheal application of DSS, proteins were extracted from whole lung tissue. The purification with anti-GFP nanobodies (GFP-Trap<sup>®</sup>) of cross-linked P2X7-EGFP complexes was analyzed via SDS-PAGE and subsequent fluorescence scanning. Almost all of the cross-linked transgenic protein was purified, while hardly any fluorescence was detected in the supernatant (SN). (B) Initial coomassie staining of the elution fraction after SDS-PAGE. A high background of unspecific protein bands was detected in both tg and wt sample. (C) Coomassie staining after the optimization of purification conditions. The GFP-Trap<sup>®</sup> agarose beads were washed in spin columns with a washing buffer containing 1% NP-40 and 150 mM NaCl and proteins were afterwards eluted with 0.2 mM glycine (pH 2.5) (for details refer to section 2.2.3.8). Distinct bands for cross-linked and monomeric P2X7-EGFP were found in the samples from the perfused transgenic animals, while no proteins were detected in the wt sample.

### 3.4.5. Identification of novel interaction partners of P2X7 by *in-situ* cross-linking mass spectrometry

For the identification of interaction partners of P2X7, tg and wt mice were perfused as described with the cross-linker solutions. The proteins from three pooled lungs were then extracted and the cross-linked complexes were purified using the anti-GFP nanobodies. After separation by SDS-PAGE, the band containing the cross-linked complex was cut out, washed, and further processed for proteolytic in gel digestion. In case of control samples from wt animals, the corresponding region of the gel was cut and further processed like the tg bands as a control to identify false positive proteins. After cleavage with trypsin, the peptide mixtures were analyzed by nano-HPLC/nano-ESI-Orbitrap-MS/MS analysis (Figure 24). See methods section 2.2.3.11.

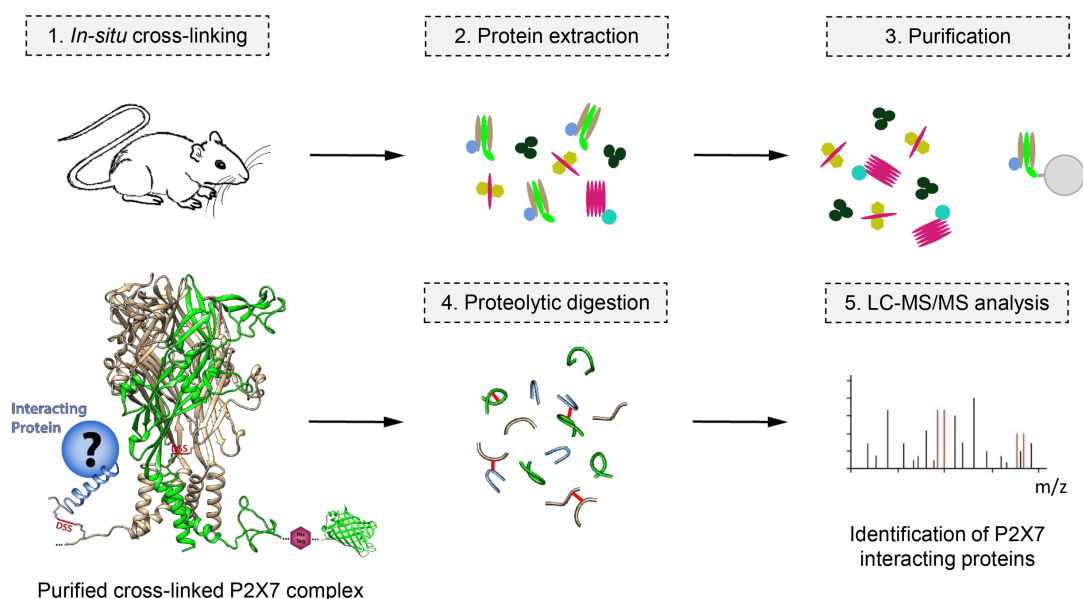


Figure 24 – Schematic illustration of the *in-situ* cross-linking experiment for the identification of novel protein interaction partners of P2X7: Proteins were cross-linked via perfusion of the lung. After the extraction of the proteins, the cross-linked transgenic P2X7 was purified via its EGFP tag. Proteins were then processed for proteolytic in gel digestion and the peptides were analyzed via nano-HPLC/nano-ESI-Orbitrap-MS/MS.

The data of three biological replicates were used for the statistical analysis via the Perseus software platform (v1.5.8.5; [Tyanova et al., 2016]) and 41 proteins were identified as significantly enriched in the tg compared to wt samples using a two sample t-test (Table 16). The results of the statistical analysis are visualized in form of a volcano plot, which shows both significance and fold-change in protein abundance between tg and wt samples (Figure 25). As expected, the target protein P2X7 was identified in all transgenic replicates with at least 44 unique peptides and a sequence coverage of 51,3%. P2X7 also showed the strongest enrichment and the lowest p value.

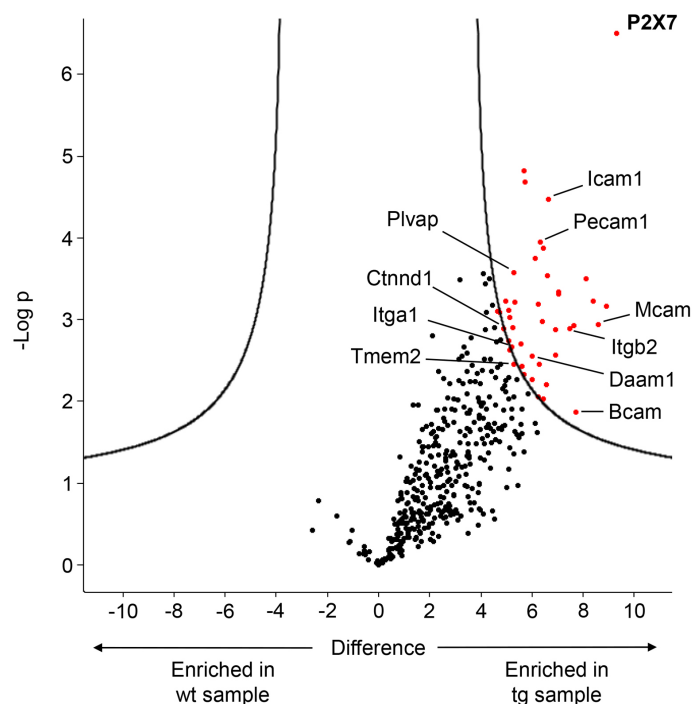


Figure 25 – **Volcano plot of the identified proteins after cross-linking with P2X7-EGFP:** Identified proteins are represented as dots. Significance ( $-\text{Log } p$ ) was plotted against the fold change in protein abundance (difference). The parameters for the cutoff curve were set to a FDR of 0.01 and  $S_0$  of 2. Significantly enriched proteins are shown in red and interesting candidates are highlighted.

All significantly enriched proteins were analyzed for known and predicted protein-protein interactions using the STRING database (v10.5; [Jensen et al., 2009]) and showed significantly more interactions than expected for a random set of proteins with the same size. This indicates that the proteins share, at least in parts, common functions and are involved in similar biological processes. Thus, fourteen proteins are involved in cell adhesion, six in processing and presentation of anti-



Protein name	Gene name	Unique peptides	Function
ADP/ATP translocase 2	Slc25a5	1	Catalyzes the exchange of cytoplasmic ADP with mitochondrial ATP.
Advanced glycosylation end product-specific receptor	Ager	3	Regulation of pro-inflammatory mediators.
Anoctamin-6	Ano6	1	Ca <sup>2+</sup> -dependent phospholipid scramblase.
<b>Basal cell adhesion molecule</b>	<b>Bcam</b>	<b>5</b>	<b>Cell adhesion molecule.</b>
Calcitonin gene-related peptide type 1 receptor	Calcr1	3	Receptor for CGRP and adrenomedullin.
<b>Catenin delta-1</b>	<b>Ctnnd1</b>	<b>9</b>	<b>Cadherin binding.</b>
CD97 antigen	Cd97	1	Promotes adhesion and migration of leukocytes.
<b>Cell surface glycoprotein MUC18</b>	<b>Mcam</b>	<b>5</b>	<b>Cell adhesion molecule.</b>
Cytochrome P450 4B1	Cyp4b1	4	Cytochrome
<b>Disheveled-associated activator of morphogenesis 1</b>	<b>Daam1</b>	<b>7</b>	<b>Reorganization of the actin cytoskeleton.</b>
Endothelial cell-selective adhesion molecule	Esam	2	Mediates endothelial cell interactions. Involved in leukocyte migration.
Ephrin-B1	Efnb1	2	Ligand for Eph receptors
H-2 class I histocompatibility antigen, D-B alpha chain	H2-D1	1	Antigen presentation
H-2 class I histocompatibility antigen, K-W28 alpha chain	H2-K1	1	Antigen presentation
H-2 class II histocompatibility antigen, A-Q alpha chain	H2-Aa	2	Antigen presentation
H-2 class II histocompatibility antigen, A-Q beta chain	H2-Ab1	5	Antigen presentation
Heat shock 70 kDa protein 12B	Hspa12b	3	Heat shock protein. Involved in angiogenesis.
<b>Integrin <math>\alpha</math>-1</b>	<b>Itga1</b>	<b>11</b>	<b>Cell adhesion molecule.</b>
<b>Integrin <math>\beta</math>-2</b>	<b>Itgb2</b>	<b>6</b>	<b>Leukocyte adhesion and transmigration.</b>
Intercellular adhesion molecule 1	Icam1	2	Leukocyte adhesion and transmigration.
Lymphatic vessel endothelial hyaluronidase 1	Lyve1	1	Autocrine regulation of cell growth
Mannose-binding protein C	Mbl2	5	Activates the lectin complement pathway.
Motile sperm domain-containing protein 2	Mospd2	1	Leukocyte migration.

NADH-cytochrome b5 reductase 3	Cyb5r3	2	Cytochrome
<b>P2X purinoceptor 7</b>	<b>P2rx7</b>	<b>48</b>	
<b>Plasmalemma vesicle-associated protein</b>	<b>Plvap</b>	<b>7</b>	<b>Regulates microvascular permeability, leukocyte migration and angiogenesis.</b>
<b>Platelet endothelial cell adhesion molecule</b>	<b>Pecam1</b>	<b>14</b>	<b>Cell adhesion molecule, required for leukocyte transendothelial migration.</b>
Podocalyxin	Podxl	1	Cell adhesion and migration.
Ras-related protein Rab-10	Rab10	1	Intracellular membrane trafficking.
Ras-related protein Rab-1A	Rab1A	1	Intracellular membrane trafficking.
Ras-related protein Rab-5A	Rab5a	2	Intracellular membrane trafficking.
Ras-related protein Rab-5C	Rab5c	3	Protein transport.
Ras-related protein Rab-7A	Rab7a	2	Endo-lysosomal trafficking. Phagosome pathway.
Ras-related protein Rras	Rras	1	Reorganization of the actin cytoskeleton.
Receptor-type tyrosine-protein phosphatase C (CD45)	Ptprc	2	T-cell activation.
Receptor-type tyrosine-protein phosphatase mu	Ptpm	5	Cell-cell adhesion.
Solute carrier organic anion transporter family member 2A1	Slco2a1	3	Prostaglandin release, transport and clearance.
Synaptosomal-associated protein 23	Snap23	2	Syntaxin binding. Regulator of transport, vesicle docking and fusion.
Syntaxin-19	Stx19	1	Intracellular protein transport.
Thrombomodulin	Thbd	2	Blood coagulation.
<b>Transmembrane protein 2</b>	<b>Tmem2</b>	<b>15</b>	<b>Regulator of angiogenesis.</b>
Vesicular integral-membrane protein VIP36	Lman2	1	Regulation of phagocytosis.

Table 16 – Significantly enriched proteins identified by XL-MS.

Interestingly, six of the proteins that were identified with at least 5 peptides were shown to be involved in leukocyte migration: platelet endothelial cell adhesion molecule 1 (PECAM-1; CD31), integrin  $\beta$ -2 (CD18), catenin delta-1 (p120 catenin), plasmalemma vesicle-associated protein (PLVAP; MECA-32; PV-1), cell surface glycoprotein MUC18 (MCAM; CD146) and integrin  $\alpha$ -1 (CD49a). Since intercellular adhesion molecule 1 (ICAM-1; CD54) is the endogenous ligand of integrin  $\beta$ -2, showed a high significant enrichment, and fits very well to

the function of the other candidates in leukocyte migration, also ICAM-1 was included as an interesting protein for further analysis, although it was only identified via two unique peptides. This could also indirectly interact with P2X7 via integrin  $\beta$ -2.

### 3.4.6. Validation of identified interaction partners

To further validate the identified potential interaction partners of P2X7, commercially available antibodies were obtained and used for co-stainings with P2X7-EGFP in lung tissue. Immunostaining with an integrin  $\beta$ -2 antibody showed the strongest signal in pulmonary macrophages in which also a high expression of P2X7-EGFP was detected (Figure 27 A). The expression of integrin  $\beta$ -2 in pulmonary macrophages is in line with previous observations [Arnaout, 2016]. An overlap of both signals was detected at the plasma membrane of these cells. To have a more detailed look at the immune cells in the lung, additional co-stainings with cells from bronchoalveolar lavage fluid were performed. Likewise, the fluorescent signals were overlapping and detected at the plasma membrane of the cells but also intracellular (Figure 27 B). To further confirm these results with another P2X7 expressing cell type from a different tissue, additional immunostainings were performed with primary microglia, the phagocytic cells of the brain. As described in section 3.2, microglia show a pronounced P2X7 expression. Interestingly, fluorescent signals were specifically co-localized at cell extensions/protrusions (Figure 27 C). This characteristic co-localization in microglia further argues for a physical and/or functional interaction of both proteins. Their localization at microglial extensions/protrusions implies a potential involvement in cell migration also in this cell type and is worth to be further investigated.

Immunostaining in lung sections with anti-PECAM-1 (CD31) antibody revealed the highest signal in endothelial cells of large blood vessels, where no expression of P2X7 was detected (Figure 28 A). In immune cells, which highly express P2X7, we did not detect any PECAM-1 signal, although this was previously described [Privatsky et al., 2013]. However, overlapping signals of both proteins were detected in the pulmonary alveoli (Figure 28 A). It is most likely that these cells represent microvascular endothelial cells, since PECAM-1 is not expressed in epithelial cells. Like PECAM-1, ICAM-1 (CD54) is expressed in pulmonary endothelial cells, but also in epithelial cells [Nomellini et al., 2012]. Fluorescence signal of the ICAM-1 was overlapping with the GFP signal in the alveolar space

but to a higher extent than PECAM-1 (Figure 28 B). Thus, P2X7 and ICAM-1 are coexpressed in epithelial as well as endothelial cells. Further analysis at sub-cellular level is required to identify a possible co-localization.

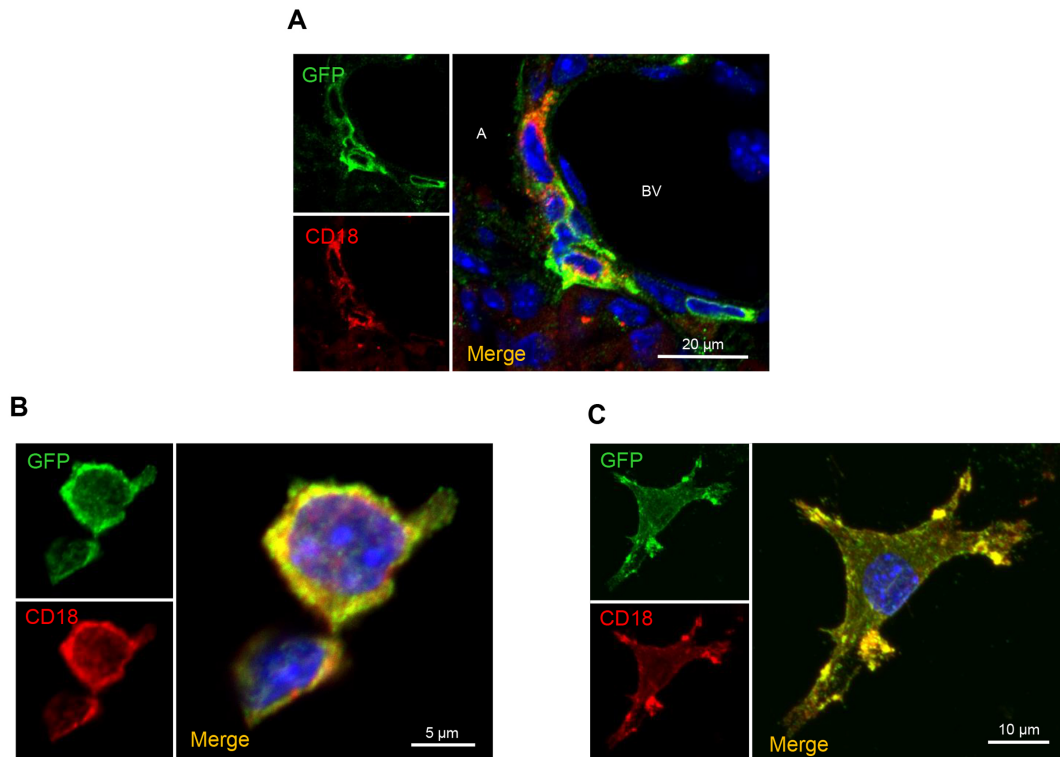


Figure 27 – **Co-staining of P2X7-EGFP and integrin  $\beta$ -2 (CD18)**: Co-stainings with GFP- and CD18- specific antibodies were performed with 10  $\mu$ m frozen lung sections (A), isolated cells from bronchoalveolar lavage fluid (B), or isolated primary microglia (C) from transgenic mice. DAPI staining is shown in blue. A = Alveolus, BV = Blood vessel

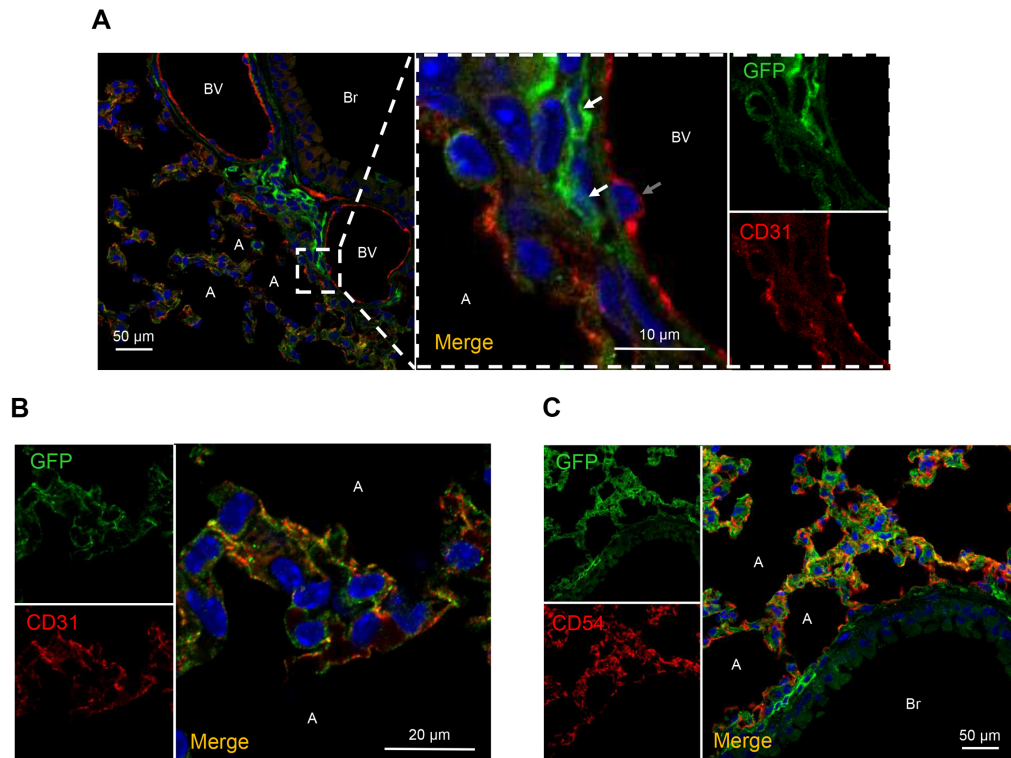


Figure 28 – **Co-staining of P2X7-EGFP with PECAM-1 (CD31) and ICAM-1 (CD54)**: (A) Lung sections from transgenic animals were stained with anti-GFP and anti-CD31 antibodies. White arrows represent immune cells with high P2X7-EGFP expression, grey arrows represent endothelial cells with strong CD31 signal. (B) Co-labeling of P2X7-EGFP and CD31 was detected in cells of the pulmonary alveoli, which most likely represent microvascular endothelial cells. (C) Co-staining of P2X7-EGFP and CD54 showed overlapping signal in alveolar epithelial as well as microvascular endothelial cells. DAPI staining is shown in blue. A = Alveolus, Br = Bronchiole, BV = Blood vessel

### 3.4.7. Identification of modified peptides and mapping of cross-linking sites

Protein cross-linking in combination with mass spectrometry does not only allow the analysis of transient protein interaction but also the mapping of inter- as well as intramolecular protein interactions. For this reason, this technique is of major interest for the field of structural biology [Sinz, 2014]. In particular, since no structural information on the P2X7 C-terminal tail is available, the MS data obtained from our pull-down experiments were used to identify the peptides that were modified by DSS via the crossfinder (v1.3) software. Around 30% of the lysines in P2X7 were modified by DSS (Figure 29).

#### Mouse P2X7 (Q9Z1M0):

<u><b>MPACCSW</b></u> <u><b>NDV</b></u>	<u><b>LOYETNKV</b></u> <u><b>TR</b></u>	<u><b>IQSTNYG</b></u> <u><b>TVK</b></u>	WVLHMIVFSY	ISFALVSDKL	50
<u><b>YQRKEP</b></u> <u><b>VISS</b></u>	<u><b>VHTKVK</b></u> <u><b>GIAE</b></u>	<u><b>VTENVTE</b></u> <u><b>GGV</b></u>	<u><b>TKL</b></u> <u><b>GHSIF</b></u> <u><b>DT</b></u>	ADYTFPLQGN	100
SFFVMTNYVK	<u><b>SEGQVQ</b></u> <u><b>TLCP</b></u>	<u><b>EYPRRGA</b></u> <u><b>QCS</b></u>	<u><b>SDRRCK</b></u> <u><b>KGWM</b></u>	<u><b>DPOS</b></u> <u><b>KGIQ</b></u> <u><b>TG</b></u>	150
<u><b>RCVPYD</b></u> <u><b>KTRK</b></u>	<u><b>TCEVSA</b></u> <u><b>WCPT</b></u>	<u><b>EEEKEA</b></u> <u><b>PRPA</b></u>	<u><b>LLRSAE</b></u> <u><b>NFTV</b></u>	<u><b>LIKNNI</b></u> <u><b>HFPG</b></u>	200
HNYTTRNILP	TMNGSCTFHK	<u><b>TWDPOC</b></u> <u><b>SIFR</b></u>	LGDIHQEAGE	NFTAVAVQGG	250
IMGIEIYWDC	NLDSWSHHC	PRYSFR <u><b>RLDD</b></u>	<u><b>KNTDES</b></u> <u><b>FVPG</b></u>	<u><b>YNFRYAK</b></u> <u><b>YYK</b></u>	300
<u><b>ENNVEK</b></u> <u><b>R</b></u> <u><b>TTLI</b></u>	KAFGIRFDIL	VFGTGGKFDI	IQLVVYIGST	LSYFGLATVC	350
IDLLINTYSS	<u><b>AFCRSG</b></u> <u><b>VYPY</b></u>	<u><b>CKCCEP</b></u> <u><b>CTVN</b></u>	<u><b>EYYR</b></u> <u><b>KKCES</b></u>	<u><b>IMEPK</b></u> <u><b>PTLKY</b></u>	400
<u><b>VSFVDE</b></u> <u><b>PHIR</b></u>	<u><b>MVDQQL</b></u> <u><b>LGKS</b></u>	<u><b>LQVVK</b></u> <u><b>QQEV</b></u> <u><b>P</b></u>	<u><b>RPQMD</b></u> <u><b>FSDL</b></u> <u><b>S</b></u>	<u><b>RLSLSL</b></u> <u><b>HDSP</b></u>	450
<u><b>LTPGQ</b></u> <u><b>SEEI</b></u> <u><b>Q</b></u>	<u><b>LLHEE</b></u> <u><b>VAPK</b></u>	<u><b>GDSPSW</b></u> <u><b>QCG</b></u>	<u><b>NCLPSR</b></u> <u><b>LPEQ</b></u>	<u><b>RRALEE</b></u> <u><b>LCCR</b></u>	500
RKPGRC <u><b>ITTS</b></u>	<u><b>KL</b></u> <u><b>FH</b></u> <u><b>KL</b></u> <u><b>VLSR</b></u>	DTLQLLLLYQ	DPLLVLGEEA	TNSRLRHRAY	550
RCYATWR <u><b>FGS</b></u>	<u><b>QDMAD</b></u> <u><b>FAILP</b></u>	<u><b>SCCR</b></u> <u><b>WRIRKE</b></u>	<u><b>FPKTEG</b></u> <u><b>QYSG</b></u>	<u><b>FKYPY</b></u>	

**PAC**: Peptide identified  
**K**: Substrate detected  
**S**: Phosphorylation

Figure 29 – **Amino acid sequence of murine P2X7 with the detected chemical modifications induced by the cross-linker DSS:** P2X7 was identified with at least 44 unique peptides and a sequence coverage of 51,3%. Identified peptides are shown in bold and underlined. Lysines with a detected substrate modification are shown in red. Identified phosphorylations are shown in blue.

Two inter-subunit cross-links within the P2X7 trimer were found, both of them showing evidence for the interaction of the same domains (AA 297-317) (Figure 30 A). Indeed, the domain is in close proximity to the corresponding domain of the respective other subunits and is located at the tip of the extracellular region (Figure 30 B). However, we did not detect any cross-link between P2X7 and one of the identified potential interaction partners.

A mixture of deuterated and non-deuterated crosslinker should allow to identify cross-links in the mass spectra more easily [Müller et al., 2001],

[Seebacher et al., 2006]. Therefore, additional cross-linking experiments were performed with a 1:1 mixture of  $d_0$  and  $d_4$  isotopes of DSS. However, also in these samples no further cross-links were identified. A possible reason for this might be the low amount of isolated protein and the high complexity of the analyzed samples. For a detailed analysis of the interaction sites, cross-linking experiments in a heterologous overexpression system would be more suited. Nevertheless, the identification of the inter-subunit cross-links provides an initial proof of concept for the technique. Therefore, XL-MS represents a promising approach to identify the interaction sites of the identified proteins as well as a powerful structural tool for the mapping of the interaction sites within the C-terminal intracellular domain of P2X7.

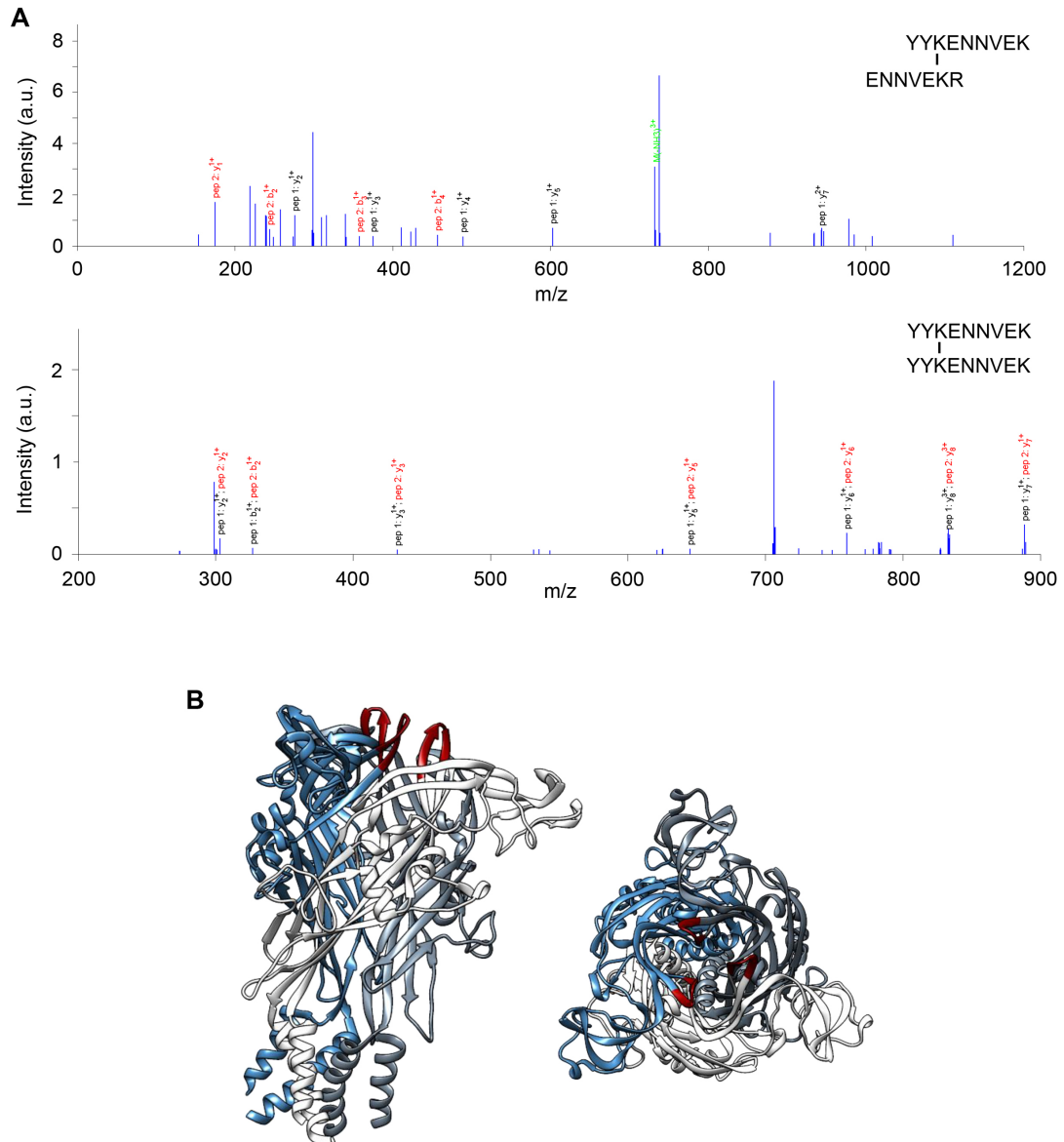


Figure 30 – **Inter-subunit cross-links within the P2X7 trimer:** (A) Mass spectra of two identified cross-links are shown. Both spectra indicate a cross-link between the same peptide of two different subunits of P2X7 (YYKENVVEKR). (B) Crystal structure of P2X7 (PDB ID: 5U1L) visualized with UCSF Chimera (v1.13.1). The domains in which the inter molecular cross-links were detected are shown in red. Crossfinder (v1.3) was used for the identification of cross-linked peptides. Analysis was conducted by Dr. Felix Müller-Planitz.

## 4. Discussion

### 4.1. P2X7 mouse models

Evolving interest in the P2X7 receptor as a novel drug target resulted in the generation of several new tools to study its function and localization. Four P2X7-deficient mouse lines have been published so far: the *P2rx7*<sup>-/-</sup> mouse line by Pfizer carries a neomycin cassette inserted into exon 13 [Solle et al., 2001], mice from GlaxoSmithKline were generated by insertion of a LacZ gene and neomycin-resistance cassette into exon 1 [Sim et al., 2004], and the mouse line generated by Lexicon genetics [Basso et al., 2009] as well as the most recent *P2rx7*<sup>-/-</sup> mouse line available at the European Conditional Mouse Mutagenesis (EUCOMM) program harbor a LacZ/neomycin selection cassette in exon 2 [Skarnes et al., 2011]. In addition to these four *P2rx7*<sup>-/-</sup> mice, a BAC transgenic P2X7 reporter mouse line (Tg(P2rx7-EGFP)FY174Gsat) was generated by the GENSAT project (<http://www.gensat.org/>) which expresses a soluble EGFP reporter under the control of the BAC-derived endogenous P2X7 promoter [Gong et al., 2003]. Just recently, also a conditional humanized mouse model was generated in which the human cDNA covering exons 2-13 is inserted in mouse exon 2 [Metzger et al., 2016].

Although these tools greatly advanced investigation of P2X7 localization and function, several unexpected findings were made and need to be considered: the Pfizer and GlaxoSmithKline *P2rx7*<sup>-/-</sup> mice were shown to be not fully deficient in P2X7 expression, since they can either express C-terminally truncated splice variants (Pfizer) or a splice variant with an alternative exon 1 (GlaxoSmithKline) [Masin et al., 2012], [Nicke et al., 2009], [Taylor et al., 2009]. Furthermore, the mice with an introduced reporter gene (LacZ or GFP) and the humanized P2X7 mice do not reveal consistent data for P2X7 localization in specific cell types [Kaczmarek-Hajek et al., 2018], [Metzger et al., 2016], [Sim et al., 2004]. Finally, also the quality of commercial available anti-P2X7 antibodies is questionable [Anderson and Nedergaard, 2006], [Sim et al., 2004]. A ‘P2X7-like’ pro-

tein with an assumingly similar recognition epitope is frequently detected with antibodies raised against the P2X7 C-terminus [Marín-García et al., 2008], [Sánchez-Nogueiro et al., 2005], [Sim et al., 2004], [Sperlágh et al., 2006]. As a consequence, published data lead to divergent conclusions and resulted in an ongoing debate about P2X7 localization, in particular concerning its existence in neurons [Illes et al., 2017], [Miras-Portugal et al., 2017].

Likewise, information about previously identified interaction partners of P2X7 is inconclusive (refer to section 1.3.4). For the identification of protein-protein interactions, co-immunoprecipitation is a standard procedure in molecular biology. However, this technique strongly relies on the expression level of the target protein, antibody quality, and good negative controls, such as knockout animals. Unfortunately, P2X7 protein expression rate in native tissue is lower than in recombinant systems and available antibodies were shown to be not selective or sensitive enough for its detection. As a consequence, analysis of protein interactions of P2X7 *in vivo* is complicated and a number of studies were performed *in vitro* with primary cells or cell lines overexpressing an affinity tagged version of P2X7. This might lead to artificial results, since the receptor is heterologously expressed in cells where it is not naturally occurring and at much higher levels, which could promote aggregation.

To overcome the described limitations in P2X7 research, a P2X7-EGFP BAC transgenic mouse model was generated in which the receptor is fused via a streptahistidyl-linker to EGFP [Kaczmarek-Hajek et al., 2018]. This mouse model allows reliable purification of P2X7-EGFP from native mouse tissue via the introduced protein tags, which makes the use of anti-P2X7 antibodies expandable. Furthermore, the protein is only moderately overexpressed and present at near physiological levels regulated by the endogenous P2X7 promotor. This also allows investigation of P2X7 protein localization *in vivo* and the identification of the respective cell types.

This BAC transgenic line was characterized in detail in this study to exclude an aberrant expression of the transgenic protein. A previous observed cell-specific localization of P2X7 in the brain was validated by conditional *P2rx7<sup>-/-</sup>* mice and underlined a dominant P2X7 expression in microglia and oligodendrocytes. Additionally, a postulated interaction with the P2X4 subunit was further investigated to resolve the distribution, mutual interrelation as well as the physical interaction of both subunits *in vivo*. No significant interaction was observed in native mouse tissue. Finally and as the major part of the study, the BAC transgenic

mouse line was used to identify novel interaction partners of the P2X7 receptor. A protocol for quantitative *in situ* cross-linking of P2X7 complexes in the lung was successfully established and used to co-purify cross-linked interacting proteins. The identified bona-fide candidates were shown to be mainly involved in leukocyte adhesion and migration. Each of these results will be discussed in detail in the following sections.

## 4.2. Validation of the P2X7-EGFP BAC transgenic mouse model

The availability of powerful tools to manipulate the mouse genome has made this organism the favorite mammalian model for *in vivo* studies. However, the generated mouse lines should be evaluated with great care to exclude an aberrant expression or unwanted effects of the transgene. Possible pitfalls of the generated P2X7-EGFP BAC transgenic mouse model will be discussed below.

### **Can an ectopic expression of the transgenic protein be excluded?**

Conventional transgenic approaches with small DNA fragments have the major limitation that expression of the transgene is influenced by its integration site. Since the integration occurs randomly and can vary in copy number, this can result in a total lack of expression, as well as ectopic or mosaic expression of the transgene [Yang and Gong, 2005]. This position effect is mainly caused by the lack of important regulatory elements. BAC transgenes, in contrast, should contain all the regulatory elements for an accurate transgene expression *in vivo*, including the endogenous promoter. Therefore, the transgene expression should be independent of its integration site and only dependent on the number of integrated BAC copies. In most cases, BAC transgenes show an expression pattern that reflects the chosen driver gene. Various other studies with BAC transgenes demonstrated that such approaches are valuable to analyze endogenous protein expression patterns [Gerfen et al., 2013], [Watanabe et al., 2019], [Yang and Gong, 2005]. However, some position effects like integration of the BAC transgene into other genes or transcriptional control elements, can result in aberrant expression or knockout of the respective other gene product. To

exclude such effects, the P2X7-EGFP BAC transgenic mouse lines were analyzed in detail. The five different transgenic lines showed different protein expression levels, which were directly correlating with the number of integrated BAC constructs and demonstrate a correct expression of the majority of integrated copies. The observed expression pattern of P2X7-EGFP was identical to the endogenous P2X7 as determined by direct comparison using a novel P2X7-specific nanobody [Danquah et al., 2016], [Kaczmarek-Hajek et al., 2018]. Moreover, conditional P2X7 knock-out mice could underline the observed expression pattern of the transgenic protein. In summary, no evidence for an ectopic or mosaic expression of the transgene was found.

### **Does the introduced protein tag influence plasma membrane targeting or protein function?**

A major drawback of large protein tags is that the bulky fluorescent reporter protein can interfere with the function of the target protein. This is especially problematic if the target protein undergoes transport processes like membrane trafficking. To exclude such influences, glycosylation analysis was performed in various tissues and it was shown that the transgenic protein possesses complex glycosylation similar to the wt P2X7. Although not all of the protein was resistant towards Endo H treatment, the overall observed glycosylation pattern was identical to the endogenous P2X7 in the tg, as well as the wt animals. Furthermore, immunofluorescence stainings were performed in different tissues and showed that the majority of P2X7-EGFP was found at the plasma membrane of the cell and also localized at specific structures, like the long ramified extension of microglia in the brain. The observed subcellular localization pattern was identical to stainings performed with an anti-P2X7 nanobody in wt animals. These results support the correct trafficking of the P2X7-EGFP to the plasma membrane and a subcellular localization that overlaps with that of the endogenous receptor. Importantly, no accumulation of aggregated protein was observed. The small amounts of intracellular P2X7 are in agreement with previous findings and might be explained by dynamic trafficking of the receptor and a high recycling rate [Guo et al., 2007], [Robinson and Murrell-Lagnado, 2013]. However, some of the intracellular signal might also be attributed to auto-fluorescence of the specific tissue since it is not always possible to distinguish precisely between a weak antibody signal and the background fluorescence. To exclude that the protein tag interferes with channel formation of the receptor, the function of the transgenic receptor was shown via

functional assays with ‘rescue mice’, which only express the transgenic but not the endogenous receptor and could confirm the functionality of the transgene.

### **Can the EGFP tag interfere with potential interaction partners?**

In the BAC transgenic P2X7-EGFP line the strep-heptahistidyl-EGFP tag was attached to the C-terminus, where the interaction with other proteins is thought to take place [Costa-Junior et al., 2011]. It is therefore crucial to ensure that the introduced EGFP does not affect protein-protein interactions of P2X7. So far no interaction partner of P2X7 has been described that achieved wide acceptance among researchers. Therefore, verified positive controls are missing and the influence of the EGFP-tag on protein interactions cannot be exactly predicted. However, the co-assembly of transgenic and endogenous P2X7 was shown via Western blot analysis after purification of the transgenic protein from various tissues. Accordingly, even if a direct interaction of the transgenic P2X7 with other proteins is hampered by EGFP, these interaction partners should still be indirectly co-purified via interaction with the endogenous subunits. Thus, the majority of endogenous P2X7 was found to be co-purified with P2X7-EGFP (compare figure 10).

In summary, all these observations indicate that the transgene mirrors the properties of the endogenous protein and forms a functional receptor at the plasma membrane. Thus, the mouse model can be used as a tool to analyze P2X7 protein expression and function. Moreover, it represents a useful tool to identify interaction partners of P2X7 in native tissue and might help to overcome previous limitations in P2X7 research.

## **4.3. P2X7 protein expression in the nervous system**

To understand the pathological role of P2X7, it is important to identify the cell types in which P2X7 is expressed. This can also help to identify cell type-specific protein-protein interactions of P2X7 in future studies. In particular, the localization of P2X7 protein in the nervous system is still ambiguous and the expression in neurons is a matter of debate in the field (refer to section 1.3.2). In this study, biochemical and microscopic analysis were performed to contribute to an in depth analysis of P2X7 expression in the nervous system

[Kaczmarek-Hajek et al., 2018]. A previously observed protein expression pattern of P2X7-EGFP in the brain was validated. Biochemical experiments with cell type-specific *P2rx7*<sup>-/-</sup> mice underlined the dominant expression of P2X7 in microglia and oligodendrocytes, while no neuronal P2X7 expression was observed in immunostainings of transgenic animals. This observation stands in contrast to other studies, where neuronal P2X7 expression was described. Possible reasons for these discrepancies will be presented and discussed in the following paragraphs.

### **Differences to other P2X7 mouse models**

Two P2X7 mouse models have been described in which neuronal expression of P2X7 was observed. In a BAC transgenic EGFP reporter mouse, generated in the Gensat project (Tg(P2rx7 EGFP)FY174Gsat; <http://www.gensat.org/>), soluble EGFP reporter is expressed under the endogenous P2X7 promoter [Gong et al., 2003]. In a humanized P2X7 mouse model, a knock-in approach was used. The murine exon 2 of *P2rx7* was replaced by a cDNA coding for human exon 2-13 [Metzger et al., 2016]. Although neuronal P2X7 was detected in both mouse models, there is a clear difference in the observed expression pattern. Especially the striking P2X7 signal in glutamatergic neurons within the CA3 region in the humanized P2X7 mouse model is not reflected by the Gensat reporter mouse [Metzger et al., 2016]. Other studies already demonstrated that expression of soluble reporter proteins does not always reproduce endogenous gene expression and should be interpreted with care. For example, in three different reporter mouse lines targeting the corticotropin-releasing hormone (CRH), a significant diversity was observed between reporter expression and endogenous CRH expression [Chen et al., 2015]. In the Gensat mice, the soluble EGFP is translated from a truncated mRNA. It might be that the strong alterations in the gene structure influence regulatory mechanisms. To avoid such influences, the *P2rx7* gene structure of the mice used in this study was kept almost untouched and all of the untranslated regions were retained. Since effects of the introduced gene modification cannot be completely ruled out, the expression pattern of the P2X7-EGFP fusion protein was compared with the endogenous P2X7 expression via the novel P2X7 nanobody and provides strong evidence that the transgenic expression corresponds to the endogenous P2X7 expression in our mouse line (as already described) [Danquah et al., 2016], [Kaczmarek-Hajek et al., 2018]. Moreover, experiments with conditional knockout mice confirmed the observed expression pattern of the transgenic animals, which is also in agreement with a

transcriptomics study of the cerebral cortex [Zhang et al., 2014]. In the humanized P2X7 mouse model, only mRNA instead of protein levels were analyzed and this might also account for some of the observed differences. Noteworthy, previous studies already demonstrated that P2X7 mRNA transcripts might not correlate with protein expression [Carpenter et al., 2014]. In addition, differences in the sensitivity of the used detection method could account for discrepancies.

#### **Is neuronal P2X7 expression below detection limit of the used method?**

The presented data clearly demonstrate that microglia and oligodendrocytes are the dominating P2X7 expressing cell types in the brain. However, this does not exclude that P2X7 protein is also expressed in other cell types like neurons. It cannot be ruled out that neuronal expression is below detection limit of the used method. A possibility is for example that the localization of the receptor is limited to fine subcellular regions like synapses or growth cones, which would be impossible to resolve with the described methods. As a possibility to boost P2X7 expression, status epilepticus was induced via intra-amygdala kainic acid injection. Even after CNS injury, no P2X7 expression in cell types other than microglia or oligodendrocytes was observed, which also argues against an induced neuronal P2X7 expression under pathological conditions.

#### **Can P2X7 splice variants escape detection via the EGFP tag?**

As already mentioned, previously generated *P2rx7<sup>-/-</sup>* mice hampered P2X7 research because of splice variants that escaped inactivation. In the BAC transgenic P2X7-EGFP line described above, the existence of a truncated neuronal splice variant that escapes the detection via the EGFP-tag cannot be fully excluded. In addition to the two previously described full-length P2X7 splice variants (splice variant a and k) that should result in EGFP-tagged P2X7 protein, also three C-terminally truncated or altered variants (splice variant b, c and d) exist [Masin et al., 2012], [Metzger et al., 2016], [Nicke et al., 2009]. However, although mRNA of the truncated splice variants b and c was detected in brain, no protein expression was observed [Masin et al., 2012]. Since the splice variant d contains only one transmembrane domain it is very unlikely that it forms a functional channel. Via Western blot analysis, a 65 kilodalton (kDa) band is frequently detected in protein extracts of brain samples, which was suggested to be an additional P2X7 splice variant [Marín-García et al., 2008], [Metzger et al., 2016], [Sánchez-Nogueiro et al., 2005]. However, unlike the P2X7 protein, the detected

band does not show a size shift after treatment with glycosidases (not shown), which indicates that, unlike P2X7, this protein is not glycosylated. Since other P2X7-specific antibodies do not detect this protein and the existence of an unglycosylated splice variant of the receptor is rather unlikely, it can be assumed that the protein does not represent a P2X7 variant.

Taken together, the presented data argue against neuronal P2X7 protein expression in the brain, as well as in DRGs, and support findings in other tissues [Kaczmarek-Hajek et al., 2018]. Thus, it can be concluded that the described P2X7-induced neurodegenerative effects might be indirect, e.g. via activated glial cells. Further experiments are needed to understand the exact effect of P2X7 activation in the brain.

## 4.4. Interaction of P2X4 and P2X7

When analyzing function and signaling of P2X7, the P2X4 subtype is frequently mentioned as a possible interacting protein that might influence processes downstream of P2X7 activation (refer to section 1.3.4.9). While an originally suggested existence of P2X4/P2X7 heterotrimers [Guo et al., 2007] could not be confirmed [Antonio et al., 2011], [Boumechache et al., 2009], [Nicke, 2008], [Torres et al., 1999], several studies argue for a physical and/or functional interaction of both subtypes (section 1.3.4.9). While most of the previous interaction studies were carried out in heterologous systems or isolated cells, here the P2X7-EGFP BAC transgenic mouse line was used to analyze their localization, mutual interrelation and physical interaction in native tissue.

### 4.4.1. Co-localization of P2X4 and P2X7 subunits

In previous studies, in which FRET analysis or an *in situ* proximity ligation assay (PLA) were used, a close association or heteromerization of both subunits was observed [Antonio et al., 2011], [Pérez-Flores et al., 2015], [Schneider et al., 2017]. These studies were performed via heterologous expression of both subtypes in *X. laevis* oocytes and HEK293 cells and might show artifacts induced by their over-expression. Over-expression of P2X4 and P2X7 might result in a stronger plasma membrane localization and therefore partial co-localization with the respective other subtype. To prevent such artifacts, experiments in this study were

conducted in tissue slices or primary cells of transgenic mice. Here, P2X7-EGFP is moderately over-expressed, while the expression of P2X4 should be unchanged. Immunostainings in native lung tissue of transgenic mice demonstrated that although both subunits are co-expressed in immune cells, they have a clear difference in their cellular as well as subcellular localization. This is in line with other findings [Bobanovic et al., 2002], [Guo et al., 2007], [Qureshi et al., 2007]. Nonetheless, recruitment of the P2X4 receptor to the cell surface was observed in studies when cells were activated by different stimuli. These studies showed that treatment of microglia with LPS or stimulation of the C-C chemokine receptor type 2 (CCR2) via its endogenous ligands (C-C motif chemokine 2 or 12) resulted in an increased fraction of P2X4 receptors at the cell surface [Boumechache et al., 2009], [Toulme et al., 2010], [Toyomitsu et al., 2012]. Also, treatment of P2X4 transfected NRK cells with the  $\text{Ca}^{2+}$  ionophore ionomycin lead to an increase in surface localization [Qureshi et al., 2007]. Accordingly, since an increase in intracellular  $\text{Ca}^{2+}$  leads to trafficking of P2X4 to the cell surface, scenarios are possible, in which P2X4 acts downstream of P2X7 and/or after activation, both receptor can co-localize at the plasma membrane. However, our data indicate that no, or only small fractions of P2X4 signal are overlapping with P2X7 at the plasma membrane, at least under physiological conditions. In addition, only a small amount of P2X7 was overlapping with the intracellular P2X4 signal. This argues against a close subcellular localization and the postulated physical interaction or heteromerization of both subtypes under physiological conditions. Additional stainings or PLA with stimulated cells, could help to investigate a close proximity of the subtypes in an activated state or under more pathological conditions.

#### **4.4.2. Mutual interrelation**

As already mentioned, both subtypes are co-expressed in immune cells and several studies also show that the two receptors share similarities in their function. For example, both receptors were shown to be involved in phagosome function [Kuehnel et al., 2009], [Qureshi et al., 2007] and autocrine or paracrine regulation of T cells activation [Manohar et al., 2012], [Schenk et al., 2008], [Wang et al., 2014], [Woehrle et al., 2010], [Yip et al., 2009]. These findings and the fact that both subtypes share a high sequence similarity imply that there

might be a compensatory relationship between P2X4 and P2X7. It can be assumed that one subtype overtakes the function of the respective other when a subtype is not functional or missing. Accordingly, a study on E10 alveolar epithelial cells could show that shRNA-mediated downregulation of P2X4 or P2X7 resulted in an increase of protein level of the respective other subunit [Weinhold et al., 2010]. However, in another study in the kidney, mRNA levels were reduced and not upregulated after genetic ablation of the respective other subtype [Craigie et al., 2013]. To investigate the mutual relationship more closely, qRT-PCR and Western blot experiments were conducted in lung tissue. Here, no mutual influences were observed. This is also in line with studies on immune cells, which showed that shRNA-mediated downregulation of P2X4 did not affect P2X7 protein expression [Kawano et al., 2012b], [Sakaki et al., 2013].

In summary, the data on mutual interrelation of the two P2X subtypes are inconclusive and might be explained by tissue and cell type specific differences. Therefore, a more detailed analysis of isolated cell types is needed.

#### 4.4.3. Physical interaction

The direct physical interaction and heteromerization of P2X4 and P2X7 receptors is an ongoing debate. Previous studies showed that both subunits could be co-immunoprecipitated from different primary cells and recombinant or native cell lines [Antonio et al., 2011], [Boumechache et al., 2009], [Guo et al., 2007], [Hung et al., 2013], [Pérez-Flores et al., 2015], [Weinhold et al., 2010]. In agreement with this, it was shown that P2X4 and P2X7 can indeed physically interact when they are heterologously co-expressed in *X. laevis* oocytes. However, an interaction was not observed in co-immunoprecipitation experiments carried out with native lung tissue from BAC transgenic P2X7-EGFP mice and moreover, P2X4 was not detected as a protein which physically interacts with P2X7 in the screening approach for novel interacting proteins by *in situ* XL-MS (section 3.4). In contrast to conventional recombinant cell lines, the BAC transgenic mouse line shows only moderate over-expression of P2X7-EGFP and allows analysis of the interaction at near physiological conditions. A physical interaction or heteromerization was also not observed in a study where different native rat tissues were used [Nicke, 2008]. A possible reason for discrepancies among the studies might be the use of different detergents, which are critical for membrane extraction and stability of protein-protein interactions. Therefore, three different non-denaturing

detergents, which are commonly used in interaction analysis, were tested. However, also here no co-precipitation of P2X4 after purification of P2X7-EGFP from lung tissue was detected. It can therefore be concluded that the detected interaction in *X. laevis* oocytes might be an artifact from the over-expression of the P2X4 and/or P2X7 receptor in recombinant systems and might be of minor relevance in native tissue. Experiments in our lab and also other studies showed that over-expressed P2X4 tends to show a high tendency to aggregate into oligomers. In support of this, Torres et al. also showed that P2X4 constructs were expressed at more than 10 times higher levels than other P2X subtypes in HEK293 cells and this resulted in unspecific interactions [Torres et al., 1999].

In conclusion, all these experiments argue against a physiological relevance of this interaction in native mouse tissue and support the assumption that a detected interaction of both subtypes in over-expression systems might result from artifacts due to heterologous over-expression.

## 4.5. Novel interaction partners of P2X7

Plasma membrane receptors are proteins that receive signals from outside the cell and are therefore the starting points for signal transduction pathways, that enable the cells to communicate, transmit signals, and react to changes in their environment. The P2X7 receptor can be described as danger sensing receptor, since it is activated by high concentrations of extracellular ATP, which is a known DAMP and released in high amounts from surrounding cells after injury or cell death. The final outcome of P2X7 activation is the induction of an inflammatory state. This pathophysiological role has made the receptor to a novel target for the treatment of a variety of diseases. However, the exact signaling cascades are still largely unknown. Knowing the first step of the cascade can be of high value for the understanding of its signaling and therefore, the identification of direct molecular interaction partners of P2X7 is of general interest. Furthermore, these direct interactions might be modulated and manipulated to enable the development of new treatment strategies for diseases in which P2X7 signaling is involved. Several proteins are reported in the literature to directly interact with the P2X7 receptor. Some of these could explain identified P2X7 effects, while the significance of others is still elusive. Most of the identified proteins were described by just one research group, while others, although reported in a number of indepen-

dent publications, are still controversial (e.g. Pannexin-1 and the P2X4 receptor). Early studies identified structural proteins that are thought to be involved in the reorganization of the plasma membrane and could explain signaling events of P2X7 like membrane blebbing and apoptosis. However, some of these proteins are frequently found as contaminants in MS-based approaches and could also represent false positive results [Mellacheruvu et al., 2013]. Subsequent studies on direct interactors of P2X7 were mainly targeted approaches with assumed candidates and investigated by co-immunoprecipitation studies followed by western blot analysis. Targeted approaches harbor the disadvantage that they are more biased than general screening approaches, since the aim is to prove a certain hypothesis. They bear the risk that experimental conditions are unintentionally adjusted to produce the expected outcome. An associated drawback of these approaches is that they are frequently carried out in heterologous expression systems and are more prone to artifacts, as for example in the case of the proposed direct interaction of P2X4 and P2X7. The use of appropriate controls in such experimental setups is therefore essential. However, in a large number of studies on P2X7, such controls are missing or not shown. Since the early studies, no major screening approaches for interactors of P2X7 were published, although several research groups have been working on this topic.

This already indicates that the identification of these proteins is not an easy task. Membrane receptors are incorporated into the cellular plasma membrane and need to be solubilized before they can be isolated from complex protein mixtures. Thus, in contrast to soluble intracellular proteins, they have to be separated from their native environment and labile signaling complexes might lose their integrity. For many membrane receptors co-precipitation experiments were successfully conducted to identify interacting proteins [Schwenk et al., 2012], [Hanack et al., 2015]. However, these interactions seem to have a more stable character, since whole signaling complexes could be resolved under native conditions in membrane extracts (e.g. via nPAGE [Schwenk et al., 2012]). For P2X7, such a stable signaling complex does not seem to exist and the bands obtained by nPAGE analysis can be quite clearly assigned to P2X7 monomers, dimers and trimers [Nicke, 2008]. That the protein-protein interactions of P2X7 have a rather transient character was also confirmed by our first co-precipitation experiments in which only the endogenous P2X7 subunit could be reproducibly enriched, while other proteins were inconsistently detected in individual pull-down experiments (section 3.4.1). In this study, a different approach has therefore been used to sta-

bilize transient protein-protein interactions before the actual purification process. By using cross-linkers, which connect proteins that are in close spatial proximity to each other via covalent bonds, labile and more dynamic interactions are preserved during the sample preparation procedure. Combined with powerful mass spectrometers, the covalent bridges between the proteins can help to identify the interacting proteins. We adapted this approach to identify transient protein-protein interactions of P2X7 by using our BAC transgenic mouse model with moderately over-expressed P2X7-EGFP as a bait for co-purification experiments, hopefully avoiding artificial protein aggregation. The cross-linking procedure was optimized to achieve high yields of P2X7 that was in its native environment covalently fixed via *in situ* cross-linking of murine lung tissue. The combination of both approaches should allow the detection of interactions in a system that is as close as possible to native and physiological conditions.

In total, 41 significantly enriched proteins were found to be specifically co-purified with P2X7-EGFP. Two of these proteins had already been described to interact with P2X7: integrin  $\beta$ -2 was found in an initial study on the P2X7 signaling complex and was co-purified among other proteins from HEK293 cells stable expressing P2X7 using an anti-P2X7 antibody [Kim et al., 2001]. However, the interaction was not further characterized. Anoctamin-6 is a  $\text{Ca}^{2+}$ -activated  $\text{Cl}^-$  channel and an interaction with P2X7 has been analyzed in detail using *X. laevis* oocytes and macrophages [Ousingsawat et al., 2015]. In this study, it was shown that anoctamin-6 is involved in several cellular responses mediated by P2X7, like membrane blebbing, apoptosis and phagocytosis. In addition, a direct interaction was detected via co-immunoprecipitation of both proteins in HEK293 cells.

In the STRING interaction network of the 41 identified proteins, two major groups are found: (I) proteins that are involved in intracellular membrane traffic, including Rab GTPases, soluble N-ethylmaleimide-sensitive-factor attachment receptor (SNARE) proteins, and proteins involved in the phagosome pathway, and (II) proteins involved in cell adhesion and leukocyte migration. These are described in the following sections.

#### **4.5.1. Proteins involved in intracellular membrane traffic**

We identified four Rab proteins to be specifically enriched after precipitation of P2X7: Rab1, Rab5, Rab7, and Rab10. Rab proteins belong to the Ras superfamily of small GTPases and serve as regulators of intracellular membrane

traffic [Hutagalung and Novick, 2011]. They are involved in membrane vesicles formation, movement, tethering, and also fusion with the target membrane. Distinct Rab proteins contribute to specific parts of the vesicular transport pathway [Zhen and Stenmark, 2015].

For example, Rab5 and Rab7 are specifically involved in the regulation of endocytosis. Rab5 localizes to early endosomes [Bucci et al., 1992] and is also found at the plasma membrane. It is required for the formation of clathrin-coated vesicles and the fusion with early endosomes [McLauchlan et al., 1998]. Rab7, in contrast, is involved in the late endocytic pathway and acts downstream of Rab5 for the transport from early to late endosome and lysosomes [Feng et al., 1995]. One explanation for the enrichment of the identified Rab proteins could be that the over-expression of P2X7 in our transgenic mouse model might lead to an artificial aggregation of the protein, which leads to a higher number of receptor recycling and degradation in which the different Rab proteins are involved. However, there is also evidence that this interaction might not be an artifact and the Rab proteins play indeed a physiological role in P2X7 receptor function.

Feng et al. described a mechanism in which the activation of P2X7 induces its endocytosis [Feng et al., 2005]. The described cascade starts with the phosphorylation of the receptors via an intracellular kinase which results in its internalization into clathrin-coated endosomes and could serve as a mechanism to modulate the receptor activity. This translocation of the receptor also explains why the P2X7 signal in immunofluorescence stainings is not restricted to the plasma membrane. Rab5 was previously identified as a key regulator of P2X4 cell surface expression and its dynamin-dependent internalization [Stokes, 2013]. Since P2X4 and P2X7 share a high sequence similarity, it is likely that this also applies for P2X7. Likewise, Rab5 was shown to control sorting of P2X3 into early endosomes [Chen et al., 2012a]. The P2X3-containing endosomes are then retrogradely transported via Rab7 [Chen et al., 2012a]. Both proteins were shown to co-localize with P2X3 in HEK293 cells. The authors propose that this mechanism is not only used for receptor degradation, but could also be used for downstream signaling via retrograde signaling endosomes.

However, Rab proteins might not only be involved in endocytosis of P2X7 receptor but also could execute other vesicular transport tasks, which are mediated by P2X7. Examples for this could be phagocytosis, microvesicle shedding, or interleukin secretion. In agreement with this, a fungal P2X ion channel was shown to regulate Rab activation and vesicle fusion [Parkinson et al., 2014].

The Rab proteins act upstream of SNARE proteins, which recognize target membranes and enable membrane docking and fusion by the formation of SNARE complexes [Wandinger-Ness and Zerial, 2014]. Interestingly, we also detected two SNARE proteins, namely Syntaxin-19 and synaptosomal-associated protein (SNAP)-23. While the exact role of Syntaxin-19 within the syntaxin family is not well described, the function of SNAP-23 has been investigated in more detail. SNAP-23 is a homologue of SNAP-25, which is a component of the best described neuronal SNARE complex consisting of vesicle associated membrane protein (VAMP)-2, syntaxin-1A, and SNAP-25 [Kunii et al., 2016]. While SNAP-25 is predominantly expressed in the brain and involved in neurotransmitter release via synaptic vesicle fusion, SNAP-23 is a ubiquitously expressed protein and modulates exocytosis in several non-neuronal cells [Kunii et al., 2016]. In the lung, SNAP-23 regulates for example surfactant secretion from alveolar epithelial cells via its interaction with syntaxins [Abonyo et al., 2004]. It has been proposed that P2X7 is involved in the secretion of surfactant in the lung, which is thought to be achieved via paracrine signaling between ATI and ATII cells [Mishra et al., 2011]. SNAP-23 is also involved in the formation and maturation of phagosomes in macrophages [Sakurai et al., 2012], a pathway that is also mediated by P2X7 signaling [Wiley and Gu, 2012].

Syntaxins, and especially the Rab GTPases Rab5 and Rab7 are also crucial components of the phagosome pathway [Vieira et al., 2003]. Phagocytosis of foreign pathogens plays a central role for the immune response and allows the presentation of phagocytosed antigens by major histocompatibility complex (MHC) class I and II by leukocytes. For the phagosome maturation, early and late endosomes fuse with the phagosome. SNAP-23 seems to be not only involved in the membrane fusion, but also in phagosomal ROS production and acidification to destroy and digest the foreign pathogens [Sakurai et al., 2012]. In a tight interplay with the adaptive immune systems, some of the phagocytosed protein fragments are presented to T lymphocytes via molecules of the MHC. Interestingly, also proteins of the MHC family were found to be specifically enriched after P2X7-EGFP precipitation.

In a previous study, it was shown that activation of P2X7 stimulates the secretion of MHC-II-containing exosomes [Qu et al., 2007], [Qu et al., 2009]. In addition, P2X7 activation also decreased the amount of MHC-I at the cell surface. The authors propose a shedding mechanism via a microvesicle release pathway independent of metalloproteinase activity [Baroja-Mazo et al., 2013].

In summary, we identified a number of proteins that are involved in membrane trafficking and could explain certain vesicular events that are associated with P2X7 activation. The identity of these proteins could for example help to explain P2X7-mediated phagocytosis, exocytosis of secretory lysosomes, membrane blebbing, shedding of microvesicles, or the formation of multinucleated giant cells, since all these mechanisms rely on proteins that control fusion of different membranes.

#### **4.5.2. Proteins involved in cell adhesion and leukocyte migration**

In the lung, P2X7 activation was found to play a role in the pathogenesis of various diseases like ALI, COPD, pulmonary fibrosis, pulmonary hypertension, and asthma [Savio et al., 2018]. Extracellular ATP serves as a danger signal and patients with idiopathic pulmonary fibrosis as well as samples from a murine bleomycin model of lung injury showed an increased ATP concentration in the BALF [Riteau et al., 2010]. Besides others, one of the hallmarks of lung injury and infection is the excessive recruitment of leukocytes, in particular neutrophils, to the site of inflammation. The involvement of P2X7 signaling in this recruitment process has been demonstrated in numerous studies via by P2X7 blockage [Mishra et al., 2016], [Wang et al., 2015] or the use of *P2rx7*<sup>-/-</sup> mice [Dagvadorj et al., 2015], [Monção-Ribeiro et al., 2011], [Riteau et al., 2010]. Here we show for the first time that P2X7 is directly interacting with proteins that participate in the process of leukocyte migration. Out of the nine bona fide candidates that were identified by a cutoff of more than five unique peptides in each replicate, six proteins are directly involved in pathways associated with leukocyte migration. All of them showed a low p-value and high enrichment compared to the control.

Transmigration of leukocytes involves a range of diverse proteins that play a role in the different steps of the migration process. Adhesion molecules are crucial for endothelial as well as epithelial transmigration of the leukocytes in the lung [Zemans et al., 2009]. Since some of the identified proteins are specifically expressed in endothelial cells, the following discussion will focus on transendothelial migration. However, it should be kept in mind that transepithelial migration occurs in a similar but slightly different manner. Transmigration processes usually start with the capture of circulating leukocytes via selectins and a subsequent

firm adhesion mediated by integrins and their endogenous binding partners. After strengthening of the adhesion, the leukocytes transmigrate by taking either a paracellular or a transcellular route [Zemans et al., 2009]. The identified proteins and their involvement in the transmigration process, their contribution to lung diseases, and the potential role of P2X7 in this signaling cascade will be described in more detail in the following sections. A simplified illustration of the transmigration process, including the identified proteins is shown in figure 31.

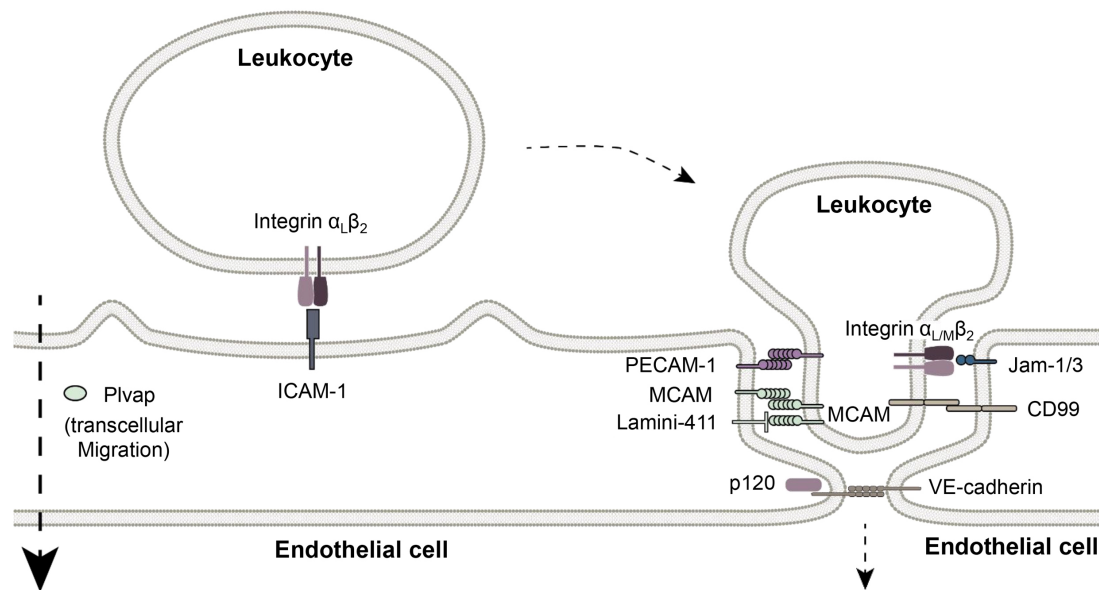


Figure 31 – **Illustration of the transendothelial migration of leukocytes:** Interaction of the heterodimeric  $\beta$ -2 integrin with ICAM-1 mediates a firm adhesion to initiate endothelial transmigration. p120 catenin regulates the loosening of adhesive VE-cadherin contacts to form gaps between endothelial cells. PECAM-1, JAM-1/3, CD99 and MCAM concentrate at the junctions to directly interact with the transmigrating leukocyte. In addition to the paracellular route, a transcellular migration is also possible. Migrating leukocytes are therefore surrounded by rings containing Plvap.

#### 4.5.2.1. Integrin $\beta$ -2 and ICAM-1

Integrins are heterodimeric cell adhesion receptors, consisting of one  $\alpha$  and one  $\beta$  subunit [Zhang and Wang, 2012]. In vertebrates, eighteen  $\alpha$  ( $\alpha_{1-11}$ ,  $\alpha_{Ib}$ ,  $\alpha_D$ ,  $\alpha_E$ ,  $\alpha_L$ ,  $\alpha_M$ ,  $\alpha_V$ ,  $\alpha_X$ ) and eight  $\beta$  subunits ( $\beta_{1-8}$ ) have been identified so far.  $\beta$ -2 integrins are the most abundant integrin subfamily expressed in leukocytes. Integrin  $\beta$ -2 (CD18) associates with one of four different  $\alpha$  integrins ( $\alpha_L$ ,  $\alpha_M$ ,  $\alpha_X$ ,  $\alpha_D$ ; also known as CD11a-d) to form the heterodimer [Arnaout, 2016].  $\beta$ -2 integrins

are usually in an inactive state, which allows the cell to freely circulate in the blood and avoid adhesion. Stimulation of the leukocyte (e.g. via chemokines or cytokines) initiates an inside-out activation (an action on the cytoplasmic part of the integrin that induces conformational changes in the extracellular domain), which is mediated by PECAM-1 and Rap1, and allows stable binding to their extracellular ligands (e.g. ICAM-1 or junctional adhesion molecule (JAM) 1/3) [Arnaout, 2016], [Muller, 2007], [Zemans et al., 2009]. ICAM-1 is expressed on epithelial and endothelial cells and the interaction with  $\beta$ -2 integrins on leukocytes mediates a firm adhesion to initiate endothelial or epithelial transmigration [Zemans et al., 2009]. In the lung, leukocyte migration can occur in a CD18-dependent or -independent manner, according to the stimulus and way of application. For example the stimulation by *E. coli*, *P. aeruginosa*, IL-1, IgG immune complexes or an intratracheal application of LPS leads to the infiltration of leukocytes in a CD18-dependent manner [Reutershan and Ley, 2004]. These stimuli also lead to an upregulation of ICAM-1. Integrin  $\beta$ -2, as well as ICAM-1, significantly co-precipitated with P2X7-EGFP in our experiments. Integrin  $\beta$ -2 was identified via six unique peptides on average in all replicates and was 7.5-fold enriched with a p-value of 0.0013. Integrin  $\beta$ -2 was also previously found as a potential interaction partner in a MS-based screening approach using P2X7 overexpressing HEK293 cells [Kim et al., 2001]. Since ICAM-1 was only identified via a small number of peptides, but highly significantly enriched in the P2X7-EGFP pull-down (6.6-fold enriched,  $p < 0.0001$ ), we speculate that the interaction of P2X7 and ICAM-1 could be indirect via its binding to integrin  $\beta$ -2. Immunostainings of lung tissue and bronchoalveolar lavage cells demonstrated that integrin  $\beta$ -2 is co-localized with P2X7-EGFP at the plasma membrane of leukocytes, most likely macrophages. Co-stainings with ICAM-1 antibody showed an overlapping signal with GFP at the plasma membrane of cells within the pulmonary alveoli, which might represent epithelial and/or endothelial cells.

#### 4.5.2.2. PECAM-1

PECAM-1 is a cell adhesion molecule that is expressed on endothelial cells, platelets, and leukocytes. PECAM-1 is frequently used as a marker for vasculature due to its high expression on endothelial cells [Muller, 2007]. The pro-inflammatory role in transendothelial leukocyte migration was the focus of early studies on its biological function [Muller et al., 1993]. However, the protein is

also involved in angiogenesis, platelet activation, T cell receptor modulation, and apoptosis [Muller, 2007]. In the process of leukocyte migration, PECAM-1 is crucial for the actual endothelial transmigration, since it promotes the adhesive interaction between leukocytes and endothelial cells. The protein forms a homophilic interaction between PECAM-1 on endothelial cells and PECAM-1 on leukocytes [Privatsky et al., 2013]. This role is best described for transmigration of neutrophils, monocytes, and natural killer cells [Muller, 2007]. Upstream of the transmigration process, PECAM-1 was found to be important for the directional migration of leukocytes to the region of inflammation [Wu et al., 2005], and the activation of  $\beta$ -2 integrins [Berman and Muller, 1995], [Berman et al., 1996]. Since it is not expressed on epithelial cells, the protein is not involved in transepithelial migration [Zemans et al., 2009]. Shedded PECAM-1 was also suggested as a biomarker for lung injury [Villar et al., 2014]. PECAM-1 was significantly enriched ( $p = 0.0001$ ) with a 6.34-fold change compared to the controls and identified via 14 unique peptides on average in all replicates. In immunostainings of lung sections we could show that PECAM-1 is co-localizing with P2X7 in specific regions of the alveoli, which might represent microvasculature endothelial cells. In pulmonary macrophages, PECAM-1 was either not expressed or below the detection limit. Since P2X7 is expressed in various leukocytes and also in endothelia cells [Ray et al., 2002], the physical interaction of both proteins could occur at the plasma membrane of one cell but also intercellularly via interaction of their extracellular domains.

#### **4.5.2.3. MCAM**

Another cell adhesion molecule found in the precipitate of P2X7-EGFP is MCAM (CD146) (8.6-fold enriched,  $p = 0.0012$ ). The majority of studies on MCAM focus on its role in cancer, since it promotes tumor growth, angiogenesis, and metastasis [Wang and Yan, 2013]. However, there is also evidence that MCAM is involved in transendothelial migration of leukocytes during inflammation, similar to PECAM-1 [Bardin et al., 2009], [Guezguez et al., 2014]. MCAM is mainly expressed on endothelial and smooth muscle cells but also found on lung epithelial cells and alveolar macrophages, where it is upregulated in pathological conditions [Huang, 2014], [Schulz et al., 2003], [Wu et al., 2013]. The protein might amplify its pro-inflammatory function through an enhanced activation of NF- $\kappa$ B [Wu et al., 2013]. Like PECAM-1, also MCAM gets re-

leased in a soluble form during inflammation [Bardin et al., 2009]. Shedding of the protein occurs through a metalloproteinase-dependent mechanism and the soluble form increases the transmigration of monocytes through endothelial cells [Bardin et al., 2009]. Like PECAM-1, also MCAM is involved in the infiltration of leukocytes during lung inflammation [Bardin et al., 2009], [Reutershan and Ley, 2004], [Zemans et al., 2009]. The protein can thereby form a homophilic interaction between leukocytes and endothelial cells to allow adhesion of the immune cells during transmigration [Johnson et al., 1997]. For MCAM expressed in T-cells, a specific interaction with endothelial laminin-411 was also shown [Flanagan et al., 2012].

#### **4.5.2.4. p120 catenin**

A protein that influences the migration of leukocytes without being directly involved in the adhesion process is catenin delta-1, also known as p120. p120 regulates the expression of vascular endothelial-cadherin (VE-cadherin) at adherens junctions between endothelial cells [Alcaide et al., 2008]. During transendothelial leukocyte migration VE-cadherin loosens the adhesive contacts to form small gaps between the cells to enable transmigration of the leukocytes [Bardin et al., 2009]. This process is regulated by p120 [Alcaide et al., 2008]. PECAM-1, JAM-1, CD99 and also MCAM concentrate then at this junction to directly interact with the transmigrating leukocyte [Aurrand-Lions et al., 2002], [Bardin et al., 2009]. p120 does also directly influence epithelial cadherin (E-cadherin) function [Ireton et al., 2002]. The fundamental role of p120 in the regulation of innate immunity in the lung was shown by ATII cell-specific p120-knockout mice. The mutant lungs showed chronic inflammation, marked leukocyte infiltration, increased NF- $\kappa$ B activity, and up-regulation of ICAM-1, TLR 4, and macrophage inflammatory protein 2 [Chignalia et al., 2015].

#### **4.5.2.5. PLVAP**

PLVAP is expressed in endothelial cells, specifically localized at caveolae, and essential for the formation of stomatal and fenestral diaphragms that maintain the integrity of vasculature [Guo et al., 2016]. It is therefore crucial for the regulation of vascular permeability. One of the first functions of PLVAP that has been described in the literature, is its role as a leukocyte trafficking molecule

[Keuschnigg et al., 2009]. Leukocytes seem to cross endothelial layers via large transcellular channels. The migrating leukocytes are therefore surrounded by rings containing PLVAP and caveolin-1 [Keuschnigg et al., 2009]. Interestingly, also caveolin-1 has been previously described to directly interact with P2X7 [Barth et al., 2007], [Barth et al., 2008], [Weinhold et al., 2010]. While the proteins described in the previous section are mainly involved in adhesion of the leukocytes and the paracellular migration, PLVAP seems to be specifically important for the transcellular migration [Keuschnigg et al., 2009].

#### **4.5.2.6. Role of P2X7 in the lung and its involvement in leukocyte migration**

In summary, we found several proteins to co-precipitate with P2X7-EGFP that are directly involved in the migration of leukocytes and fit well to the described role of P2X7 in the pathogenesis of lung disease via recruitment of leukocytes to the site of inflammation. We propose that P2X7 is influencing the process via the direct interaction with adhesion molecules that are mainly expressed in macrophages and microvascular endothelial cells, as well as alveolar epithelial cells. Since pull-down experiments were conducted with whole lung tissue, the exact cell type-specific localization of each interaction remains elusive. Further co-purification experiments with cross-linked proteins from isolated primary cells could provide an insight into the specific cell type in which the interaction takes place.

Interestingly, other P2X7-mediated mechanisms have been described that influence leukocyte migration, and also proteins that were previously identified to directly interact with P2X7 were shown to be involved in these processes but have not been put into this context so far. For example, myosin-9 was shown to control cell adhesion and migration [Vicente-Manzanares et al., 2009] and to facilitate the transendothelial migration process by regulating endothelial cell-cell junctions [Newell-Litwa et al., 2015]. Furthermore, myosin-9 was shown to mediate adhesion of integrin  $\beta$ -2 and to be particularly important for the release of the leukocyte after transmigration [Morin et al., 2008]. P2X7-induced PS exposure was also described to be important for leukocyte migration. PS flip to the outer leaflets of the plasma membrane is considered as an indicator of apoptosis. However, a brief activation of P2X7 can result in a reversible PS translocation [Mackenzie et al., 2005]. It was proposed that the increase in

membrane fluidity resulting from P2X7-mediated PS flip leads to an improved plasticity of the cell and change of its shape, which finally facilitates the transmigration process [Qu and Dubyak, 2009]. The translocation of PS also increased the adhesion of cells to endothelial cells [Manodori et al., 2000] and lead to shedding of L-selectin (CD62L) [Elliott et al., 2005]. L-selectin is a cell adhesion molecule that initiates leukocyte tethering, the first step of the adherence and migration cascade [Ivetic, 2018]. Shedding of L-selectin from human monocytes occurs precisely during transmigration and is important for the invasion and direction of migration [Rzeniewicz et al., 2015]. Receptor-type tyrosine-protein phosphatase C (CD45) is a negative regulator of PS translocation and subsequent L-selectin shedding [Elliott et al., 2005]. Interestingly CD45 was also found to significantly co-precipitate with P2X7-EGFP in our experiments. In addition to L-selectin shedding [Labasi et al., 2002], other proteins that are involved in leukocyte migration are described to be shedded after P2X7 activation, like low affinity immunoglobulin Fc $\epsilon$  receptor (CD23) [Chen et al., 1999], [Sluyter and Wiley, 2002], [Pupovac et al., 2015] or vascular cell adhesion protein 1 (VCAM-1) [Mishra et al., 2016]. After activation of P2X7 soluble VCAM-1 is released from ATI cells through P2X7 receptor-mediated activation of disintegrin and metalloproteinase domain-containing protein 17 (ADAM17). The soluble form of VCAM-1 then serves as a chemoattractant for neutrophils and as an activator for alveolar macrophages [Mishra et al., 2016]. A similar function could apply for shedded PECAM-1 and MCAM, which are both released in their soluble form during inflammation [Bardin et al., 2009], [Villar et al., 2014]. Since PECAM-1 and MCAM are released via shedded microparticles during COPD, activation of P2X7 could play a major role in their release. The role of the P2X7 secretome in inflammatory processes has recently been analyzed and interestingly also integrin  $\beta$ -2 was found via an antibody protein array in the P2X7 secretome of M1 macrophages [De Torre-Minguela et al., 2016].

## 4.6. Identification of cross-linking sites

The combination of cross-linking with MS does not only allow the identification of transient interactions but also the detection of the cross-linked peptides. The position of the cross-linked amino acids can be identified from the mass spectra using specific programs and this data can be used to get valuable information about

single protein domains which interact with each other. The distance constraints from these experiments can even be used for computational modeling of whole protein complexes and also enables the analysis of dynamic structural changes [Chavez et al., 2018], [Doberenz et al., 2014]. Due to these advantages, XL-MS has become an important addition to the more established structural methods like nuclear magnetic resonance (NMR) spectroscopy or X-ray crystallography [Leitner et al., 2016], [Sinz et al., 2015].

We aimed to identify the interaction domains of P2X7 and its identified potential interaction partners. However, in the analyzed mass spectra only very few cross-linked peptides were detected and no protein-protein cross-links between P2X7 and one of the most enriched proteins were found. As a proof of concept, however, we could detect two inter-molecular cross-links within the P2X7 trimer, between two peptides in the extracellular region that are indeed in close proximity. It is a general problem of XL-MS to identify the cross-linked peptides in the MS spectra, since the number of potential cross-links generates highly complex data sets. Several working groups have developed distinct software to analyze these data [Sinz et al., 2015]. The cross-linked peptides generate a different fragmentation pattern than normal peptides and the small number of cross-linked peptides is overlaid by the high number of linear peptides, which makes analysis even more sophisticated [Holding, 2015].

As a possibility to overcome this problem we used in addition to experiments with DSS, samples that were cross-linked with a 1:1 mixture of non-deuterated ( $d_0$ ) and fourfold-deuterated ( $d_4$ ) DSS. This should lead to the formation of distinct  $d_0/d_4$  isotope patterns in the mass spectra and peptides carrying the cross-linker can thereby be more easily identified [Müller et al., 2001], [Seebacher et al., 2006]. However, also with this modification in the experimental setup we could not detect cross-linked peptides between P2X7 and an interacting protein. As a major problem in our approach, we speculate that the sample mixture is too complex and the abundance of the enriched proteins is too low. For approaches which aim to allow structural modeling via identification of cross-linked peptides, it is common to use larger amounts of protein, that are usually purified from heterologous expression systems (e.g. [Doberenz et al., 2014]). Although the use of deuterated cross-linkers can help to identify modified peptides more easily, they also harbor the problem that the overall intensity gets distributed on both isotopes,  $d_0$  and  $d_4$ . Taking into account that only accessible parts of the proteins do react with the cross-linker, it is highly probable that the signal of the low abundant cross-

linked peptides is overlaid by the dominating unmodified peptides in the mass spectra. For future studies, the use of more advanced MS-cleavable cross-linkers could help to identify modified peptides more easily and recombinant overexpression of P2X7 together with an identified potential interaction partner could yield higher amounts of cross-linked complexes.

## List of Figures

1.	Different classes of purinergic receptors . . . . .	11
2.	Structure of P2X receptors . . . . .	13
3.	Role of P2X7 in the maturation and release of the pro-inflammatory cytokine IL-1 $\beta$ . . . . .	17
4.	The P2X7-EGFP BAC transgenic mouse model: . . . . .	29
5.	Comparison of the number of integrated BAC copies and protein expression levels of the five different transgenic mouse lines . . . . .	56
6.	Comparison of P2X7-EGFP expression of animals from different generations, with different age, or different gender . . . . .	57
7.	Influence of P2X7-EGFP overexpression on the endogenous protein . . . . .	58
8.	Ratios of transgenic and wild type P2X7 protein in different brain regions . . . . .	59
9.	Glycosylation status and membrane targeting of P2X7-EGFP . . . . .	60
10.	Purification of the transgenic protein via its His- and/or GFP-tag . . . . .	62
11.	Functionality of the transgenic P2X7-EGFP . . . . .	63
12.	Reduction of P2X7 protein expression in cell type-specific knockout mice (CNP-cre and Cx3cr1-cre) . . . . .	64
13.	Co-staining of EGFP with cell type-specific markers in hypothalamus (Hy), caudoputamen (CPu), pallidum (Pal) and substantia nigra (SN) . . . . .	66
14.	Expression of P2X7-EGFP after kainic acid-induced status epilepticus . . . . .	68
15.	Localization of P2X7 in dorsal root ganglions . . . . .	70
16.	Cell type-specific P2X7 protein expression in the lung . . . . .	72
17.	Subcellular localization of P2X4 and P2X7 protein . . . . .	74
18.	Mutual interrelation of P2X4 and P2X7 expression . . . . .	76
19.	Physical interaction of P2X4 and P2X7 receptors . . . . .	78
20.	Immunoprecipitation of P2X7-EGFP reveals variable enrichment of potential interaction partners . . . . .	79

---

21.	P2X7 cross-linking with DSS in protein extract, homogenate and tissue samples . . . . .	82
22.	Optimization of cross-linking conditions for <i>in-situ</i> cross-linking of lung tissue . . . . .	83
23.	Optimization of purification conditions . . . . .	85
24.	Schematic illustration of the <i>in-situ</i> cross-linking experiment for the identification of novel protein interaction partners of P2X7 . .	86
25.	Volcano plot of the identified proteins after cross-linking with P2X7-EGFP . . . . .	87
26.	Protein-protein interaction network of the identified proteins . . .	88
27.	Co-staining of P2X7-EGFP and integrin $\beta$ -2 (CD18) . . . . .	92
28.	Co-staining of P2X7-EGFP with PECAM-1 (CD31) and ICAM-1 (CD54) . . . . .	93
29.	Amino acid sequence of murine P2X7 with the detected chemical modifications induced by the cross-linker DSS . . . . .	94
30.	Inter-subunit cross-links within the P2X7 trimer . . . . .	96
31.	Illustration of the transendothelial migration of leukocytes . . . .	113

## List of Tables

2.	Identified interaction partners of P2X7. . . . .	20
3.	Mouse lines used in this study. . . . .	31
4.	Chemicals and materials. . . . .	32
5.	Commercial kits and solutions. . . . .	33
6.	Buffers and media for molecular biology. . . . .	33
7.	Buffers for <i>X. laevis</i> oocytes. . . . .	34
8.	Buffers for biochemical applications. . . . .	35
9.	Buffers and media for immunohistochemistry. . . . .	35
10.	Buffers and media for FACS analysis and cell culture. . . . .	35
11.	Primary antibodies used in this study. . . . .	36
12.	Secondary antibodies used in this study. . . . .	37
13.	Enzymes used in this study. . . . .	37
14.	Oligonucleotides used in this study. . . . .	38
15.	Special equipment used for this study. . . . .	39
16.	Significantly enriched proteins identified by XL-MS. . . . .	90

## References

- [Abonyo et al., 2004] Abonyo, B. O., Gou, D., Wang, P., Narasaraaju, T., Wang, Z., and Liu, L. (2004). Syntaxin 2 and SNAP-23 Are Required for Regulated Surfactant Secretion. *Biochemistry*, 43(12):3499–3506. 4.5.1
- [Adinolfi et al., 2003] Adinolfi, E., Kim, M., Young, M. T., Di Virgilio, F., and Surprenant, A. (2003). Tyrosine phosphorylation of HSP90 within the P2X7 receptor complex negatively regulates P2X7 receptors. *The Journal of biological chemistry*, 278(39):37344–51. 2, 1.3.4.1
- [Adriouch et al., 2002] Adriouch, S., Dox, C., Welge, V., Seman, M., Koch-Nolte, F., and Haag, F. (2002). Cutting edge: a natural P451L mutation in the cytoplasmic domain impairs the function of the mouse P2X7 receptor. *Journal of immunology (Baltimore, Md. : 1950)*, 169(8):4108–4112. 3.1.1
- [Alberto et al., 2013] Alberto, A. V., Faria, R. X., Couto, C. G., Ferreira, L. G., Souza, C. A., Teixeira, P. C., Fróes, M. M., and Alves, L. A. (2013). Is pannexin the pore associated with the P2X7 receptor? *Naunyn-Schmiedeberg's Archives of Pharmacology*, 386(9):775–787. 1.3.4.2
- [Alcaide et al., 2008] Alcaide, P., Newton, G., Auerbach, S., Sehrawat, S., Mayadas, T. N., Golan, D. E., Yacono, P., Vincent, P., Kowalczyk, A., and Luscinskas, F. W. (2008). p120-catenin regulates leukocyte transmigration through an effect on VE-cadherin phosphorylation. *Blood*, 112(7):2770–2779. 4.5.2.4
- [Anderson and Nedergaard, 2006] Anderson, C. M. and Nedergaard, M. (2006). Emerging challenges of assigning P2X7 receptor function and immunoreactivity in neurons. *Trends in Neurosciences*, 29(5):257–262. 1.3.2, 4.1
- [Antonio et al., 2011] Antonio, L. S., Stewart, a. P., Xu, X. J., Varanda, W. a., Murrell-Lagnado, R. D., and Edwardson, J. M. (2011). P2X4 receptors interact with both P2X2 and P2X7 receptors in the form of homotrimers. *British*

- journal of pharmacology*, 163(5):1069–77. 1.3.1, 2, 1.3.4.9, 1.3.4.9, 3.3.3, 4.4, 4.4.1, 4.4.3
- [Arnaout, 2016] Arnaout, M. A. (2016). Biology and structure of leukocyte  $\beta 2$  integrins and their role in inflammation. *F1000Research*, 5(0):2433. 3.4.6, 4.5.2.1
- [Aurrand-Lions et al., 2002] Aurrand-Lions, M., Johnson-Leger, C., and Imhof, B. A. (2002). The last molecular fortress in leukocyte trans-endothelial migration. *Nature Immunology*, 3(2):116–118. 4.5.2.4
- [Babelova et al., 2009] Babelova, A., Moreth, K., Tsalastra-Greul, W., Zeng-Brouwers, J., Eickelberg, O., Young, M. F., Brucker, P., Pfeilschifter, J., Schaefer, R. M., Gröne, H. J., and Schaefer, L. (2009). Biglycan, a danger signal that activates the NLRP3 inflammasome via toll-like and P2X receptors. *Journal of Biological Chemistry*, 284(36):24035–24048. 2, 1.3.4.7, 1.3.4.9
- [Bardin et al., 2009] Bardin, N., Blot-Chabaud, M., Despoix, N., Kebir, A., Harhour, K., Arsanto, J. P., Espinosa, L., Perrin, P., Robert, S., Vely, F., Sabatier, F., Le Bivic, A., Kaplanski, G., Sampol, J., and Dignat-George, F. (2009). CD146 and its soluble form regulate monocyte transendothelial migration. *Arteriosclerosis, Thrombosis, and Vascular Biology*, 29(5):746–753. 4.5.2.3, 4.5.2.4, 4.5.2.6
- [Baroja-Mazo et al., 2013] Baroja-Mazo, A., Barberà-Cremades, M., and Pelegrín, P. (2013). P2X7 Receptor Activation Impairs Exogenous MHC Class I Oligopeptides Presentation in Antigen Presenting Cells. *PLoS ONE*, 8(8). 4.5.1
- [Barth and Kasper, 2009] Barth, K. and Kasper, M. (2009). Membrane compartments and purinergic signalling: Occurrence and function of P2X receptors in lung. *FEBS Journal*, 276(2):341–353. 1.3.2, 1.3.4.4
- [Barth et al., 2008] Barth, K., Weinhold, K., Guenther, A., Linge, A., Gereke, M., and Kasper, M. (2008). Characterization of the molecular interaction between caveolin-1 and the P2X receptors 4 and 7 in E10 mouse lung alveolar epithelial cells. *International Journal of Biochemistry and Cell Biology*, 40(10):2230–2239. 2, 1.3.4.4, 4.5.2.5

- [Barth et al., 2007] Barth, K., Weinhold, K., Guenther, a., Young, M. T., Schnitler, H., and Kasper, M. (2007). Caveolin-1 influences P2X7 receptor expression and localization in mouse lung alveolar epithelial cells. *The FEBS journal*, 274(12):3021–33. 1.3.4.4, 4.5.2.5
- [Bartlett et al., 2014] Bartlett, R., Stokes, L., and Sluyter, R. (2014). The P2X7 Receptor Channel: Recent Developments and the Use of P2X7 Antagonists in Models of Disease. *Pharmacological Reviews*, 66(3):638–675. 1.3.3
- [Basso et al., 2009] Basso, A. M., Bratcher, N. A., Harris, R. R., Jarvis, M. F., Decker, M. W., and Rueter, L. E. (2009). Behavioral profile of P2X7 receptor knockout mice in animal models of depression and anxiety: Relevance for neuropsychiatric disorders. *Behavioural Brain Research*, 198(1):83–90. 4.1
- [Berman and Muller, 1995] Berman, M. E. and Muller, W. A. (1995). Ligation of platelet/endothelial cell adhesion molecule 1 (PECAM-1/CD31) on monocytes and neutrophils increases binding capacity of leukocyte CR3 (CD11b/CD18). *The Journal of Immunology*, 154(1):299 LP – 307. 4.5.2.2
- [Berman et al., 1996] Berman, M. E., Xie, Y., and Muller, W. A. (1996). Roles of platelet/endothelial cell adhesion molecule-1 (PECAM-1, CD31) in natural killer cell transendothelial migration and beta 2 integrin activation. *The Journal of Immunology*, 156(4):1515 LP – 1524. 4.5.2.2
- [Bobanovic et al., 2002] Bobanovic, L. K., Royle, S. J., and Murrell-Lagnado, R. D. (2002). P2X receptor trafficking in neurons is subunit specific. *The Journal of neuroscience : the official journal of the Society for Neuroscience*, 22(12):4814–4824. 1.3.4.9, 4.4.1
- [Boumechache et al., 2009] Boumechache, M., Masin, M., Edwardson, J. M., Górecki, D., and Murrell-Lagnado, R. (2009). Analysis of assembly and trafficking of native P2X4 and P2X7 receptor complexes in rodent immune cells. *Journal of Biological Chemistry*, 284(20):13446–13454. 2, 1.3.4.9, 4.4, 4.4.1, 4.4.3
- [Bowler et al., 2003] Bowler, J. W., Jayne Bailey, R., Alan North, R., and Surprenant, A. (2003). P2X4 , P2Y1 and P2Y2 receptors on rat alveolar macrophages. *British Journal of Pharmacology*, 140(3):567–575. 1.3.4.9, 3.3.1

- [Boyce and Swayne, 2017] Boyce, A. K. and Swayne, L. A. (2017). P2X7 receptor cross-talk regulates ATP-induced pannexin 1 internalization. *Biochemical Journal*, 474(13):2133–2144. 2, 1.3.4.2
- [Boyce et al., 2015] Boyce, A. K. J., Kim, M. S., Wicki-Stordeur, L. E., and Swayne, L. A. (2015). ATP stimulates pannexin 1 internalization to endosomal compartments. *Biochemical Journal*, 470(3):319–330. 1.3.4.2
- [Brake et al., 1994] Brake, A. J., Wagenbach, M. J., and Julius, D. (1994). New structural motif for ligand-gated ion channels defined by an ionotropic ATP receptor. *Nature*, 371(6497):519–23. 1.2
- [Browne et al., 2010] Browne, L. E., Jiang, L. H., and North, R. A. (2010). New structure enlivens interest in P2X receptors. *Trends in Pharmacological Sciences*, 31(5):229–237. 1.2
- [Bucci et al., 1992] Bucci, C., Parton, R. G., Mather, I. H., Stunnenberg, H., Simons, K., Hoflack, B., and Zerial, M. (1992). The small GTPase rab5 functions as a regulatory factor in the early endocytic pathway. *Cell*, 70(5):715–728. 4.5.1
- [Burnstock, 1972] Burnstock, G. (1972). Purinergic Nerves. *Pharmacological Reviews*, 24(3):509 LP – 581. 1.1
- [Burnstock, 2012] Burnstock, G. (2012). Discovery of purinergic signalling, the initial resistance and current explosion of interest. *British Journal of Pharmacology*, 167(2):238–255. 1.1
- [Burnstock, 2014] Burnstock, G. (2014). Purinergic signalling: From discovery to current developments. *Experimental Physiology*, 99(1):16–34. 1.3.2
- [Burnstock et al., 2012] Burnstock, G., Brouns, I., Adriaensen, D., and Timmermans, J.-P. (2012). Purinergic Signaling in the Airways. *Pharmacological Reviews*, 64(4):834–868. 3.3.1
- [Burnstock and Knight, 2004] Burnstock, G. and Knight, G. E. (2004). Cellular Distribution and Functions of P2 Receptor Subtypes in Different Systems. *Int Rev Cytol.*, (240):31–304. 1.3.2
- [Carpenter et al., 2014] Carpenter, S., Ricci, E. P., Mercier, B. C., Moore, M. J., and Fitzgerald, K. A. (2014). Post-transcriptional regulation of gene expression in innate immunity. *Nature Reviews Immunology*, 14(6):361–376. 4.3

- [Casas-Pruneda et al., 2009] Casas-Pruneda, G., Reyes, J. P., Pérez-Flores, G., Pérez-Cornejo, P., and Arreola, J. (2009). Functional interactions between P2X4 and P2X7 receptors from mouse salivary epithelia. *The Journal of physiology*, 587(Pt 12):2887–901. 1.3.4.9
- [Chavez et al., 2018] Chavez, J. D., Lee, C. F., Caudal, A., Keller, A., Tian, R., and Bruce, J. E. (2018). Chemical Crosslinking Mass Spectrometry Analysis of Protein Conformations and Supercomplexes in Heart Tissue. *Cell systems*, 6(1):136–141.e5. 3.4.3, 4.6
- [Chekeni et al., 2010] Chekeni, F. B., Elliott, M. R., Sandilos, J. K., Walk, S. F., Kinchen, J. M., Lazarowski, E. R., Armstrong, A. J., Penuela, S., Laird, D. W., Salvesen, G. S., Isakson, B. E., Bayliss, D. A., and Ravichandran, K. S. (2010). Pannexin 1 channels mediate 'find-me' signal release and membrane permeability during apoptosis. *Nature*, 467(7317):863–867. 1.3.4.2
- [Chen et al., 1999] Chen, J. R., Ben, J. G., Dao, L. P., Bradley, C. J., Mulligan, S. P., and Wiley, J. S. (1999). Transendothelial migration of lymphocytes in chronic lymphocytic leukaemia is impaired and involves down-regulation of both L-selectin and CD23. *British Journal of Haematology*, 105(1):181–189. 4.5.2.6
- [Chen et al., 2014] Chen, Q., Jin, Y., Zhang, K., Li, H., Chen, W., Meng, G., and Fang, X. (2014). Alarmin HNP-1 promotes pyroptosis and IL-1 $\beta$  release through different roles of NLRP3 inflammasome via P2X7 in LPS-primed macrophages. *Innate Immunity*, 20(3):290–300. 2
- [Chen et al., 2012a] Chen, X. Q., Wang, B., Wu, C., Pan, J., Yuan, B., Su, Y. Y., Jiang, X. Y., Zhang, X., and Bao, L. (2012a). Endosome-mediated retrograde axonal transport of P2X 3 receptor signals in primary sensory neurons. *Cell Research*, 22(4):677–696. 4.5.1
- [Chen et al., 2012b] Chen, Y., Li, G., and Huang, L. Y. M. (2012b). P2X7 receptors in satellite glial cells mediate high functional expression of P2X3 receptors in immature dorsal root ganglion neurons. *Molecular Pain*, 8(1):9. 3.2.2
- [Chen et al., 2015] Chen, Y., Molet, J., Gunn, B. G., Ressler, K., and Baram, T. Z. (2015). Diversity of reporter expression patterns in transgenic mouse lines targeting corticotropin-releasing hormone-expressing neurons. *Endocrinology*, 156(12):4769–4780. 4.3

- [Chignalia et al., 2015] Chignalia, A. Z., Vogel, S. M., Reynolds, A. B., Mehta, D., Dull, R. O., Minshall, R. D., Malik, A. B., and Liu, Y. (2015). p120-catenin expressed in alveolar type II cells is essential for the regulation of lung innate immune response. *American Journal of Pathology*, 185(5):1251–1263. 4.5.2.4
- [Collo et al., 1997] Collo, G., Neidhart, S., Kawashima, E., Kosco-Vilbois, M., North, R. A., and Buell, G. (1997). Tissue distribution of the P2X7 receptor. *Neuropharmacology*, 36(9):1277–1283. 1.3.2
- [Costa-Junior et al., 2011] Costa-Junior, H. M., Vieira, F. S., and Coutinho-Silva, R. (2011). C terminus of the P2X7 receptor: Treasure hunting. *Purinergic Signalling*, 7(1):7–19. 4.2
- [Cox et al., 2011] Cox, J., Neuhauser, N., Michalski, A., Scheltema, R. A., Olsen, J. V., and Mann, M. (2011). Andromeda: A peptide search engine integrated into the MaxQuant environment. *Journal of Proteome Research*, 10(4):1794–1805. 2.2.3.11
- [Craigie et al., 2013] Craigie, E., Birch, R. E., Unwin, R. J., and Wildman, S. S. (2013). The relationship between P2X4 and P2X7: A physiologically important interaction? *Frontiers in Physiology*, 4 AUG(August):1–6. 1.3.4.9, 3.3.2, 4.4.2
- [Dagvadorj et al., 2015] Dagvadorj, J., Shimada, K., Chen, S., Jones, H. D., Tumorhhuu, G., Zhang, W., Wawrowsky, K. A., Crother, T. R., and Arditi, M. (2015). Lipopolysaccharide Induces Alveolar Macrophage Necrosis via CD14 and the P2X7 Receptor Leading to Interleukin-1 $\alpha$  Release. *Immunity*, 42(4):640–653. 1.3.3, 2, 1.3.4.7, 4.5.2
- [Danquah et al., 2016] Danquah, W., Catherine, M. S., Rissiek, B., Pinto, C., Arnau, S. P., Amadi, M., Iacenda, D., Knop, J. H., Hammel, A., Bergmann, P., Schwarz, N., Assunção, J., Rotthier, W., Haag, F., Tolosa, E., Bannas, P., Eric, B. G., Magnus, T., Laeremans, T., Stortelers, C., and Friedrich, K. N. (2016). Nanobodies that block gating of the P2X7 ion channel ameliorate inflammation. *Science Translational Medicine*, 8(366). 3.2.2, 4.2, 4.3
- [De Torre-Minguela et al., 2016] De Torre-Minguela, C., Barberà-Cremades, M., Gómez, A. I., Martín-Sánchez, F., and Pelegrín, P. (2016). Macrophage activation and polarization modify P2X7 receptor secretome influencing the inflammatory process. *Scientific Reports*, 6(October 2015):22586. 4.5.2.6

- [Denlinger et al., 2001] Denlinger, L. C., Fiset, P. L., Sommer, J. A., Watters, J. J., Prabhu, U., Dubyak, G. R., Proctor, R. A., and Bertics, P. J. (2001). Cutting Edge: The Nucleotide Receptor P2X7 Contains Multiple Protein- and Lipid-Interaction Motifs Including a Potential Binding Site for Bacterial Lipopolysaccharide. *The Journal of Immunology*, 167(4):1871–1876. 1.3.4.7
- [Di Virgilio et al., 2017] Di Virgilio, F., Dal Ben, D., Sarti, A. C., Giuliani, A. L., and Falzoni, S. (2017). The P2X7 Receptor in Infection and Inflammation. *Immunity*, 47(1):15–31. 1.3.3
- [Di Virgilio et al., 2018] Di Virgilio, F., Schmalzing, G., and Markwardt, F. (2018). The Elusive P2X7 Macropore. *Trends in Cell Biology*, 28(5):392–404. 1.3.1, 1.3.4.2
- [Doberenz et al., 2014] Doberenz, C., Zorn, M., Falke, D., Nannemann, D., Hunger, D., Beyer, L., Ihling, C. H., Meiler, J., Sinz, A., and Sawers, R. G. (2014). Pyruvate formate-lyase interacts directly with the formate channel FocA to regulate formate translocation. *Journal of Molecular Biology*, 426(15):2827–2839. 4.6
- [Elliott et al., 2005] Elliott, J. I., Surprenant, A., Marelli-Berg, F. M., Cooper, J. C., Cassady-Cain, R. L., Wooding, C., Linton, K., Alexander, D. R., and Higgins, C. F. (2005). Membrane phosphatidylserine distribution as a non-apoptotic signalling mechanism in lymphocytes. *Nature Cell Biology*, 7(8):808–816. 4.5.2.6
- [Engel et al., 2012] Engel, T., Gomez-Villafuertes, R., Tanaka, K., Mesuret, G., Sanz-Rodriguez, A., Garcia-Huerta, P., Miras-Portugal, M. T., Henshall, D. C., and Diaz-Hernandez, M. (2012). Seizure suppression and neuroprotection by targeting the purinergic P2X7 receptor during status epilepticus in mice. *The FASEB Journal*, 26(4):1616–1628. 3.2.1
- [Farley et al., 2000] Farley, F. W., Soriano, P., Steffen, L. S., and Dymecki, S. M. (2000). Widespread recombinase expression using FLPeR (flipper) mice. *Genesis (New York, N.Y. : 2000)*, 28(3-4):106–110. 3
- [Feng et al., 2015] Feng, J.-F., Gao, X.-F., Pu, Y.-y., Burnstock, G., Xiang, Z., and He, C. (2015). P2X7 receptors and Fyn kinase mediate ATP-induced oligodendrocyte progenitor cell migration. *Purinergic Signalling*, 11(3):361–369. 2

- [Feng et al., 1995] Feng, Y., Press, B., and Wandinger-Ness, A. (1995). Rab 7: An important regulator of late endocytic membrane traffic. *Journal of Cell Biology*, 131(6 I):1435–1452. 4.5.1
- [Feng et al., 2005] Feng, Y.-H., Wang, L., Wang, Q., Li, X., Zeng, R., and Gorodeski, G. I. (2005). ATP stimulates GRK-3 phosphorylation and beta-arrestin-2-dependent internalization of P2X7 receptor. *American journal of physiology. Cell physiology*, 288(6):C1342–56. 2, 1.3.4.6, 4.5.1
- [Ferrari et al., 1997] Ferrari, D., Chiozzi, P., Falzoni, S., Dal Susino, M., Melchiorri, L., Baricordi, O. R., and Di Virgilio, F. (1997). Extracellular ATP triggers IL-1 beta release by activating the purinergic P2Z receptor of human macrophages. *The Journal of Immunology*, 159(3):1451 LP – 1458. 1.3.3
- [Flanagan et al., 2012] Flanagan, K., Fitzgerald, K., Baker, J., Regnstrom, K., Gardai, S., Bard, F., Mocci, S., Seto, P., You, M., Larochelle, C., Prat, A., Chow, S., Li, L., Vandevent, C., Zago, W., Lorenzana, C., Nishioka, C., Hoffman, J., Botelho, R., Willits, C., Tanaka, K., Johnston, J., and Yednock, T. (2012). Laminin-411 Is a Vascular Ligand for MCAM and Facilitates TH17 Cell Entry into the CNS. *PLoS ONE*, 7(7):e40443. 4.5.2.3
- [Forné et al., 2012] Forné, I., Ludwigsen, J., Imhof, A., Becker, P. B., and Mueller-Planitz, F. (2012). Probing the Conformation of the ISWI ATPase Domain With Genetically Encoded Photoreactive Crosslinkers and Mass Spectrometry. *Molecular & Cellular Proteomics*, 11(4):M111.012088. 2.2.3.11
- [Franceschini et al., 2015] Franceschini, A., Capece, M., Chiozzi, P., Falzoni, S., Sanz, J. M., Sarti, A. C., Bonora, M., Pinton, P., and Di Virgilio, F. (2015). The P2X7 receptor directly interacts with the NLRP3 inflammasome scaffold protein. *The FASEB Journal*, 29(6):2450–2461. 1.3.3, 2, 1.3.4.7
- [Franco et al., 2013] Franco, M. C., Ye, Y., Refakis, C. A., Feldman, J. L., Stokes, A. L., Basso, M., Melero Fernandez de Mera, R. M., Sparrow, N. A., Calingasan, N. Y., Kiaei, M., Rhoads, T. W., Ma, T. C., Grumet, M., Barnes, S., Beal, M. F., Beckman, J. S., Mehl, R., and Estevez, A. G. (2013). Nitration of Hsp90 induces cell death. *Proceedings of the National Academy of Sciences*, 110(12):E1102–E1111. 2, 1.3.4.1

- [Gerfen et al., 2013] Gerfen, C. R., Paletzki, R., and Heintz, N. (2013). GEN-SAT BAC cre-recombinase driver lines to study the functional organization of cerebral cortical and basal ganglia circuits. *Neuron*, 80(6):1368–1383. 4.2
- [Gibson et al., 2009] Gibson, D. G., Young, L., Chuang, R.-Y., Venter, J. C., Hutchison, C. a., and Smith, H. O. (2009). Enzymatic assembly of DNA molecules up to several hundred kilobases. *Nature methods*, 6(5):343–5. 2.2.2.1
- [Giuliani et al., 2017] Giuliani, A. L., Sarti, A. C., Falzoni, S., and Di Virgilio, F. (2017). The P2X7 receptor-interleukin-1 liaison. *Frontiers in Pharmacology*, 8(MAR):1–10. 1.3.3
- [Gong et al., 2003] Gong, S., Zheng, C., Doughty, M. L., Losos, K., Didkovsky, N., Schambra, U. B., Nowak, N. J., Joyner, A., Leblanc, G., Hatten, M. E., and Heintz, N. (2003). A gene expression atlas of the central nervous system based on bacterial artificial chromosomes. *Nature*, 425(6961):917–925. 4.1, 4.3
- [Gu et al., 2009] Gu, B. J., Rathsam, C., Stokes, L., McGeachie, A. B., and Wiley, J. S. (2009). Extracellular ATP dissociates nonmuscle myosin from P2X(7) complex: this dissociation regulates P2X(7) pore formation. *American journal of physiology. Cell physiology*, 297(2):C430–9. 1.3.4, 2, 1.3.4.1, 1.3.4.5
- [Gu et al., 2010] Gu, B. J., Saunders, B. M., Jursik, C., and Wiley, J. S. (2010). The P2X7-nonmuscle myosin membrane complex regulates phagocytosis of nonopsonized particles and bacteria by a pathway attenuated by extracellular ATP. *Blood*, 115(8):1621–1631. 1.3.4.5
- [Guezguez et al., 2014] Guezguez, B., Vigneron, P., Lamerant, N., Kieda, C., Jaffredo, T., and Dunon, D. (2014). Dual Role of Melanoma Cell Adhesion Molecule (MCAM)/CD146 in Lymphocyte Endothelium Interaction: MCAM/CD146 Promotes Rolling via Microvilli Induction in Lymphocyte and Is an Endothelial Adhesion Receptor. *The Journal of Immunology*, 179(10):6673–6685. 4.5.2.3
- [Guo et al., 2007] Guo, C., Masin, M., Qureshi, O. S., and Murrell-Lagnado, R. D. (2007). Evidence for functional P2X4/P2X7 heteromeric receptors. *Molecular pharmacology*, 72(6):1447–56. 2, 1.3.4.9, 1.3.4.9, 1.3.4.9, 1.3.4.9, 1.3.4.9, 3.3.1, 4.2, 4.4, 4.4.1, 4.4.3

- [Guo et al., 2016] Guo, L., Zhang, H., Hou, Y., Wei, T., and Liu, J. (2016). Plasmalemma vesicle-associated protein: A crucial component of vascular homeostasis. *Experimental and Therapeutic Medicine*, 12(3):1639–1644. 4.5.2.5
- [Hanack et al., 2015] Hanack, C., Moroni, M., Lima, W. C., Wende, H., Kirchner, M., Adelfinger, L., Schrenk-Siemens, K., Tappe-Theodor, A., Wetzels, C., Kuich, P. H., Gassmann, M., Roggenkamp, D., Bettler, B., Lewin, G. R., Selbach, M., and Siemens, J. (2015). GABA blocks pathological but not acute TRPV1 pain signals. *Cell*, 160(4):759–770. 4.5
- [Hanley et al., 2012] Hanley, P. J., Kronlage, M., Kirschning, C., Del Rey, A., Di Virgilio, F., Leipziger, J., Chessell, I. P., Sargin, S., Filippov, M. A., Lindemann, O., Mohr, S., Königs, V., Schillers, H., Bähler, M., and Schwab, A. (2012). Transient P2X7 receptor activation triggers macrophage death independent of toll-like receptors 2 and 4, caspase-1, and pannexin-1 proteins. *Journal of Biological Chemistry*, 287(13):10650–10663. 1.3.4.2
- [Harkat et al., 2017] Harkat, M., Peverini, L., Cerdan, A. H., Dunning, K., Beudez, J., Martz, A., Calimet, N., Specht, A., Cecchini, M., Chataigneau, T., and Grutter, T. (2017). On the permeation of large organic cations through the pore of ATP-gated P2X receptors. *Proceedings of the National Academy of Sciences*, 114(19):E3786–E3795. 1.3.4.2
- [He et al., 2016] He, Y., Zeng, M. Y., Yang, D., Motro, B., and Núñez, G. (2016). NEK7 is an essential mediator of NLRP3 activation downstream of potassium efflux. *Nature*, 530(7590):354–357. 1.3.3
- [Holding, 2015] Holding, A. N. (2015). XL-MS: Protein cross-linking coupled with mass spectrometry. *Methods*, 89:54–63. 4.6
- [Hou and Cao, 2016] Hou, Z. and Cao, J. (2016). Comparative study of the P2X gene family in animals and plants. *Purinergic Signalling*, 12(2):269–281. 1.3.4.9
- [Huang, 2014] Huang, C. (2014). MUC18 Differentially Regulates Pro-Inflammatory and Anti-Viral Responses in Human Airway Epithelial Cells. *Journal of Clinical & Cellular Immunology*, 05(05). 4.5.2.3
- [Hung et al., 2005] Hung, A. C., Chu, Y. J., Lin, Y. H., Weng, J. Y., Chen, H. B., Au, Y. C., and Sun, S. H. (2005). Roles of protein kinase C in regulation of

- P2X7 receptor-mediated calcium signalling of cultured type-2 astrocyte cell line, RBA-2. *Cellular Signalling*, 17(11):1384–1396. 2
- [Hung et al., 2013] Hung, S.-C., Choi, C. H., Said-Sadier, N., Johnson, L., Atanasova, K. R., Sellami, H., Yilmaz, Ö., and Ojcius, D. M. (2013). P2X4 assembles with P2X7 and pannexin-1 in gingival epithelial cells and modulates ATP-induced reactive oxygen species production and inflammasome activation. *PloS one*, 8(7):e70210. 2, 1.3.4.2, 1.3.4.9, 1.3.4.9, 4.4.3
- [Hutagalung and Novick, 2011] Hutagalung and Novick (2011). Role of Rab GT-Pases in Membrane Traffic and Cell Physiology. *Physiol Rev*, 91(1):119–149. 4.5.1
- [Iglesias et al., 2008] Iglesias, R., Locovei, S., Roque, A., Alberto, A. P., Dahl, G., Spray, D. C., and Scemes, E. (2008). P2X7 receptor-Pannexin1 complex: pharmacology and signaling. *AJP: Cell Physiology*, 295(3):C752–C760. 2, 1.3.4.2
- [Illes et al., 2017] Illes, P., Khan, T. M., and Rubini, P. (2017). Neuronal P2X7 Receptors Revisited: Do They Really Exist? *The Journal of Neuroscience*, 37(30):7049–7062. 1.3.2, 4.1
- [Ireton et al., 2002] Ireton, R. C., Davis, M. A., Van Hengel, J., Mariner, D. J., Barnes, K., Thoreson, M. A., Anastasiadis, P. Z., Matrisian, L., Bundy, L. M., Sealy, L., Gilbert, B., Van Roy, F., and Reynolds, A. B. (2002). A novel role for p120 catenin in E-cadherin function. *Journal of Cell Biology*, 159(3):465–476. 4.5.2.4
- [Isakson and Thompson, 2014] Isakson, B. E. and Thompson, R. J. (2014). Pannexin-1 as a potentiator of ligand-gated receptor signaling. *Channels*, 8(2):118–123. 1.3.4.2
- [Ivetic, 2018] Ivetic, A. (2018). A head-to-tail view of L-selectin and its impact on neutrophil behaviour. *Cell and Tissue Research*, 371(3):437–453. 4.5.2.6
- [Jacobson and Müller, 2016] Jacobson, K. A. and Müller, C. E. (2016). Medicinal chemistry of adenosine, P2Y and P2X receptors. *Neuropharmacology*, 104:31–49. 1.1

- [Jager and Vaegter, 2016] Jager, S. B. and Vaegter, C. B. (2016). Avoiding experimental bias by systematic antibody validation. *Neural Regeneration Research*, 11(7):1079–1080. 1.3.2
- [Jensen et al., 2009] Jensen, L. J., Kuhn, M., Stark, M., Chaffron, S., Creevey, C., Muller, J., Doerks, T., Julien, P., Roth, A., Simonovic, M., Bork, P., and von Mering, C. (2009). STRING 8 - A global view on proteins and their functional interactions in 630 organisms. *Nucleic Acids Research*, 37(SUPPL. 1):412–416. 3.4.5, 26
- [Jiang et al., 2013] Jiang, L.-H., Baldwin, J. M., Roger, S., and Baldwin, S. a. (2013). Insights into the Molecular Mechanisms Underlying Mammalian P2X7 Receptor Functions and Contributions in Diseases, Revealed by Structural Modeling and Single Nucleotide Polymorphisms. *Frontiers in pharmacology*, 4(May):55. 2, 1.3.1
- [Jiang et al., 2015] Jiang, T., Hoekstra, J., Heng, X., Kang, W., Ding, J., Liu, J., Chen, S., and Zhang, J. (2015). P2X7 receptor is critical in alpha-synuclein-mediated microglial NADPH oxidase activation. *Neurobiology of Aging*, 36(7):2304–2318. 2
- [Jimenez-Pacheco et al., 2013] Jimenez-Pacheco, A., Mesuret, G., Sanz-Rodriguez, A., Tanaka, K., Mooney, C., Conroy, R., Miras-Portugal, M. T., Diaz-Hernandez, M., Henshall, D. C., and Engel, T. (2013). Increased neocortical expression of the P2X7 receptor after status epilepticus and anticonvulsant effect of P2X7 receptor antagonist A-438079. *Epilepsia*, 54(9):1551–1561. 2.2.5.2
- [Johnson et al., 1997] Johnson, J. P., Bar-Eli, M., Jansen, B., and Markhof, E. (1997). Melanoma progression-associated glycoprotein MUC18/MCAM mediates homotypic cell adhesion through interaction with a heterophilic ligand. *International journal of cancer*, 73(5):769–74. 4.5.2.3
- [Jun et al., 2007] Jun, D. J., Kim, J., Jung, S. Y., Song, R., Noh, J. H., Park, Y. S., Ryu, S. H., Kim, J. H., Kong, Y. Y., Chung, J. M., and Kim, K. T. (2007). Extracellular ATP mediates necrotic cell swelling in SN4741 dopaminergic neurons through P2X7 receptors. *Journal of Biological Chemistry*, 282(52):37350–37358. 3.2.1

- [Kaake et al., 2014] Kaake, R. M., Wang, X., Burke, A., Yu, C., Kandur, W., Yang, Y., Novtisky, E. J., Second, T., Duan, J., Kao, A., Guan, S., Vellucci, D., Rychnovsky, S. D., and Huang, L. (2014). A New in Vivo Cross-linking Mass Spectrometry Platform to Define Protein-Protein Interactions in Living Cells. *Molecular & Cellular Proteomics*, 13(12):3533–3543. 3.4.3
- [Kaczmarek-Hajek et al., 2018] Kaczmarek-Hajek, K., Zhang, J., Kopp, R., Grosche, A., Rissiek, B., Saul, A., Bruzzone, S., Engel, T., Jooss, T., Krautloher, A., Schuster, S., Magnus, T., Stadelmann, C., Sirko, S., Koch-Nolte, F., Eulenburg, V., and Nicke, A. (2018). Re-evaluation of neuronal P2X7 expression using novel mouse models and a P2X7-specific nanobody. *eLife*, 7:1–29. 1.3.2, 1.4, 3, 2.2.2.8, 2.2.4, 2.2.5.2, 3.1.1, 3.2.1, 3.2.1, 4.1, 4.2, 4.3, 4.3, 4.3
- [Kalkhof and Sinz, 2008] Kalkhof, S. and Sinz, A. (2008). Chances and pitfalls of chemical cross-linking with amine-reactive N-hydroxysuccinimide esters. *Analytical and Bioanalytical Chemistry*, 392(1-2):1–8. 3.4.2
- [Kanjanamekanant et al., 2014] Kanjanamekanant, K., Luckprom, P., and Pavasant, P. (2014). P2X7 receptor-Pannexin1 interaction mediates stress-induced interleukin-1 beta expression in human periodontal ligament cells. *Journal of Periodontal Research*, 49(5):595–602. 2, 1.3.4.2
- [Karasawa et al., 2017] Karasawa, A., Michalski, K., Mikhelzon, P., and Kawate, T. (2017). The P2X7 receptor forms a dye-permeable pore independent of its intracellular domain but dependent on membrane lipid composition. *eLife*, 6(1):1–22. 1.3.1, 1.3.4.2
- [Kawano et al., 2012a] Kawano, A., Tsukimoto, M., Mori, D., Noguchi, T., Harada, H., Takenouchi, T., Kitani, H., and Kojima, S. (2012a). Regulation of P2X7-dependent inflammatory functions by P2X4 receptor in mouse macrophages. *Biochemical and Biophysical Research Communications*, 420(1):102–107. 1.3.4.9
- [Kawano et al., 2012b] Kawano, A., Tsukimoto, M., Noguchi, T., Hotta, N., Harada, H., Takenouchi, T., Kitani, H., and Kojima, S. (2012b). Involvement of P2X4 receptor in P2X7 receptor-dependent cell death of mouse macrophages. *Biochemical and Biophysical Research Communications*, 419(2):374–380. 1.3.4.9, 1.3.4.9, 1.3.4.9, 4.4.2

- [Kawate et al., 2009] Kawate, T., Michel, J. C., Birdsong, W. T., and Gouaux, E. (2009). Crystal structure of the ATP-gated P2X<sub>4</sub> ion channel in the closed state. *Nature*, 460(7255):592–598. 1.2
- [Kayagaki et al., 2015] Kayagaki, N., Stowe, I. B., Lee, B. L., O’Rourke, K., Anderson, K., Warming, S., Cuellar, T., Haley, B., Roose-Girma, M., Phung, Q. T., Liu, P. S., Lill, J. R., Li, H., Wu, J., Kummerfeld, S., Zhang, J., Lee, W. P., Snipas, S. J., Salvesen, G. S., Morris, L. X., Fitzgerald, L., Zhang, Y., Bertram, E. M., Goodnow, C. C., and Dixit, V. M. (2015). Caspase-11 cleaves gasdermin D for non-canonical inflammasome signalling. *Nature*, 526(7575):666–671. 1.3.3
- [Keuschnigg et al., 2009] Keuschnigg, J., Henttinen, T., Auvinen, K., Karikoski, M., Salmi, M., and Jalkanen, S. (2009). The prototype endothelial marker PAL-E is a leukocyte trafficking molecule. *Blood*, 114(2):478–484. 4.5.2.5
- [Kim et al., 2001] Kim, M., Jiang, L. H., Wilson, H. L., North, R. A., and Surprenant, A. (2001). Proteomic and functional evidence for a P2X<sub>7</sub> receptor signalling complex. *EMBO Journal*, 20(22):6347–6358. 1.3.4, 2, 1.3.4.1, 3.4.5, 4.5, 4.5.2.1
- [Klockenbusch and Kast, 2010] Klockenbusch, C. and Kast, J. (2010). Optimization of Formaldehyde Cross-Linking for Protein Interaction Analysis of Non-Tagged Integrin  $\beta$  1. *Journal of Biomedicine and Biotechnology*, 2010:1–13. 3.4.2
- [Kuehnel et al., 2009] Kuehnel, M. P., Rybin, V., Anand, P. K., Anes, E., and Griffiths, G. (2009). Lipids regulate P2X<sub>7</sub>-receptor-dependent actin assembly by phagosomes via ADP translocation and ATP synthesis in the phagosome lumen. *Journal of Cell Science*, 122(4):499–504. 1.3.4.9, 4.4.2
- [Kunii et al., 2016] Kunii, M., Ohara-Imaizumi, M., Takahashi, N., Kobayashi, M., Kawakami, R., Kondoh, Y., Shimizu, T., Simizu, S., Lin, B., Nunomura, K., Aoyagi, K., Ohno, M., Ohmuraya, M., Sato, T., Yoshimura, S. I., Sato, K., Harada, R., Kim, Y. J., Osada, H., Nemoto, T., Kasai, H., Kitamura, T., Nagamatsu, S., and Harada, A. (2016). Opposing roles for SNAP23 in secretion in exocrine and endocrine pancreatic cells. *Journal of Cell Biology*, 215(1). 4.5.1
- [Labasi et al., 2002] Labasi, J. M., Petrushova, N., Donovan, C., McCurdy, S., Lira, P., Payette, M. M., Brissette, W., Wicks, J. R., Audoly, L., and Gabel,

- C. A. (2002). Absence of the P2X7 Receptor Alters Leukocyte Function and Attenuates an Inflammatory Response. *The Journal of Immunology*, 168(12):6436–6445. 4.5.2.6
- [Lakso et al., 1996] Lakso, M., Pichel, J. G., Gorman, J. R., Sauer, B., Okamoto, Y., Lee, E., Alt, F. W., and Westphal, H. (1996). Efficient in vivo manipulation of mouse genomic sequences at the zygote stage. *Proc. Natl. Acad. Sci. USA*, 93:5860–5865. 3
- [Lappe-Siefke et al., 2003] Lappe-Siefke, C., Goebbels, S., Gravel, M., Nicksch, E., Lee, J., Braun, P. E., Griffiths, I. R., and Navel, K. A. (2003). Disruption of *Cnp1* uncouples oligodendroglial functions in axonal support and myelination. *Nature Genetics*, 33(3):366–374. 3, 3.2.1
- [Leitner et al., 2016] Leitner, A., Faini, M., Stengel, F., and Aebersold, R. (2016). Crosslinking and Mass Spectrometry: An Integrated Technology to Understand the Structure and Function of Molecular Machines. *Trends in Biochemical Sciences*, 41(1):20–32. 4.6
- [Li et al., 2017] Li, J., Zhang, W., Yang, H., Howrigan, D. P., Wilkinson, B., Souaiaia, T., Evgrafov, O. V., Genovese, G., Clementel, V. A., Tudor, J. C., Abel, T., Knowles, J. A., Neale, B. M., Wang, K., Sun, F., and Coba, M. P. (2017). Spatiotemporal profile of postsynaptic interactomes integrates components of complex brain disorders. *Nature Neuroscience*, 20(8):1150–1161. 1.3.4, 2
- [Li et al., 2011] Li, S., Tomić, M., and Stojilkovic, S. S. (2011). Characterization of novel Pannexin 1 isoforms from rat pituitary cells and their association with ATP-gated P2X channels. *General and Comparative Endocrinology*, 174(2):202–210. 2, 1.3.4.2
- [Liu et al., 2011] Liu, Y., Xiao, Y., and Li, Z. (2011). P2X7 receptor positively regulates MyD88-dependent NF- $\kappa$ B activation. *Cytokine*, 55(2):229–236. 2, 1.3.4.7
- [Locovei et al., 2007] Locovei, S., Scemes, E., Qiu, F., Spray, D. C., and Dahl, G. (2007). Pannexin1 is part of the pore forming unit of the P2X7 receptor death complex. *FEBS Letters*, 581(3):483–488. 1.3.4.2

- [Lopez-Castejon and Brough, 2011] Lopez-Castejon, G. and Brough, D. (2011). Understanding the mechanism of IL-1 $\beta$  secretion. *Cytokine and Growth Factor Reviews*, 22(4):189–195. 1.3.3
- [Ma et al., 2006] Ma, W., Korngreen, A., Weil, S., Cohen, E. B.-T., Priel, A., Kuzin, L., and Silberberg, S. D. (2006). Pore properties and pharmacological features of the P2X receptor channel in airway ciliated cells. *The Journal of physiology*, 571(Pt 3):503–17. 1.3.4.9, 1.3.4.9
- [Mackenzie et al., 2005] Mackenzie, A. B., Young, M. T., Adinolfi, E., and Surprenant, A. (2005). Pseudoapoptosis Induced by Brief Activation of ATP-gated P2X7 Receptors. *Journal of Biological Chemistry*, 280(40):33968–33976. 4.5.2.6
- [Manodori et al., 2000] Manodori, a. B., Barabino, G. A., Lubin, B. H., and Kuypers, F. a. (2000). Adherence of phosphatidylserine-exposing erythrocytes to endothelial matrix thrombospondin. *Blood*, 95(4):1293–1300. 4.5.2.6
- [Manohar et al., 2012] Manohar, M., Hirsh, M. I., Chen, Y., Woehrle, T., Karande, A. A., and Junger, W. G. (2012). ATP release and autocrine signaling through P2X4 receptors regulate  $\gamma\delta$  T cell activation. *Journal of Leukocyte Biology*, 92(4):787–794. 4.4.2
- [Marín-García et al., 2008] Marín-García, P., Sánchez-Nogueiro, J., Gómez-Villafuertes, R., León, D., and Miras-Portugal, M. T. (2008). Synaptic terminals from mice midbrain exhibit functional P2X7 receptor. *Neuroscience*, 151(2):361–373. 4.1, 4.3
- [Martin et al., 2009] Martin, U., Scholler, J., Gurgel, J., Renshaw, B., Sims, J. E., and Gabel, C. A. (2009). Externalization of the Leaderless Cytokine IL-1F6 Occurs in Response to Lipopolysaccharide/ATP Activation of Transduced Bone Marrow Macrophages. *The Journal of Immunology*, 183(6):4021–4030. 1.3.3
- [Masin et al., 2012] Masin, M., Young, C., Lim, K., Barnes, S. J., Xu, X. J., Marschall, V., Brutkowski, W., Mooney, E. R., Gorecki, D. C., and Murrell-Lagnado, R. (2012). Expression, assembly and function of novel C-terminal truncated variants of the mouse P2X7 receptor: Re-evaluation of P2X7 knock-outs. *British Journal of Pharmacology*, 165(4):978–993. 4.1, 4.3

- [McLauchlan et al., 1998] McLauchlan, H., Newell, J., Morrice, N., Osborne, A., West, M., and Smythe, E. (1998). A novel role for Rab5-GDI in ligand sequestration into clathrin-coated pits. *Current Biology*, 8(1):34–45. 4.5.1
- [Mehta et al., 2001] Mehta, V. B., Hart, J., and Wewers, M. D. (2001). ATP-stimulated Release of Interleukin (IL)-1 $\beta$  and IL-18 Requires Priming by Lipopolysaccharide and Is Independent of Caspase-1 Cleavage. *Journal of Biological Chemistry*, 276(6):3820–3826. 1.3.3
- [Mellacheruvu et al., 2013] Mellacheruvu, D., Wright, Z., Couzens, A. L., Lambert, J. P., St-Denis, N. A., Li, T., Miteva, Y. V., Hauri, S., Sardi, M. E., Low, T. Y., Halim, V. A., Bagshaw, R. D., Hubner, N. C., Al-Hakim, A., Bouchard, A., Faubert, D., Fermin, D., Dunham, W. H., Goudreault, M., Lin, Z. Y., Badillo, B. G., Pawson, T., Durocher, D., Coulombe, B., Aebersold, R., Superti-Furga, G., Colinge, J., Heck, A. J. R., Choi, H., Gstaiger, M., Mohammed, S., Cristea, I. M., Bennett, K. L., Washburn, M. P., Raught, B., Ewing, R. M., Gingras, A. C., and Nesvizhskii, A. I. (2013). The CRAPome: A contaminant repository for affinity purification-mass spectrometry data. *Nature Methods*, 10(8):730–736. 1.3.4, 2, 4.5
- [Metzger et al., 2016] Metzger, M. W., Walser, S. M., Aprile-Garcia, F., Dedic, N., Chen, A., Holsboer, F., Arzt, E., Wurst, W., and Deussing, J. M. (2016). Genetically dissecting P2rx7 expression within the central nervous system using conditional humanized mice. *Purinergic Signalling*, 13(2):153–170. 4.1, 4.3, 4.3
- [Migita et al., 2016] Migita, K., Ozaki, T., Shimoyama, S., Yamada, J., Nikaido, Y., Furukawa, T., Shiba, Y., Egan, T. M., and Ueno, S. (2016). HSP90 Regulation of P2X7 Receptor Function Requires an Intact Cytoplasmic C-Terminus. *Molecular Pharmacology*, 90(2):116–126. 1.3.4.1
- [Miklavc et al., 2011] Miklavc, P., Mair, N., Wittekindt, O. H., Haller, T., Dietl, P., Felder, E., Timmler, M., and Frick, M. (2011). Fusion-activated Ca<sup>2+</sup> entry via vesicular P2X4 receptors promotes fusion pore opening and exocytotic content release in pneumocytes. *Proceedings of the National Academy of Sciences*, 108(35):14503–14508. 3.3.1
- [Miklavc et al., 2013] Miklavc, P., Thompson, K. E., and Frick, M. (2013). A new role for P2X4 receptors as modulators of lung surfactant secretion. *Frontiers in Cellular Neuroscience*, 7(October):2009–2014. 3.3.1, 3.3.1

- [Minkiewicz et al., 2013] Minkiewicz, J., de Rivero Vaccari, J. P., and Keane, R. W. (2013). Human astrocytes express a novel NLRP2 inflammasome. *Glia*, 61(7):1113–1121. 1.3.3, 2, 1.3.4.7
- [Miras-Portugal et al., 2017] Miras-Portugal, M. T., Sebastián-Serrano, Á., de Diego García, L., and Díaz-Hernández, M. (2017). Neuronal P2X7 Receptor: Involvement in Neuronal Physiology and Pathology. *The Journal of Neuroscience*, 37(30):7063–7072. 1.3.2, 4.1
- [Mishra et al., 2011] Mishra, A., Chintagari, N. R., Guo, Y., Weng, T., Su, L., and Liu, L. (2011). Purinergic P2X7 receptor regulates lung surfactant secretion in a paracrine manner. *Journal of Cell Science*, 124(4):657–668. 3.3.1, 4.5.1
- [Mishra et al., 2016] Mishra, A., Guo, Y., Zhang, L., More, S., Weng, T., Chintagari, N. R., Huang, C., Liang, Y., Pushparaj, S., Gou, D., Breshears, M., and Liu, L. (2016). A Critical Role for P2X7 Receptor-Induced VCAM-1 Shedding and Neutrophil Infiltration during Acute Lung Injury. *The Journal of Immunology*, 197(7):2828–2837. 4.5.2, 4.5.2.6
- [Monção-Ribeiro et al., 2011] Monção-Ribeiro, L. C., Cagido, V. R., Lima-Murad, G., Santana, P. T., Riva, D. R., Borojevic, R., Zin, W. A., Cavalcante, M. C., Riça, I., Brando-Lima, A. C., Takiya, C. M., Faffe, D. S., and Coutinho-Silva, R. (2011). Lipopolysaccharide-induced lung injury: Role of P2X7 receptor. *Respiratory Physiology & Neurobiology*, 179(2-3):314–325. 4.5.2
- [Morin et al., 2008] Morin, N. A., Oakes, P. W., Hyun, Y.-M., Lee, D., Chin, Y. E., King, M. R., Springer, T. A., Shimaoka, M., Tang, J. X., Reichner, J. S., and Kim, M. (2008). Nonmuscle myosin heavy chain IIA mediates integrin LFA-1 de-adhesion during T lymphocyte migration. *The Journal of Experimental Medicine*, 205(1):195–205. 4.5.2.6
- [Moura et al., 2015] Moura, G., Lucena, S., Lima, M., Nascimento, F., Gesteira, T., Nader, H., Paredes-Gamero, E., and Tersariol, I. (2015). Post-translational allosteric activation of the P2X7 receptor through glycosaminoglycan chains of CD44 proteoglycans. *Cell Death Discovery*, 1(1):15005. 2
- [Müller et al., 2001] Müller, D. R., Schindler, P., Towbin, H., Wirth, U., Voshol, H., Hoving, S., and Steinmetz, M. O. (2001). Isotope tagged cross linking

- reagents. A new tool in mass spectrometric protein interaction analysis. *Analytical Chemistry*, 73(9):1927–1934. 3.4.7, 4.6
- [Muller, 2007] Muller, W. A. (2007). PECAM: Regulating the start of diapedesis. *Adhesion Molecules Function and Inhibition*, pages 201–220. 4.5.2.1, 4.5.2.2
- [Muller et al., 1993] Muller, W. A., Weigl, S. A., Deng, X., and Phillips, D. M. (1993). PECAM-1 is required for transendothelial migration of leukocytes. *The Journal of experimental medicine*, 178(2):449–60. 4.5.2.2
- [Muñoz-Planillo et al., 2013] Muñoz-Planillo, R., Kuffa, P., Martínez-Colón, G., Smith, B., Rajendiran, T., and Núñez, G. (2013). K<sup>+</sup> Efflux Is the Common Trigger of NLRP3 Inflammasome Activation by Bacterial Toxins and Particulate Matter. *Immunity*, 38(6):1142–1153. 1.3.3
- [Newell-Litwa et al., 2015] Newell-Litwa, K. A., Horwitz, R., and Lamers, M. L. (2015). Non-muscle myosin II in disease: mechanisms and therapeutic opportunities. *Disease Models & Mechanisms*, 8(12):1495–1515. 4.5.2.6
- [Nicke, 2008] Nicke, A. (2008). Homotrimeric complexes are the dominant assembly state of native P2X7 subunits. *Biochemical and biophysical research communications*, 377(3):803–8. 1.3.1, 1.3.4.9, 4.4, 4.4.3, 4.5
- [Nicke et al., 1998] Nicke, A., Bäumer, H. G., Rettinger, J., Eichele, A., Lambrecht, G., Mutschler, E., and Schmalzing, G. (1998). P2X1 and P2X3 receptors form stable trimers: A novel structural motif of ligand-gated ion channels. *EMBO Journal*, 17(11):3016–3028. 1.2
- [Nicke et al., 2009] Nicke, A., Kuan, Y.-H., Masin, M., Rettinger, J., Marquez-Klaka, B., Bender, O., Górecki, D. C., Murrell-Lagnado, R. D., and Soto, F. (2009). A functional P2X7 splice variant with an alternative transmembrane domain 1 escapes gene inactivation in P2X7 knock-out mice. *The Journal of biological chemistry*, 284(38):25813–22. 4.1, 4.3
- [Nomellini et al., 2012] Nomellini, V., Brubaker, A. L., Mahbub, S., Palmer, J. L., Gomez, C. R., and Kovacs, E. J. (2012). Dysregulation of neutrophil CXCR2 and pulmonary endothelial icam-1 promotes age-related pulmonary inflammation. *Aging and Disease*, 3(3):234–247. 3.4.6
- [North, 2002] North, R. (2002). Molecular physiology of P2X receptors. *Physiological reviews*, 82(4):1013–67. 1.2

- [Ohishi et al., 2016] Ohishi, A., Keno, Y., Marumiya, A., Sudo, Y., Uda, Y., Matsuda, K., Morita, Y., Furuta, T., Nishida, K., and Nagasawa, K. (2016). Expression level of P2X7 receptor is a determinant of ATP-induced death of mouse cultured neurons. *Neuroscience*, 319:35–45. 1.3.2, 3.2.1
- [Ousingsawat et al., 2015] Ousingsawat, J., Wanitchakool, P., Kmit, A., Romao, A. M., Jantarajit, W., Schreiber, R., and Kunzelmann, K. (2015). Anoctamin 6 mediates effects essential for innate immunity downstream of P2X7 receptors in macrophages. *Nature Communications*, 6:6245. 2, 1.3.4.8, 3.4.5, 4.5
- [Parkinson et al., 2014] Parkinson, K., Baines, A. E., Keller, T., Gruenheit, N., Bragg, L., North, A., and Thompson, C. R. L. (2014). Calcium dependent regulation of Rab activation and vesicle fusion by an intracellular P2X ion channel. *Nat Cell Biol.*, 16(1):87–98. 4.5.1
- [Pelegrin et al., 2008] Pelegrin, P., Barroso-Gutierrez, C., and Surprenant, A. (2008). P2X7 Receptor Differentially Couples to Distinct Release Pathways for IL-1 $\beta$  in Mouse Macrophage. *The Journal of Immunology*, 180:7147–7157. 1.3.3
- [Pelegrin and Surprenant, 2006] Pelegrin, P. and Surprenant, A. (2006). Pannexin-1 mediates large pore formation and interleukin-1 $\beta$  release by the ATP-gated P2X7 receptor. *EMBO Journal*, 25(21):5071–5082. 1.3.1, 2, 1.3.4.2
- [Pereira et al., 2013] Pereira, V. S., Casarotto, P. C., Hiroaki-Sato, V. A., Sartim, A. G., Guimarães, F. S., and Joca, S. R. (2013). Antidepressant- and anticomulsive-like effects of purinergic receptor blockade: Involvement of nitric oxide. *European Neuropsychopharmacology*, 23(12):1769–1778. 2
- [Pérez-Flores et al., 2015] Pérez-Flores, G., Lévesque, S. A., Pacheco, J., Vaca, L., Pérez-Cornejo, P., Arreola, J., Lacroix, S., Pérez-Cornejo, P., and Arreola, J. (2015). The P2X7/P2X4 interaction shapes the purinergic response in murine macrophages. *Biochemical and Biophysical Research Communications*, 467(3):484–490. 2, 1.3.4.9, 1.3.4.9, 1.3.4.9, 1.3.4.9, 3.3.3, 4.4.1, 4.4.3
- [Pfleger et al., 2012] Pfleger, C., Ebeling, G., Bläsche, R., Patton, M., Patel, H. H., Kasper, M., and Barth, K. (2012). Detection of caveolin-3/caveolin-1/P2X7R complexes in mice atrial cardiomyocytes in vivo and in vitro. *Histochemistry and Cell Biology*, 138(2):231–241. 2, 1.3.4.4

- [Pippel et al., 2017] Pippel, A., Stolz, M., Woltersdorf, R., Kless, A., Schmalzing, G., and Markwardt, F. (2017). Localization of the gate and selectivity filter of the full-length P2X7 receptor. *Proceedings of the National Academy of Sciences*, 114(11):E2156–E2165. 1.3.1, 1.3.4.2
- [Poornima et al., 2012] Poornima, V., Madhupriya, M., Kootar, S., Sujatha, G., Kumar, A., and Bera, A. K. (2012). P2X7 receptor-pannexin 1 hemichannel association: Effect of extracellular calcium on membrane permeabilization. *Journal of Molecular Neuroscience*, 46(3):585–594. 2, 1.3.4.2
- [Privatsky et al., 2013] Privatsky, J. R., Newman, D. K., and Newman, P. J. (2013). PECAM-1: Conflicts of Interest in Inflammation. *Magn Reson Imaging*, 31(3):477–479. 3.4.6, 4.5.2.2
- [Pupovac et al., 2015] Pupovac, A., Geraghty, N. J., Watson, D., and Sluyter, R. (2015). Activation of the P2X7 receptor induces the rapid shedding of CD23 from human and murine B cells. *Immunology and Cell Biology*, 93(1):77–85. 4.5.2.6
- [Qiu and Dahl, 2008] Qiu, F. and Dahl, G. (2008). A permeant regulating its permeation pore: inhibition of pannexin 1 channels by ATP. *American Journal of Physiology-Cell Physiology*, 296(2):C250–C255. 1.3.4.2
- [Qu and Dubyak, 2009] Qu, Y. and Dubyak, G. R. (2009). P2X7 receptors regulate multiple types of membrane trafficking responses and non-classical secretion pathways. *Purinergic Signalling*, 5(2):163–173. 4.5.2.6
- [Qu et al., 2007] Qu, Y., Franchi, L., Nunez, G., and Dubyak, G. R. (2007). Nonclassical IL-1 Secretion Stimulated by P2X7 Receptors Is Dependent on Inflammasome Activation and Correlated with Exosome Release in Murine Macrophages. *The Journal of Immunology*, 179(3):1913–1925. 4.5.1
- [Qu et al., 2011] Qu, Y., Misaghi, S., Newton, K., Gilmour, L. L., Louie, S., Cupp, J. E., Dubyak, G. R., Hackos, D., and Dixit, V. M. (2011). Pannexin-1 Is Required for ATP Release during Apoptosis but Not for Inflammasome Activation. *The Journal of Immunology*, 186(11):6553–6561. 1.3.4.2
- [Qu et al., 2009] Qu, Y., Ramachandra, L., Mohr, S., Franchi, L., Harding, C. V., Nunez, G., and Dubyak, G. R. (2009). P2X7 Receptor-Stimulated Secretion of MHC Class II-Containing Exosomes Requires the ASC/NLRP3 Inflammasome

- but Is Independent of Caspase-1. *The Journal of Immunology*, 182(8):5052–5062. 4.5.1
- [Qureshi et al., 2007] Qureshi, O. S., Paramasivam, A., Yu, J. C. H., and Murrell-Lagnado, R. D. (2007). Regulation of P2X4 receptors by lysosomal targeting, glycan protection and exocytosis. *Journal of Cell Science*, 120(21):3838–3849. 1.3.4.9, 1.3.4.9, 3.3.1, 4.4.1, 4.4.2
- [Ray et al., 2002] Ray, F. R., Huang, W., Slater, M., and Barden, J. A. (2002). Purinergic receptor distribution in endothelial cells in blood vessels: A basis for selection of coronary artery grafts. *Atherosclerosis*, 162(1):55–61. 4.5.2.2
- [Reutershan and Ley, 2004] Reutershan, J. and Ley, K. (2004). Bench-to-bedside review: Acute respiratory distress syndrome - How neutrophils migrate into the lung. *Critical Care*, 8(6):453–461. 4.5.2.1, 4.5.2.3
- [Riteau et al., 2010] Riteau, N., Gasse, P., Fauconnier, L., Gombault, A., Couegnat, M., Fick, L., Kanellopoulos, J., Quesniaux, V. F. J., Marchand-Adam, S., Crestani, B., Ryffel, B., and Couillin, I. (2010). Extracellular ATP is a danger signal activating P2X 7 receptor in lung inflammation and fibrosis. *American Journal of Respiratory and Critical Care Medicine*, 182(6):774–783. 4.5.2
- [Robinson and Murrell-Lagnado, 2013] Robinson, L. E. and Murrell-Lagnado, R. D. (2013). The trafficking and targeting of P2X receptors. *Frontiers in Cellular Neuroscience*, 7(November):1–6. 4.2
- [Roger et al., 2010] Roger, S., Gillet, L., Baroja-Mazo, A., Surprenant, A., and Pelegrin, P. (2010). C-terminal calmodulin-binding motif differentially controls human and rat P2X7 receptor current facilitation. *The Journal of biological chemistry*, 285(23):17514–24. 2, 1.3.4.3
- [Roger et al., 2008] Roger, S., Pelegrin, P., and Surprenant, A. (2008). Facilitation of P2X7 receptor currents and membrane blebbing via constitutive and dynamic calmodulin binding. *The Journal of Neuroscience*, 28(25):6393–401. 2, 1.3.4.3
- [Rzeniewicz et al., 2015] Rzeniewicz, K., Newe, A., Rey Gallardo, A., Davies, J., Holt, M. R., Patel, A., Charras, G. T., Stramer, B., Molenaar, C., Tedder, T. F., Parsons, M., and Ivetic, A. (2015). L-selectin shedding is activated specifically within transmigrating pseudopods of monocytes to regulate cell polarity in

- vitro. *Proceedings of the National Academy of Sciences*, 112(12):201417100. 4.5.2.6
- [Sakaki et al., 2013] Sakaki, H., Fujiwaki, T., Tsukimoto, M., Kawano, A., Harada, H., and Kojima, S. (2013). P2X4 receptor regulates P2X7 receptor-dependent IL-1 $\beta$  and IL-18 release in mouse bone marrow-derived dendritic cells. *Biochemical and Biophysical Research Communications*, 432(3):406–411. 1.3.4.9, 1.3.4.9, 4.4.2
- [Sakurai et al., 2012] Sakurai, C., Hashimoto, H., Nakanishi, H., Arai, S., Wada, Y., Sun-Wada, G.-H., Wada, I., and Hatsuzawa, K. (2012). SNAP-23 regulates phagosome formation and maturation in macrophages. *Molecular Biology of the Cell*, 23(24):4849–4863. 4.5.1
- [Salas et al., 2013] Salas, E., Carrasquero, L. M. G., Olivos-Ore, L. A., Bustillo, D., Artalejo, A. R., Miras-Portugal, M. T., and Delicado, E. G. (2013). Purinergic P2X7 Receptors Mediate Cell Death in Mouse Cerebellar Astrocytes in Culture. *Journal of Pharmacology and Experimental Therapeutics*, 347(3):802–815. 3.2.1
- [Sánchez-Nogueiro et al., 2005] Sánchez-Nogueiro, J., Marín-García, P., and Miras-Portugal, M. T. (2005). Characterization of a functional P2X7-like receptor in cerebellar granule neurons from P2X7 knockout mice. *FEBS Letters*, 579(17):3783–3788. 4.1, 4.3
- [Saul et al., 2013] Saul, A., Hausmann, R., Kless, A., and Nicke, A. (2013). Heteromeric assembly of P2X subunits. *Frontiers in cellular neuroscience*, 7(December):250. 1.2
- [Savio et al., 2018] Savio, L. E., Mello, P. d. A., da Silva, C. G., and Coutinho-Silva, R. (2018). The P2X7 receptor in inflammatory diseases: Angel or demon? *Frontiers in Pharmacology*, 9(FEB). 1.4, 3.3.1, 4.5.2
- [Schenk et al., 2008] Schenk, U., Westendorf, A. M., Radaelli, E., Casati, A., Ferro, M., Fumagalli, M., Verderio, C., Buer, J., Scanziani, E., and Grassi, F. (2008). Purinergic control of T cell activation by ATP released through pannexin-1 hemichannels. *Science Signaling*, 1(39):ra6. 4.4.2
- [Schmitt-Ulms et al., 2004] Schmitt-Ulms, G., Hansen, K., Liu, J., Cowdrey, C., Yang, J., DeArmond, S. J., Cohen, F. E., Prusiner, S. B., and Baldwin, M. a.

- (2004). Time-controlled transcardiac perfusion cross-linking for the study of protein interactions in complex tissues. *Nature Biotechnology*, 22(6):724–731. 3.4.3
- [Schmittgen and Livak, 2008] Schmittgen, T. D. and Livak, K. J. (2008). Analyzing real-time PCR data by the comparative CT method. *Nature Protocols*, 3(6):1101–1108. 2.2.2.3
- [Schneider et al., 2017] Schneider, M., Prudic, K., Pippel, A., Klapperstück, M., Braam, U., Müller, C. E., Schmalzing, G., and Markwardt, F. (2017). Interaction of Purinergic P2X4 and P2X7 Receptor Subunits. *Frontiers in Pharmacology*, 8(November):1–14. 1.3.4.9, 1.3.4.9, 3.3.3, 4.4.1
- [Schulz et al., 2003] Schulz, C., Petrig, V., Wolf, K., Krätzel, K., Köhler, M., Becker, B., and Pfeifer, M. (2003). Upregulation of MCAM in primary bronchial epithelial cells from patients with COPD. *European Respiratory Journal*, 22(3):450–456. 4.5.2.3
- [Schwenk et al., 2012] Schwenk, J., Harmel, N., Brechet, A., Zolles, G., Berkefeld, H., Müller, C. S., Bildl, W., Baehrens, D., Hüber, B., Kulik, A., Klöcker, N., Schulte, U., and Fakler, B. (2012). High-resolution proteomics unravel architecture and molecular diversity of native AMPA receptor complexes. *Neuron*, 74(4):621–33. 4.5
- [Seebacher et al., 2006] Seebacher, J., Mallick, P., Zhang, N., Eddes, J. S., Aebbersold, R., and Gelb, M. H. (2006). Protein cross-linking analysis using mass spectrometry, isotope-coded cross-linkers, and integrated computational data processing. *Journal of Proteome Research*, 5(9):2270–2282. 3.4.7, 4.6
- [Shi et al., 2015] Shi, J., Zhao, Y., Wang, K., Shi, X., Wang, Y., Huang, H., Zhuang, Y., Cai, T., Wang, F., and Shao, F. (2015). Cleavage of GSDMD by inflammatory caspases determines pyroptotic cell death. *Nature*, 526(7575):660–665. 1.3.3
- [Shieh et al., 2014] Shieh, C. H., Heinrich, A., Serchov, T., van Calker, D., and Biber, K. (2014). P2X7-dependent, but differentially regulated release of IL-6, CCL2, and TNF- $\alpha$  in cultured mouse microglia. *Glia*, 62(4):592–607. 1.3.3
- [Silverman et al., 2009] Silverman, W. R., de Rivero Vaccari, J. P., Locovei, S., Qiu, F., Carlsson, S. K., Scemes, E., Keane, R. W., and Dahl, G. (2009). The

- pannexin 1 channel activates the inflammasome in neurons and astrocytes. *Journal of Biological Chemistry*, 284(27):18143–18151. 1.3.3, 2, 1.3.4.2, 1.3.4.7
- [Sim et al., 2006] Sim, J. A., Chaumont, S., Jo, J., Ulmann, L., Young, M. T., Cho, K., Buell, G., North, R. A., and Rassendren, F. (2006). Altered Hippocampal Synaptic Potentiation in P2X4 Knock-Out Mice. *Journal of Neuroscience*, 26(35):9006–9009. 3
- [Sim et al., 2004] Sim, J. A., Young, M. T., Sung, H.-Y., North, R. A., and Surprenant, A. (2004). Reanalysis of P2X7 Receptor Expression in Rodent Brain. *Journal of Neuroscience*, 24(28):6307–6314. 1.3.2, 4.1
- [Sinz, 2014] Sinz, A. (2014). The advancement of chemical cross-linking and mass spectrometry for structural proteomics: from single proteins to protein interaction networks. *Expert Review of Proteomics*, 11(6):733–743. 3.4.7
- [Sinz et al., 2015] Sinz, A., Arlt, C., Chorev, D., and Sharon, M. (2015). Chemical cross-linking and native mass spectrometry: A fruitful combination for structural biology. *Protein Science*, 24(8):1193–1209. 4.6
- [Skarnes et al., 2011] Skarnes, W. C., Rosen, B., West, A. P., Koutsourakis, M., Bushell, W., Iyer, V., Mujica, A. O., Thomas, M., Harrow, J., Cox, T., Jackson, D., Severin, J., Biggs, P., Fu, J., Nefedov, M., de Jong, P. J., Stewart, A. F., and Bradley, A. (2011). A conditional knockout resource for the genome-wide study of mouse gene function. *Nature*, 474(7351):337–342. 4.1
- [Sluyter and Wiley, 2002] Sluyter, R. and Wiley, J. S. (2002). Extracellular adenosine 5'-triphosphate induces a loss of CD23 from human dendritic cells via activation of P2X7 receptors. *International immunology*, 14(12):1415–21. 4.5.2.6
- [Solle et al., 2001] Solle, M., Labasi, J., Perregaux, D. G., Stam, E., Petrushova, N., Koller, B. H., Griffiths, R. J., and Gabel, C. A. (2001). Altered cytokine production in mice lacking P2X7 receptors. *Journal of Biological Chemistry*, 276(1):125–132. 1.3.3, 4.1
- [Sorge et al., 2013] Sorge, R. E., Trang, T., Dorfman, R., Smith, S. B., Beggs, S., Ritchie, J., Austin, J.-S., Zaykin, D. V., Vander Meulen, H., Costigan, M., Herbert, T. A., Yarkoni-Abitbul, M., Tichauer, D., Livneh, J., Gershon, E., Zheng, M., Tan, K., John, S. L., Slade, G. D., Jordan, J., Woolf, C. J.,

- Peltz, G., Maixner, W., Diatchenko, L., Seltzer, Z., Salter, M. W., and Mogil, J. S. (2013). Genetically determined P2X7 receptor pore formation regulates variability in chronic pain sensitivity. *Nature medicine*, 18(4):595–9. 3.1.1
- [Sperlágh and Illes, 2014] Sperlágh, B. and Illes, P. (2014). P2X7 receptor: an emerging target in central nervous system diseases. *Trends in Pharmacological Sciences*, 35(10):537–547. 1.3.2
- [Sperlágh et al., 2006] Sperlágh, B., Vizi, E. S., Wirkner, K., and Illes, P. (2006). P2X7 receptors in the nervous system. *Progress in Neurobiology*, 78(6):327–346. 4.1
- [Stelmashenko et al., 2012] Stelmashenko, O., Lalo, U., Yang, Y., Bragg, L., North, R. A., and Compan, V. (2012). Activation of Trimeric P2X2 Receptors by Fewer than Three ATP Molecules. *Molecular Pharmacology*, 82(4):760–766. 1.2
- [Stokes, 2013] Stokes, L. (2013). Rab5 regulates internalisation of P2X4 receptors and potentiation by ivermectin. *Purinergic Signalling*, 9(1):113–121. 4.5.1
- [Stolz et al., 2015] Stolz, M., Klapperstück, M., Kendzierski, T., Detoro-dassen, S., Panning, A., Schmalzing, G., and Markwardt, F. (2015). Homodimeric anoctamin-1, but not homodimeric anoctamin-6, is activated by calcium increases mediated by the P2Y1 and P2X7 receptors. *Pflügers Archiv European Journal of Physiology*, 467(10):2121–2140. 1.3.4.8
- [Subbotin and Chait, 2014] Subbotin, R. I. and Chait, B. T. (2014). A Pipeline for Determining Protein-Protein Interactions and Proximities in the Cellular Milieu. *Molecular & Cellular Proteomics*, 13(11):2824–2835. 3.4.2
- [Sun et al., 2017] Sun, F., Xiao, G., and Qu, Z. (2017). Murine Bronchoalveolar Lavage. *Bio Protoc.*, 7(10):1–7. 2.2.6.1
- [Sutherland et al., 2008] Sutherland, B. W., Toews, J., and Kast, J. (2008). Utility of formaldehyde cross-linking and mass spectrometry in the study of protein-protein interactions. *Journal of mass spectrometry : JMS*, 43(7):854–864. 3.4.2

- [Tardiff et al., 2007] Tardiff, D. F., Abruzzi, K. C., and Rosbash, M. (2007). Protein characterization of *Saccharomyces cerevisiae* RNA polymerase II after in vivo cross-linking. *Proceedings of the National Academy of Sciences*, 104(50):19948–19953. 3.4.3
- [Taylor et al., 2009] Taylor, S. R. J., Gonzalez-Begne, M., Sojka, D. K., Richardson, J. C., Sheardown, S. A., Harrison, S. M., Pusey, C. D., Tam, F. W. K., and Elliott, J. I. (2009). Lymphocytes from P2X7 -deficient mice exhibit enhanced P2X7 responses. *Journal of Leukocyte Biology*, 85(6):978–986. 4.1
- [Torres et al., 1999] Torres, G. E., Egan, T. M., and Voigt, M. M. (1999). Heterooligomeric Assembly of P2X Receptor Subunits. *The Journal of biological chemistry*, 274(10):6653–6659. 1.2, 1.3.1, 1.3.4.9, 4.4, 4.4.3
- [Toulme et al., 2010] Toulme, E., Garcia, A., Samways, D., Egan, T. M., Carson, M. J., and Khakh, B. S. (2010). P2X4 receptors in activated C8-B4 cells of cerebellar microglial origin. *The Journal of general physiology*, 135(4):333–53. 4.4.1
- [Toyomitsu et al., 2012] Toyomitsu, E., Tsuda, M., Yamashita, T., Tozaki-Saitoh, H., Tanaka, Y., and Inoue, K. (2012). CCL2 promotes P2X4 receptor trafficking to the cell surface of microglia. *Purinergic Signalling*, 8(2):301–310. 4.4.1
- [Tyanova et al., 2016] Tyanova, S., Temu, T., Sinitcyn, P., Carlson, A., Hein, M. Y., Geiger, T., Mann, M., and Cox, J. (2016). The Perseus computational platform for comprehensive analysis of (prote)omics data. *Nature Methods*, 13(9):731–740. 3.4.5
- [Valera et al., 1994] Valera, S., Hussy, N., Evans, R. J., Adami, N., North, R. a., Surprenant, A., and Buell, G. (1994). A new class of ligand-gated ion channel defined by P2x receptor for extracellular ATP. *Nature*, 371(6497):516–9. 1.2
- [Vasilescu et al., 2004] Vasilescu, J., Guo, X., and Kast, J. (2004). Identification of protein-protein interactions using in vivo cross-linking and mass spectrometry. *Proteomics*, 4(12):3845–3854. 3.4.3
- [Vénéreau et al., 2015] Vénéreau, E., Ceriotti, C., and Bianchi, M. E. (2015). DAMPs from cell death to new life. *Frontiers in Immunology*, 6(AUG):1–11. 1.3.3

- [Vicente-Manzanares et al., 2009] Vicente-Manzanares, M., Ma, X., Adelstein, R. S., and Horwitz, A. R. (2009). Non-muscle myosin II takes centre stage in cell adhesion and migration. *Nature reviews. Molecular cell biology*, 10(11):778–90. 4.5.2.6
- [Vieira et al., 2003] Vieira, O. V., Bucci, C., Harrison, R. E., Trimble, W. S., Lanzetti, L., Gruenberg, J., Schreiber, A. D., Stahl, P. D., and Grinstein, S. (2003). Modulation of Rab5 and Rab7 Recruitment to Phagosomes by Phosphatidylinositol 3-Kinase. *Molecular and Cellular Biology*, 23(7):2501–2514. 4.5.1
- [Villar et al., 2014] Villar, J., Muros, M., Cabrera-Benítez, N. E., Valladares, F., López-Hernández, M., Flores, C., Martín-Barrasa, J. L., Blanco, J., Liu, M., and Kacmarek, R. M. (2014). Soluble platelet-endothelial cell adhesion molecule-1, a biomarker of ventilator-induced lung injury. *Critical Care*, 18(2). 4.5.2.2, 4.5.2.6
- [Wandinger-Ness and Zerial, 2014] Wandinger-Ness, A. and Zerial, M. (2014). Rab Proteins and the Compartmentalization of the Endosomal system. *Cold Spring Harbor Perspectives in Biology*, 6(11):1–25. 4.5.1
- [Wang et al., 2014] Wang, C. M., Ploia, C., Anselmi, F., Sarukhan, A., and Viola, A. (2014). Adenosine triphosphate acts as a paracrine signaling molecule to reduce the motility of T cells. *The EMBO Journal*, 33(12):1354–1364. 4.4.2
- [Wang et al., 2011] Wang, J., Huo, K., Ma, L., Tang, L., Li, D., Huang, X., Yuan, Y., Li, C., Wang, W., Guan, W., Chen, H., Jin, C., Wei, J., Zhang, W., Yang, Y., Liu, Q., Zhou, Y., Zhang, C., Wu, Z., Xu, W., Zhang, Y., Liu, T., Yu, D., Zhang, Y., Chen, L., Zhu, D., Zhong, X., Kang, L., Gan, X., Yu, X., Ma, Q., Yan, J., Zhou, L., Liu, Z., Zhu, Y., Zhou, T., He, F., and Yang, X. (2011). Toward an understanding of the protein interaction network of the human liver. *Molecular Systems Biology*, 7(536):1–10. 1.3.4, 2
- [Wang et al., 2015] Wang, S., Zhao, J., Wang, H., Liang, Y., Yang, N., and Huang, Y. (2015). Blockage of P2X7 attenuates acute lung injury in mice by inhibiting NLRP3 inflammasome. *International Immunopharmacology*, 27(1):38–45. 4.5.2
- [Wang and Yan, 2013] Wang, Z. and Yan, X. (2013). CD146, a multi-functional molecule beyond adhesion. *Cancer Letters*, 330(2):150–162. 4.5.2.3

- [Watanabe et al., 2019] Watanabe, C., Matsushita, J., Azami, T., Tsukiyama-Fujii, S., Tsukiyama, T., Mizuno, S., Takahashi, S., and Ema, M. (2019). Generating Vegfr3 reporter transgenic mouse expressing membrane-tagged Venus for visualization of VEGFR3 expression in vascular and lymphatic endothelial cells. *PLoS ONE*, 14(1):1–16. 4.2
- [Weinhold et al., 2010] Weinhold, K., Krause-Buchholz, U., Rödel, G., Kasper, M., and Barth, K. (2010). Interaction and interrelation of P2X7 and P2X4 receptor complexes in mouse lung epithelial cells. *Cellular and molecular life sciences : CMLS*, 67(15):2631–42. 2, 1.3.4.4, 1.3.4.9, 1.3.4.9, 3.3.2, 4.4.2, 4.4.3, 4.5.2.5
- [Wiley and Gu, 2012] Wiley, J. S. and Gu, B. J. (2012). A new role for the P2X7 receptor: a scavenger receptor for bacteria and apoptotic cells in the absence of serum and extracellular ATP. *Purinergic signalling*, 8(3):579–86. 4.5.1
- [Wilkinson et al., 2006] Wilkinson, W. J., Jiang, L.-H., Surprenant, A., and North, R. A. (2006). Role of ectodomain lysines in the subunits of the heteromeric P2X2/3 receptor. *Molecular pharmacology*, 70(4):1159–1163. 1.2
- [Wilson et al., 2004] Wilson, H. L., Francis, S. E., Dower, S. K., and Crossman, D. C. (2004). Secretion of Intracellular IL-1 Receptor Antagonist (Type 1) Is Dependent on P2X7 Receptor Activation. *The Journal of Immunology*, 173(2):1202–1208. 1.3.3
- [Wilson et al., 2002] Wilson, H. L., Wilson, S. a., Surprenant, A., and North, R. A. (2002). Epithelial membrane proteins induce membrane blebbing and interact with the P2X7 receptor C terminus. *The Journal of biological chemistry*, 277(37):34017–23. 1.3.4, 2
- [Woehrle et al., 2010] Woehrle, T., Yip, L., Elkhail, A., Sumi, Y., Chen, Y., Yao, Y., Insel, P. A., and Junger, W. G. (2010). Pannexin-1 hemichannel-mediated ATP release together with P2X1 and P2X4 receptors regulate T-cell activation at the immune synapse. *Blood*, 116(18):3475–3484. 4.4.2
- [Wu et al., 2007] Wu, C., Ma, M. H., Brown, K. R., Geisler, M., Li, L., Tzeng, E., Jia, C. Y., Jurisica, I., and Li, S. S. (2007). Systematic identification of SH3 domain-mediated human protein-protein interactions by peptide array target screening. *Proteomics*, 7(11):1775–1785. 1.3.4, 2

- [Wu et al., 2013] Wu, Q., Case, S. R., Minor, M. N., Jiang, D., Martin, R. J., Bowler, R. P., Wang, J., Hartney, J., Karimpour-Fard, A., and Chu, H. W. (2013). A novel function of MUC18: Amplification of lung inflammation during bacterial infection. *American Journal of Pathology*, 182(3):819–827. 4.5.2.3
- [Wu et al., 2005] Wu, Y., Stabach, P., Michaud, M., and Madri, J. A. (2005). Neutrophils Lacking Platelet-Endothelial Cell Adhesion Molecule-1 Exhibit Loss of Directionality and Motility in CXCR2-Mediated Chemotaxis. *The Journal of Immunology*, 175(6):3484–3491. 4.5.2.2
- [Xiang and Burnstock, 2005] Xiang, Z. and Burnstock, G. (2005). Expression of P2X receptors on rat microglial cells during early development. *Glia*, 52(2):119–126. 1.3.4.9
- [Yang and Gong, 2005] Yang, X. W. and Gong, S. (2005). An overview on the generation of BAC transgenic mice for neuroscience research. *Current Protocols in Neuroscience*, Chapter 5:Unit 5.20. 4.2
- [Yip et al., 2009] Yip, L., Woehrle, T., Corriden, R., Hirsh, M., Chen, Y., Inoue, Y., Ferrari, V., Insel, P. A., and Junger, W. G. (2009). Autocrine regulation of T-cell activation by ATP release and P2X7 receptors. *The FASEB Journal*, 23(6):1685–1693. 4.4.2
- [Yona et al., 2013] Yona, S., Kim, K. W., Wolf, Y., Mildner, A., Varol, D., Breker, M., Strauss-Ayali, D., Viukov, S., Guillemins, M., Misharin, A., Hume, D. A., Perlman, H., Malissen, B., Zelzer, E., and Jung, S. (2013). Fate Mapping Reveals Origins and Dynamics of Monocytes and Tissue Macrophages under Homeostasis. *Immunity*, 38(1):79–91. 3, 3.2.1
- [Young et al., 2015] Young, C. N., Sinadinos, A., Lefebvre, A., Chan, P., Arkle, S., Vaudry, D., and Gorecki, D. C. (2015). A novel mechanism of autophagic cell death in dystrophic muscle regulated by P2RX7 receptor large-pore formation and HSP90. *Autophagy*, 11(1):113–130. 1.3.4.1
- [Yu et al., 2008] Yu, Y., Ugawa, S., Ueda, T., Ishida, Y., Inoue, K., Kyaw Nyunt, A., Umemura, A., Mase, M., Yamada, K., and Shimada, S. (2008). Cellular localization of P2X7 receptor mRNA in the rat brain. *Brain Research*, 1194:45–55. 1.3.2

- [Zech et al., 2016] Zech, A., Wiesler, B., Ayata, C. K., Schlaich, T., Dürk, T., Hoßfeld, M., Ehrat, N., Cicko, S., and Idzko, M. (2016). P2rx4 deficiency in mice alleviates allergen-induced airway inflammation. *Oncotarget*, 7(49):80288–80297. 3.3.1
- [Zemans et al., 2009] Zemans, R. L., Colgan, S. P., and Downey, G. P. (2009). Transepithelial migration of neutrophils: Mechanisms and implications for acute lung injury. *American Journal of Respiratory Cell and Molecular Biology*, 40(5):519–535. 4.5.2, 4.5.2.1, 4.5.2.2, 4.5.2.3
- [Zhang et al., 2005] Zhang, X. F., Han, P., Faltynek, C. R., Jarvis, M. F., and Shieh, C. C. (2005). Functional expression of P2X7 receptors in non-neuronal cells of rat dorsal root ganglia. *Brain Research*, 1052(1):63–70. 3.2.2
- [Zhang et al., 2014] Zhang, Y., Chen, K., Sloan, S. A., Bennett, M. L., Scholze, A. R., O’Keeffe, S., Phatnani, H. P., Guarnieri, P., Caneda, C., Ruderisch, N., Deng, S., Liddelow, S. A., Zhang, C., Daneman, R., Maniatis, T., Barres, B. A., and Wu, J. Q. (2014). An RNA-Sequencing Transcriptome and Splicing Database of Glia, Neurons, and Vascular Cells of the Cerebral Cortex. *Journal of Neuroscience*, 34(36):11929–11947. 4.3
- [Zhang and Wang, 2012] Zhang, Y. and Wang, H. (2012). Integrin signalling and function in immune cells. *Immunology*, 135(4):268–275. 4.5.2.1
- [Zhen and Stenmark, 2015] Zhen, Y. and Stenmark, H. (2015). Cellular functions of Rab GTPases at a glance. *Journal of Cell Science*, 128(17):3171–3176. 4.5.1
- [Zuo et al., 2018] Zuo, Y., Wang, J., Liao, F., Yan, X., Li, J., Huang, L., and Liu, F. (2018). Inhibition of Heat Shock Protein 90 by 17-AAG Reduces Inflammation via P2X7 Receptor/NLRP3 Inflammasome Pathway and Increases Neurogenesis After Subarachnoid Hemorrhage in Mice. *Frontiers in Molecular Neuroscience*, 11(November):401. 1.3.4.1

## **A. Appendix**

### **A.1. Acknowledgement**

First of all, I would like to express my deep gratitude to my supervisor Prof. Dr. Annette Nicke for the opportunity to conduct my research in her lab and to write this dissertation. I want to thank you for your patient guidance, the useful critiques, and your contagious passion for science.

I am particularly grateful for the assistance given by the group of Prof. Dr. Axel Imhof and in particular by Dr. Andreas Schmidt, who conducted the MS analysis. I would also like to acknowledge my colleagues at the Walther Straub Institute for the great working atmosphere and for their support in various ways. I would like to particularly single out Anna Krautloher, Jiong Zhang, Johann Schredelseker, Jonas Weber, and Susanne Fiedler. I want to thank you for the helpful discussions and for spending your time teaching me new techniques. Moreover, I would like to extend my gratitude to Heinz Janser, who provided technical assistance in many ways.

I would like to express my deep and sincere gratitude to my family for their continuous love and support. I want to thank my parents, Monika and Siegfried, who always believed in me and backed me up. I am grateful to my wife Miriam for always being there for me and supporting me during this entire journey, even in difficult times. I would also like to extend my deepest gratitude to my parents-in-law, Brigitte and Hans-Walter, who made it possible to spend several hours on writing, without being distracted by taking care of the everyday problems. Hans, thank you for everything!

Finally, I want to thank my daughter Greta and all of my friends for providing the distraction I needed, to rest my mind outside of my research.

Thanks to all of you! Without you, this thesis would not have been possible!

## A.2. Eidesstattliche Versicherung

Kopp, Robin Edwin

---

Name, Vorname

Ich erkläre hiermit an Eides statt, dass ich die vorliegende Dissertation mit dem Thema:

**"Analysis of P2X7 protein complexes in a P2X7-EGFP BAC transgenic mouse model."**

selbständig verfasst, mich außer der angegebenen keiner weiteren Hilfsmittel bedient und alle Erkenntnisse, die aus dem Schrifttum ganz oder annähernd übernommen sind, als solche kenntlich gemacht und nach ihrer Herkunft unter Bezeichnung der Fundstelle einzeln nachgewiesen habe.

Ich erkläre des Weiteren, dass die hier vorgelegte Dissertation nicht in gleicher oder in ähnlicher Form bei einer anderen Stelle zur Erlangung eines akademischen Grades eingereicht wurde.

München, 08.04.2020

---

Ort, Datum

Robin Kopp

---

Unterschrift